

EXTRINSIC REGULATION OF INTESTINAL STEM CELL
PROLIFERATION AND DIFFERENTIATION BY NICHE COMPONENTS

Bailey Zwarycz

A dissertation submitted to the faculty at the University of North Carolina at Chapel Hill
in partial fulfillment of the requirements for the degree of Doctor of Philosophy in the
Department of Cell Biology and Physiology in the School of Medicine.

Chapel Hill
2018

Approved by:

Scott T. Magness

Carol A. Otey

Susan J. Henning

Keith Burridge

Michael B. Major

© 2018
Bailey Zwarycz
ALL RIGHTS RESERVED

ABSTRACT

Bailey Zwarycz: Extrinsic Regulation of Intestinal Stem Cell Proliferation and Differentiation by Niche Components
(Under the direction of Scott T. Magness)

The small intestinal epithelium facilitates the absorption of nutrients and provides a barrier against damaging toxins, indigestible contents, and microbes in the intestinal lumen. The epithelium is maintained by a pool of intestinal stem cells (ISCs) that reside at the base of the crypt in a supportive niche environment, made up of both cellular and non-cellular components. Niche cells, including epithelial Paneth cells, subepithelial myofibroblasts, and immune cells, along with the non-cellular extracellular matrix (ECM) provide cues that promote ISC proliferation and differentiation. The niche environment is complex and dynamic, with various cell types present that secrete different growth factors and cytokines in response to intestinal damage, inflammation, and regeneration.

Extrinsic niche factors are integral for the survival and proliferation of ISCs; therefore, understanding the influence of individual niche components on ISC behavior is essential for the development of therapeutics for patient health. Here, two components of the ISC niche are investigated for their influence on ISC proliferation and differentiation: cytokines secreted from local immune cells and the underlying ECM scaffold. Through a screen of inflammatory bowel disease-related cytokines, Interleukin 22 demonstrated a concentration-dependent effect on ileal organoid size and survival *in vitro*. Elevated levels of Interleukin 22 limited ISC expansion in favor of increased progenitor cell differentiation

and proliferation, resulting in increased organoids size and expression of antimicrobial gene products. ISC cultures rely on the use of non-intestinal based ECM components for the survival of ISCs *in vitro*. Using a natural, acellular intestinal scaffold provides a more physiologically relevant substrate for use both *in vitro* culture systems and for tissue engineering applications. By optimizing decellularization techniques, an acellular porcine small intestinal scaffold was created that retained mucosal architecture, preserved key ECM components, and supported the proliferation and differentiation of mouse small intestinal epithelium. Together, these to findings further the understanding of how extrinsic factors from the niche influence ISCs, which is of particular importance when developing therapies for intestinal disease.

To my Mom and Dad for always being my biggest fans.

ACKNOWLEDGEMENTS

If I actually wrote out my sincerest thanks to everyone who has helped me while I've been at UNC, this dissertation would be twice as long. The friendships that I have made while working here are irreplaceable to me and I value each and every one of them.

I am forever grateful to Dr. Scott Magness for training me to become the scientist I am today—without you none of this would be possible. I would like to particularly thank Drs. Susan Henning and Lola Reid who provided invaluable mentorship for my fellowship research. I would like to acknowledge my current and former committee members, Drs. Carol Otey, Susan Henning, Ben Major, Keith Burrige, and Kay Lund for all of the guidance throughout the evolution of this dissertation. Thank you to the Gastrointestinal Stem Cell group, the Center for Gastrointestinal Biology & Disease, and Department of Cell Biology & Physiology for the continuous support, feedback, and encouragement.

A big thank you to everyone, past and present, from the Magness Lab. My experience in the lab would not have been the same without each and every one of you. I would like to specifically acknowledge Ian Williamson, Kristina Rivera, Dr. Kyle Roche, and Dr. Eric Bankaitis, for their help with fellowship and manuscript development and writing. I would especially like to acknowledge Dr. Adam Gracz and Dr. Leigh Ann Samsa who were integral in the encouragement towards and completion of this dissertation.

Finally, thank you to my family. Your constant love, support, and encouragement are the reasons I am who I am today. I promise that I'm done with school now and we can properly plan family get-togethers without me having to leave early to feed my cells.

TABLE OF CONTENTS

LIST OF TABLES.....	ix
LIST OF FIGURES	x
LIST OF ABBREVIATIONS	xii
CHAPTER 1: INTRODUCTION	1
Small Intestinal Epithelium: Structure, Function, and Cellular Composition	1
Genes and Pathways Regulating Epithelial Cell Differentiation	3
Intestinal Stem Cells: Identification and Maintenance	4
Studying Intestinal Stem Cells <i>in vitro</i> : Organoid Culture System	8
Components of the Intestinal Stem Cell Niche	10
Immune Cell Components of the Small Intestine	13
Intestinal Mucosal Response to Inflammation and Healing	15
CHAPTER 2: ELEVATED IL22 INHIBITS EPITHELIAL STEM CELL EXPANSION IN AN ILEAL ORGANOID MODEL	23
Overview	23
Introduction	24
Results	26
Discussion	36
Methods	41

CHAPTER 3: DEVELOPMENT OF EXTRACELLULAR MATRIX SCAFFOLDS FROM PORCINE SMALL INTESTINE THAT SUPPORT THE PROLIFERATION AND DIFFERENTIATION OF INTESTINAL EPITHELIAL CELLS	59
Overview	59
Introduction	60
Results	62
Discussion	67
Methods	70
CHAPTER 4: SCOPE OF WORK, SIGNIFICANCE, AND IMPLICATIONS FOR FUTURE STUDIES	80
IL22 levels are physiologically important.....	80
Acellular porcine intestine is an attractive scaffold for intestinal tissue engineering	83
Extrinsic niche factors influence ISC proliferation and differentiation	86
APPENDIX A: ORGANOID CULTURES FOR ASSESSING INTESTINAL EPITHELIAL DIFFERENTIATION AND FUNCTION IN RESPONSE TO TYPE-2 INFLAMMATION	87
Overview	87
Introduction	88
Materials.....	92
Methods	97
Notes.....	110
REFERENCES	122

LIST OF TABLES

Table 2.1. List of Taqman probes for qRT-PCR.....	58
Table 5.1 Suggested Taqman probes for qRT-PCR analysis	121

LIST OF FIGURES

Figure 1.1. Small intestinal anatomy and epithelial cell lineages	20
Figure 1.2. ISCs form organoids in vitro.....	21
Figure 1.3. The intestinal stem cell niche.....	22
Figure 2.1. A focused screen of IBD-related cytokines reveals that IL22 causes a dose-dependent decrease in organoid survival and increase in organoid size	51
Figure 2.2. IL22ra1 is heterogeneously expressed throughout the crypt	53
Figure 2.3. COMSOL Multiphysics simulation of IL22 diffusion.	54
Figure 2.4. Cell lineage analysis in single ISCs and ileal organoids treated with IL22.	55
Figure 2.5. IL22 limits ISC expansion	56
Figure 2.6. Elevated IL22 causes an increase in TA progenitors.....	57
Figure 3.1. Porcine intestine throughout the decellularization process	76
Figure 3.2. Intestinal scaffolds retain architecture and ECM composition.....	77
Figure 3.3. Intestinal scaffolds support intestinal epithelial cell proliferation	78
Figure 3.4. Intestinal scaffolds support intestinal epithelial cell differentiation	79
Figure 5.1 A cellular mechanism to resolve helminth infections in the gastrointestinal tract.....	115
Figure 5.2 Quality control steps in intestinal crypt isolation.....	116
Figure 5.3 Best practices for placing ECM, and adding/removing media from ECM-based cultures	117

Figure 5.4 Organoids in culture form crypt buds118

Figure 5.5 Sectioned organoids can be identified by light microscopy.....119

Figure 5.6 Wild-type intestinal organoids contain tuft, goblet, and
Paneth cell populations.....120

LIST OF ABBREVIATIONS

aISC	“actively cycling” ISCs
ANOVA	Analysis of Variance
Ascl2	Achaete-scute family bHLH transcription factor 2
Atoh1	Atonal bLHL transcription factor 1
Axin2	Axin 2
β -catenin	Cadherin associated protein, beta 1
BMP	Bone morphogenic protein
Ccnd1	Cyclin D1
ChgA	Chromagranin A
Col1a1	Collagen Type I
Col18a1	Collagen Type XVIII
Dcamk1	Doublecortin and calcium/calmodulin-dependent protein kinase-like-1
Dll1	Delta-like 1
DPBS	Dulbecco’s phosphate-buffered saline
ECM	Extracellular matrix
EDTA	ethylenediaminetetraacetic acid
EdU	5-ethynyl-2’-deoxyuridine
EGF	Epidermal growth factor
EGFP	Enhanced green fluorescent protein
E1f3	E74-like factor 3
Epcam	Epithelial cell adhesion molecule

FACS	Fluorescence-activated cell sorting
GALT	Gut-associated lymphoid tissue
GFP	Green florescent protein
Grem1	Gremlin 1
HBSS	Hank's balanced salt solution
Hes1	Hes family bHLH transcription factor 1
IBD	Inflammatory bowel disease
IHC	immunohistochemistry
IL	Interleukin
IL22	Interleukin 22
IL22BP	Interleukin 22 binding protein (IL22ra2)
IL22ra1	Interleukin 22 receptor, alpha 1
IL22ra2	Interleukin 22, receptor, alpha 2
ILC	Innate lymphoid cell
ILF	Isolated lymphoid follicle
ISC	Intestinal stem cell
LC3	Microtubule-associated protein 1A/1B-light chain 3
Lgr4	Leucine-rich-repeat-containing G protein coupled receptor 4
LGR5	Leucine-rich-repeat-containing G protein coupled receptor 5
Lyz2	Lysozyme 2
MAPK	Mitogen-activated protein kinases
mRNA	Messenger ribonucleic acid
Muc2	Mucin 2

Myc	Myelocytomatosis oncogene
NAC	N-acetylcysteine
Nog	Noggin
OCT	Optimal Cutting Temperature
Olfm4	Olfactomedin 4
PFA	paraformaldehyde
PLA ₂	Phospholipase A ₂
PN	Parenteral nutrition
REG	Regenerating family member 3
rISC	“reserve” ISC
RNA-seq	RNA-sequencing
ROR γ	Retinoic-acid-receptor-related orphan nuclear receptor gamma
RT-qPCR	Quantitative reverse transcription polymerase chain reaction
SBS	Short bowel syndrome
SDC	Sodium deoxycholate
SI	Sucrose isomaltase
SILT	Solitary isolated lymphoid tissue
SMAD	SMAD family members
Sox9	SRY (sex determining region Y)-box 9
Stat3	Signal transducer and activator of transcription 3
TA	Transit-amplifying
TCF/LEF	T-cell factor/lymphoid enhancer factor
TNF	Tumor necrosis factor

Ubq

Ubiquitin

Wnt3a

Wingless-type MMTV integration site family, member 3A

CHAPTER 1: INTRODUCTION

Small Intestinal Epithelium: Structure, Function, and Cellular Composition

In the gastrointestinal tract, the small intestine specializes in the digestion and absorption of food and nutrients. Although all regions of the gastrointestinal tract are integral for efficient food and water intake, digestion, and absorption, the focus of this dissertation will be on the small intestine. The small intestine is divided into three distinct anatomical segments: the duodenum, jejunum, and ileum. The first segment is the duodenum where intestinal contents mix with digestive enzymes from the pancreas and liver after exiting the stomach. The next, and longest, segment is the jejunum, which is the main segment for nutrient absorption. Finally, the ileum is the most distal segment of the small intestine and functions to absorb remaining nutrients and bile acids before intestinal contents move into the large intestine.

All three regions – the duodenum, jejunum, and ileum – share a similar layered anatomy with an outermost serosa, followed by the muscularis propria (layers of longitudinal and circular muscle), submucosa, and innermost mucosa (Figure 1.1A)¹. The mucosa is comprised of the innermost epithelium and is supported by the lamina propria and the muscularis mucosae, a thin smooth muscle layer. In direct contact with the luminal contents, the simple monolayer of columnar epithelium facilitates the absorption of nutrients and provides a barrier between the rest of the body and indigestible luminal

contents, damaging toxins, and microbes that reside in the intestinal lumen. The lamina propria resides directly underneath the epithelium and contains supportive structural components, including a complex and highly patterned extracellular matrix (ECM) architecture, vasculature, mesenchymal cells, and immune cells that directly support epithelial structure and function². In particular, subepithelial myofibroblasts and immune cells are in close contact with the epithelium and secrete growth factors and cytokines to influence epithelial cell function.

The epithelium of the small intestine is distinctly organized into a crypt-villus architecture (Figure 1.1A). Crypts are invaginations of the epithelium embedded into the lamina propria and contain mostly proliferative cells. Epithelial proliferation occurs within the crypt and is driven by intestinal stem cells (ISCs) residing at the base. ISCs rapidly divide approximately once every 24 hours³ and self-renew to give rise to more ISCs or differentiate to a proliferative transit-amplifying (TA) progenitor cell with each division. TA progenitor cells divide 2-3 times every 12-16 hours⁴ and migrate away from the base of the crypt before terminally differentiating as they exit the crypt. Crypts surround large, finger-like projections called villi, which contain differentiated cells and protrude into the intestinal lumen to increase absorptive surface area.

Differentiated cells migrate from the crypt to the tip of the villus, where they ultimately undergo anoikis (a programmed cell death process triggered by loss of contact with the basement membrane) and are sloughed off into the intestinal lumen^{5,6}. This process of differentiation and migration takes approximately 3-5 days and is integral to maintaining epithelial barrier integrity⁷. In the mouse, there are approximately 6-12 crypts per villus depending on the location within the small intestine⁸, providing a constant

“conveyer belt” of differentiated cells for each villus. Regional differences in epithelial architecture and differentiated cell composition are also found along the small intestine to meet functional requirements. Villi in the duodenum are longest to facilitate nutrient absorption and increased secretion of hydrolytic enzymes, whereas villi in the ileum are shorter and contain more mucus-secreting cells to facilitate passage of food into the colon^{9,10}.

Genes and Pathways Regulating Epithelial Cell Differentiation

By the time an epithelial cell has migrated to the villus, its identity has been established based on gene expression signatures. There are two main lineages of differentiated cells – absorptive cells and secretory cells (Figure 1.1B). The initial fate decision committing a nascent epithelial cell to an absorptive versus secretory identity is strongly controlled by Notch signaling. Notch signaling activates expression of hes family bHLH transcription factor 1 (*Hes1*), which in turn represses the expression of atonal bHLH transcription factor 1 (*Atoh1*). Under homeostatic Notch signaling, the majority of epithelial cells differentiate towards the absorptive lineage and become enterocytes. Similarly, *Atoh1* deletion results in differentiation towards enterocytes^{11,12}. Approximately 80% of the cells on the villus are enterocytes, which absorb nutrients through their apical brush border¹³. Enterocytes also provide hydrolytic brush border enzymes to facilitate the breakdown of dietary carbohydrates and proteins and can therefore be identified by their expression of enzymes including sucrose isomaltase (*SI*) and lactase.

Inhibition of Notch signaling, or overexpression of *Atoh1*, causes differentiation towards a secretory fate¹⁴⁻¹⁷. Cells of the secretory lineage include goblet,

enteroendocrine, and tuft cells found on the villi and Paneth cells found at the base of the crypt. Goblet cells secrete mucins to coat and protect the epithelium from the luminal contents and microbiota and are identified by their expression of mucin genes, including mucin 2 (*Muc2*)¹⁸. Enteroendocrine cells comprise approximately 1% of intestinal epithelial cells and secrete hormones that regulate digestion¹⁹. Although enteroendocrine cells include more than 10 different cell types producing distinct hormones, they can be identified by their general expression of chromogranin A (*ChgA*) and Synaptophysin²⁰. Finally, the rare tuft cell is thought to play an essential role in the initiation of Type 2 immune responses to helminth infections and is identified by expression of doublecortin and calcium/calmodulin-dependent protein kinase-like-1 (*Dcamk1l*)^{21,22}.

Paneth cells are of the secretory lineage, but remain at the crypt base intercalated between ISCs. Each crypt contains approximately 15 ISCs and 10 Paneth cells²³. Compared to other differentiated cells types, Paneth cells are long-lived with a life-span of approximately 60 days²⁴. Paneth cells have long been known to secrete antimicrobial peptides for protection from luminal microbes and are identified by expression of antimicrobials including Lysozyme and cryptidins^{23,25}. A more recently established role for Paneth cells is the secretion of growth factors, including epidermal growth factor (EGF), wntless-type MMTV integration site family, member 3A (Wnt3a) and Notch ligands²⁶ to support ISC maintenance and proliferation.

Intestinal Stem Cells: Identification and Maintenance

ISCs reside at the base of the crypt and drive constant regeneration of the intestinal epithelium, with epithelial turnover occurring every 3-5 days⁷. Two distinct ISC types been

identified, with varying proliferative capacities. Traditionally, ISCs were termed “crypt-based-columnar” cells in reference to their position at the crypt base intercalated among Paneth cells. These “actively cycling” ISCs (aISCs) divide approximately once every 24 hours⁴, give rise to TA progenitor cells, and maintain the day to day epithelial turnover during homeostasis. In contrast, facultative or “reserve” ISCs (rISC) found in the ‘+4 position’ (4 cell positions up from the base of the crypt) are slowly cycling or quiescent during homeostasis²⁷ and only become activated following intestinal damage²⁸. These rISCs have historically been described as “label-retaining” cells based on their functional capacity to retain expression of DNA-labeling agents²⁹. Their capacity for activation and renewal in response to injury has made rISCs the focus of many recent studies^{7,30}. This dissertation will focus only on regulation of the aISC population by extrinsic factors, so from here on aISCs will be referred to simply as ISCs.

Biomarkers that enable isolation of live ISCs have only recently been identified. The first ISC biomarker identified was the leucine-rich-repeat-containing G protein coupled receptor 5 (*Lgr5*)³¹. By linking *Lgr5* expression with EGFP protein expression *in vivo*, the *Lgr5*EGFPiresCreERT2 knock-in mouse model (from here on to be referred to as *Lgr5*-EGFP) allowed for *Lgr5*-GFP+ ISCs to be directly visualized in the intestinal crypt³¹. By crossing the *Lgr5*-EGFP mouse with a *Rosa26LacZ* reporter mouse, administration of Tamoxifen allowed the inducible CreERT2 to recombine floxed alleles to permanently label *Lgr5*-expressing cells and all their progeny³². These early lineage tracing studies demonstrated that the *Lgr5*+ ISC marked aISCs that were able to give rise to all other epithelial cell lineages *in vivo*³¹. Deletion of *Lgr5* has little effect on crypt proliferation; however, mutation of leucine-rich-repeat-containing G protein coupled

receptor 4 (*Lgr4*), which is also found in intestinal crypt cells, greatly decreases crypt epithelial cell proliferation³³. Most prominently, knockout both of *Lgr4* and *Lgr5* entirely stops crypt proliferation³⁴. LGR4 and LGR5 promote Wnt signaling³⁴, suggesting the strong dependence of ISC function on the Wnt signaling pathway.

Wnt signaling is integral in many tissues to promote proliferation³⁵ and is found in a gradient along the crypt^{36,37}. Expression of specific Wnts (mice have 19 of them) is regional along the crypt-villus axis, with epithelial-derived Wnts being found in a gradient that is highest at the base of the crypt and decreases moving towards the villus^{36,37}. To briefly summarize relevant canonical Wnt signaling, in the absence of receptor activation, cytoplasmic β -catenin (catenin (cadherin associated protein) beta 1, *Ctnnb1*) is destroyed by the APC destruction complex. To activate Wnt signaling, Wnt proteins bind to the cysteine-rich domain of Frizzled-Lrp5/6 receptors and dephosphorylates the APC destruction complex, rendering it incapable of interacting with β -catenin. This allows β -catenin to accumulate within the cell, travel to the nucleus, and bind to TCF/LEF proteins to regulate expression of Wnt target genes including myelocytomatosis oncogene (*Myc*), cyclin D1 (*Ccnd1*), CD44 antigen (*Cd44*), and axin 2 (*Axin2*)³⁸. In mice, loss of TCF3 causes loss of proliferative crypts³⁹ and loss of β -catenin causes loss of ISC markers, terminal differentiation of epithelium and ultimately a fatal loss of intestinal function⁴⁰, highlighting the importance of Wnt signaling for ISC proliferation.

Since the discovery of *Lgr5* as an ISC biomarker, additional biomarkers that are also Wnt target genes, including SRY (sex determining region Y)-box 9 (*Sox9*)⁴¹, achaete-scute family bHLH transcription factor 2 (*Ascl2*)⁴², and olfactomedin 4 (*Olfm4*)^{43,44} have been identified. The transcription factor *Sox9* is a Wnt target gene and has been shown

to regulate ISC proliferation^{45,46}. Not only was *Sox9* found to be an ISC marker, it also marked all proliferating cell types in the crypt at various expression levels: at high levels in rISCs and enteroendocrine cells, low levels in aISCs, and sublow levels in TA progenitor cells^{41,47}. The ability to isolate ISCs and other crypt epithelial cells by expression of enhanced green fluorescent protein (EGFP) driven by a *Sox9* promoter has allowed for the development of elegant, high-throughput studies of ISCs *in vitro*⁴⁸.

In order for ISCs to maintain their proliferative capacity and an appropriate ratio of ISC renewal versus differentiation, a delicate balance of growth factor signaling is required. Gradients of Wnts and bone morphogenic proteins (BMPs) have been found to be inversely related and influence proliferative capacity as cells migrate away from the crypt base^{36,37,49}. In contrast to Wnt signaling, BMP signaling restricts stemness and proliferation. Binding of BMPs to their receptors leads to phosphorylation and activation of receptor-regulated SMAD family members (SMAD) 1, 5, and 8 (*Smad1*, *Smad5*, and *Smad8*) to form complexes with *Smad4* and regulate gene expression in the nucleus⁵⁰. In the intestine, BMP2 and BMP4 is secreted by intra-villus and inter-crypt mesenchymal cells,⁵¹ whereas the BMP antagonists noggin (*Nog*) and gremlin 1 (*Grem1*) are mainly expressed in mesenchymal cells beneath the crypt⁴⁹, resulting in a gradient of BMP activity along the crypt-villus axis. BMP signaling is required for intestinal homeostasis, as BMP inhibition causes abnormal villus morphogenesis, epithelial hyperplasia, and ectopic crypt formation⁵². Recently, BMP has been shown to limit ISC self-renewal and decrease expression of the ISC genes *Lgr5*, *Olfm4*, and *Ascl2* via Smad⁵³. In conjunction with ISC biomarker identification, the identification of epithelial and mesenchymal growth

factors required for ISC maintenance have allowed for the development of *in vitro* ISC culture methods.

Studying Intestinal Stem Cells in vitro: Organoid Culture System

The ability to culture ISCs has only been developed in the last ten years after the isolation of single LGR5+ ISCs. When grown in an ECM-rich culture substrate, single ISCs and crypts form into 3-dimensional structures⁵⁴. When initial culture conditions were established in 2009, resulting self-organizing crypt-villus structures (or “mini-guts”) that formed from single Lgr5+ ISCs were termed “organoids”^{32,54}. Additionally, 3-dimensional structures resulting from human pluripotent ISCs that are differentiated into intestinal tissue *in vitro* were also termed “organoids”⁵⁵. However, debate has been had on the proper nomenclature of these *in vitro* structures. In 2012, members of the NIH Intestinal Stem Cell Consortium proposed a systematic nomenclature to more specifically describe the 3-dimensional structures based on source tissue and cell types present⁵⁶. Multi-lobed structures that develop from isolated intestinal epithelial cells are referred to as “enteroids” (isolated from the small intestine) or “colonoids” (isolated from the colon), whereas an the term “organoid” refers to a multicellular cluster of epithelial and mesenchymal elements⁵⁶. Both “organoids” and “enteroids” are regularly used to define 3-dimensional structures that arise from isolated epithelial cells from the small intestine; therefore, they will here on be referred to as “organoids.”

Growth factors that recapitulate the factors observed in the ISC niche *in vivo* are required for ISC maintenance and expansion *in vitro*. When culturing isolated crypts that contain ISCs and Paneth cells (Figure 1.2A), exogenous Wnt is not required since it is

supplied by Paneth cells. However, EGF, R-Spondin, and Noggin are required for ISC survival³². EGF drives Mitogen-activated protein kinases (MAPK) signaling to inhibit epithelial cell shedding and extrusion^{57,58}, R-Spondin, a Wnt agonist, further activates the Wnt pathway⁵⁹, and Noggin inhibits BMP signaling allowing ISCs to remain undifferentiated^{51,52}. When single ISCs are cultured, no source of Wnt is present; therefore, exogenous Wnt is also needed to support isolated ISC growth. Recent creation of cell lines that create R-spondin, Wnt, and Noggin conditioned media have reduced the cost of growth factors for *in vitro* organoid cultures⁶⁰.

Manipulation of key signaling pathways has been shown to increase the survival of ISCs *in vitro*. Addition of CHIR99021, a glycogen synthase kinase 3 β inhibitor that enhances Wnt signaling⁶¹, promotes proliferation of ISCs⁶². Furthermore, addition of Valproic acid, a histone deacetylase inhibitor that activates Notch signaling^{63,64}, and CHIR99021 resulted in nearly homogenous cultures of ISCs in organoids⁶². Importantly, a 100-fold increase was observed in the survival of single ISCs when cultured with CHIR99021 and Valproic acid⁶², suggesting the need for niche cell-derived growth factors for enhanced ISC survival *in vitro*.

An essential requirement for the survival of ISCs *ex vivo* and culture of ISCs *in vitro* is an ECM substrate due to the requirement of integrin binding⁶⁵. Traditionally, ISCs have been grown in either Type I Collagen⁶⁶ or Matrigel³², a basement membrane preparation from an Engelbreth-Holm-Swarm mouse sarcoma. Recent development of tunable synthetic matrices has allowed for the use of defined ECM to finely regulate the ISC expansion and organoid formation⁶⁷. Enrichment of hydrogels supplemented with key ECM components found within the ISC niche *in vivo*, including fibronectin, laminin,

collagen IV, hyaluronic acid and perlecan, have also been shown to further enhance ISC survival and proliferation⁶⁷.

Organoids accurately recapitulate the architecture of native intestine with proliferative crypt-like buds and zones of differentiated cells (Figure 1.2B)⁶⁸. The crypt-like buds contain Lgr5+ ISCs intercalated among Paneth cells located at the bud base. ISCs give rise to TA progenitors that differentiate as they migrate out of the bud into an inter-villus domain where they form all of the cell types found *in vivo*³². Differentiated cells ultimately undergo anoikis and slough off into the organoid lumen, mimicking the physiological turnover of the epithelium *in vivo*. Organoids grow to have many buds, and thus expanding the number of ISCs per organoid. Organoids can also be dissociated into crypt bud units or to single cells and expanded indefinitely *in vitro*³². Although culture conditions are able to recapitulate the essential factors to support ISCs, the niche environment that provides these factors *in vivo* is dynamic depending on the physiologic state of the intestine.

Components of the Intestinal Stem Cell Niche

The ISC niche environment is made up of both cellular and non-cellular components (Figure 1.3). Cells in the niche are in close proximity to ISCs and include epithelial Paneth cells that are intercalated between ISCs, subepithelial pericryptal myofibroblasts that encapsule the crypt, and immune cell types that vary depending on the state of intestinal inflammation. All of these cells interact with and are supported by the non-cellular extracellular matrix (ECM), which provides a biological scaffold for cellular interaction.

The two main cellular components of the niche, the Paneth cells and the pericryptal myofibroblasts, secrete various mitogens and morphogens, including Wnts, the Notch ligand Delta-like 1 (DLL1), EGF, and Noggin, that regulate ISC survival and function⁷. Genetic ablation of Paneth cells does not critically impair epithelial function in the mouse intestine suggesting a functional overlap of cellular roles within the niche^{69,70}, with the likely candidate being the subepithelial myofibroblast. A heterogeneous population of myofibroblasts exists throughout the lamina propria⁷¹; however, pericryptal myofibroblasts, which are intimately associated with the ISCs *in vivo* secrete Wnt proteins^{72,73}, supplying a non-epithelial source of Wnt to drive epithelial regeneration. When ISCs are cultured *in vitro*, co-culture with subepithelial myofibroblasts enhances ISC survival and organoid size and removes the need for exogenous Wnt agonists⁷³. Myofibroblasts have also been found to secrete other cytokines, growth factors, and essential ECM proteins for ISC survival and maintenance⁷¹.

Supporting the ISC niche, a physical scaffold of ECM is in contact with all the cellular components (Figure 1.3)⁷⁴. The ECM is secreted by resident niche cells to provide support for and influence neighboring cells⁷⁵. Both epithelial and mesenchymal compartments contribute to ECM in the niche⁷⁶; however, specific ECM contributions of individual cell types have not been determined. The basolateral membrane of epithelial cells lies directly on the basement membrane, a thin sheet of ECM composed mostly of laminins and collagen IV and interacts with epithelial cells through integrin binding⁷⁴. This basement membrane also physically separates the epithelium from pericryptal myofibroblasts and other cells residing in the lamina propria⁷⁴. ECM is also found throughout the lamina propria supporting other cell types including fibroblasts, blood

vessels, and neurons. In general, this more diffuse ECM is composed of an intertwining mix of glycosaminoglycans and proteins, including collagens, laminins, elastin, and fibronectin, found in 3-dimensional patterns and gradients⁷⁵. While studies in other tissues, like mammary gland⁷⁷ and bladder⁷⁸, establish a role for ECM in stem cell niches, the influence of ECM on ISCs is still being defined².

ECM can impact cell behavior by modulating signaling pathways that control cell proliferation, growth, and death by serving as a substrate to physically anchor cells, providing biomechanical stiffness, and creating reservoirs of soluble factors^{75,79}. Anchorage to ECM is essential for ISC survival, as intestinal epithelial cells undergo apoptosis without an ECM substrate for epithelial beta 1 integrins to interact with⁶⁵. Stiffness of the surrounding ECM has also been found to direct ISC fate, with a high matrix stiffness of a synthetic scaffold enhancing ISC expansion and a low matrix stiffness supporting ISC differentiation⁶⁷.

The role of ECM as a reservoir for soluble factors has not been studied in the context of the intestinal crypt; however, gradients of growth factors, including Wnt and BMP, exist along the crypt-villus axis. Heparan sulfate proteoglycans, found on many ECM proteins, can help to form gradients by stabilizing growth factors such as Wnt and preventing protein aggregation^{80,81}. In the intestine, mice broadly lacking heparan sulfate proteoglycans have reduced expression of Wnt target genes during crypt regeneration after irradiation⁸⁰. ECM proteins with attached heparin sulfate proteoglycans, such as Collagen XVIII (Col18a1), are found in the basement membrane in the ISC niche and potentially play a critical a role in niche dynamics⁸². Other basement membrane proteins,

including laminins, are regionally distributed along the crypt villus axis⁷⁴, suggesting a relationship between regional ECM composition and epithelial cell function.

Immune Cell Components of the Small Intestine

The cellular and ECM components of the ISC niche remain relatively constant throughout the homeostatic life of the animal; however, immune system components dynamically interact with niche cells depending on tissue damage and inflammation^{83,84}. The immune system in the intestine is the largest compartment of the immune system in the body, as it is constantly exposed to antigens from the diet and microbiota found in the intestinal lumen¹⁰. Regional differences in intestinal immunity are prominent, as the luminal microbial load and the amount immune cell tissue increases from proximal to distal small intestine¹⁰. The majority of immune cells are located in the lamina propria either individually scattered or in organized lymphoid structures collectively termed gut-associated lymphoid tissue (GALT)¹⁰.

Two types of GALT exist: larger Peyer's patches and smaller lymphoid aggregates collectively termed solitary isolated lymphoid tissue (SILTs)¹⁰. Peyer's patches are large aggregates of B cell lymphoid cells that are macroscopic⁸⁵. B cells present antigens and secrete antibodies and cytokines⁸⁶. Peyer's patches have germinal centers, which contain active B cells, suggesting continual immune stimulation by luminal antigens^{10,85}. Intercalated among B cell aggregates are smaller areas of T cells¹⁰. T cells can bind to antigen-presenting B cells to cause further antibody secretion, as well as to other antigen-presenting cells, including dendritic cells and macrophages, and secrete cytokines to cause inflammation⁸⁷. Peyer's patches increase in size, density and number from the

duodenum to the ileum as the microbial burden in the intestinal lumen increases, with approximately 100-200 in humans⁸⁸ and 6-12 in mice⁸⁵. Like Peyer's patches, SILTs contain a germinal center and B cells, but no clear T cell zone⁸⁹ and are smaller¹⁰. Throughout the small intestine, mice have up to 1,500 SILTs and humans have more than 30,000 SILTs^{90,91}. SILTs include cryptopatches and isolated lymphoid follicles (ILFs) that are found more interspersed throughout the lamina propria¹⁰. These aggregates range in size dependent upon their maturity, as cryptopatches mature into ILFs with age and bacterial burden⁹⁰. The human ileum has the highest concentration of ILFs, with one ILF for every 28 villi, due to increased microbial presence⁹².

In addition to aggregates of immune cells, individual T and B cells are found throughout the lamina propria and have been extensively researched due to their definitive roles in both intestinal homeostasis and disease¹⁰. Innate lymphoid cells (ILCs) are a relatively newly identified subset of immune cells that are unique in they lack antigen-specific receptors, unlike the T and B cells, and are thought to play a large role in the immune defense at mucosal surfaces⁹³. ILCs can be categorized based on their cytokine production into three main groups, termed ILC1, ILC2 and ILC3s. Group 1 ILCs are primarily involved in intracellular pathogens, viruses and tumors, Group 2 ILCs are primarily involved in protecting against helminth invasion, wound healing, and allergic responses, and Group 3 ILCs are primarily involved in resistance to bacterial and fungal infections^{93,94}. Importantly, ILCs participate in cytokine and chemokine signaling, and can impact epithelial cells to promote regeneration and repair^{95,96}.

Although the intestinal immune system is vast, the intestinal epithelium has protective abilities that allow it to act as the primary line of defense against luminal

microbiota before antigens interact with underlying immune cells. Goblet cells secrete mucins to form a strong mucus barrier extending 150 μ M above the epithelium, with a loose outer layer to immobilize bacteria and a firm inner layer devoid of bacteria to protect the epithelium⁹⁷. Paneth cells can directly sense microbiota and regulate production of antimicrobials and defensins⁹⁸. Additionally, epithelial cells themselves can secrete pro-inflammatory cytokines to elicit an immune response⁹⁹. Although these defenses limit barrier breaching by luminal bacteria and pathogens, invasion does occur and subsequently faces both a strong adaptive and innate immune response from the intestine¹⁰. Immune sensors, including dendritic cells and macrophages, respond to broad stimuli found in the intestinal lumen. Dendritic cells, found mostly in SILT, can directly sense intestinal contents by extending their dendritic processes into the intestinal lumen¹⁰⁰. Dendritic cells and macrophages in the lamina propria respond to intestinal antigens by activating T cells and promoting activation of other lymphoid cells^{101,102}. Depending upon the antigen sensed, dendritic cells and macrophages can also secrete cytokines to influence lymphoid and epithelial cell responses^{103,104}. Failure of the immune response towards invading bacteria and pathogens can result in chronic inflammation and intestinal disorders and diseases, including malabsorption, enteritis, diarrhea, inflammatory bowel disease, and cancer.

Intestinal Mucosal Response to Inflammation and Healing

Chronic inflammation of the intestine can result in loss of the epithelium and impaired epithelial regeneration, producing painful lesions that are unable resolve. An impaired epithelial barrier allows for the constant infiltration of luminal bacteria and pathogens into the lamina propria, resulting in the inability for the intestine to fully heal.

Inflammatory bowel disease (IBD) is a chronic inflammatory disorder of the intestine that affects over 1 million patients in the United States and recent epidemiologic studies suggest the incidence is expected to exponentially increase over the next 10 years¹⁰⁵. IBD is characterized into two main types: 1. Crohn's disease, which can affect any part of the gastrointestinal tract in patches and extend throughout all intestinal layers, and 2. Ulcerative colitis, which only affects the innermost layer of colon and rectum in continuous fashion⁸³. The mechanisms of IBD etiology remain largely unknown; however, leading hypotheses suggest that disease results from a dynamic mix of genetic, immunological, and genetic risk factors¹⁰⁶. For the purpose of this dissertation that concentrates on the small intestine, Crohn's disease will be the focus from here on as 65% of Crohn's disease patients have ileal involvement¹⁰⁷.

Crohn's disease features an exaggerated immune response, impaired barrier function, and progressive microbial product invasion^{107,108}. These factors fuel chronic inflammation, which leads to lifelong disease even with therapy. However, the natural course of Crohn's disease has unpredictable periods of remission, where disease symptoms are minimal, and relapse (or "flares"), where inflammation and disease symptoms are present¹⁰⁹. Overall, 20% of Crohn's disease patients have relapses of disease every year and 67% of patients have relapses within the first eight years post-diagnosis¹¹⁰. The damage and repair that results from cycles of relapse and remission make it challenging for the epithelium to regenerate and allow the wound to completely heal.

Epithelial response to damage is a two-step process. First, during the repair process after injury, the epithelium adjacent to the injury undergoes restitution, where

epithelial cells migrate over the damaged area to reconstitute the epithelial barrier¹¹¹. This redistribution of cells is rapid, does not require epithelial proliferation, and is regulated by cytokines¹¹². After epithelial restitution, epithelial cells begin to proliferate to increase the pool of epithelial cells that can reconstitute the epithelial barrier¹¹¹. During this phase, crypts become elongated as more undifferentiated cells proliferate to increase the total epithelial cell number^{111,113}. Additionally, crypt fission, or the division of one crypt into two crypts, may occur to also increase the available pool of proliferating cells¹¹³. Finally, differentiation of epithelial cells occurs to re-form the epithelium and create all of the differentiated cell lineages to reconstitute the homeostatic epithelial barrier¹¹¹. A prognostic factor of long-term IBD remission is mucosal healing, as compared to improvement in clinical symptoms^{109,114}, suggesting that complete mucosal healing or remission is the goal for IBD treatment. This goal of remission is not trivial as there are many components of the mucosa that interact in concert to maintain mucosal integrity.

Intestinal damage in Crohn's disease is more than just epithelial damage and can be present in subepithelial tissue. In inflamed lesions, local immune cells secrete serine proteases and matrix metalloproteases to degrade ECM and allow for the influx of infiltrating immune cells and myofibroblasts¹¹⁵. However, when the inflammation subsides, the ECM and sub-epithelial tissue need to undergo wound healing to create a new environment for epithelial proliferation and differentiation. During the initial phases of wound healing and epithelial restitution, myofibroblasts migrate to the site of the lesion and proliferate by growth factors and cytokines secreted from platelets, inflammatory cells, and endothelium¹¹⁶. Fibroblasts and myofibroblasts then deposit ECM, mainly collagen and fibronectin. Depending on how large the wound is, myofibroblasts also

contract the wound to limit the area the epithelium has to cover¹¹⁵. As repair continues, neovascularization occurs, more ECM is synthesized, and the number of recruited immune and mesenchymal cells diminishes¹¹⁶. Finally, remodeling of the ECM is critical to support appropriate angiogenesis, innervation, immune cell response, and epithelial proliferation¹¹⁷.

Healing of the epithelium to restore barrier function is of utmost importance to limit microbial product invasion and restore the homeostatic immune response. In addition, epithelial goblet and Paneth cells are required to re-create the epithelial barrier¹¹⁸. Although it is known that ISCs are integral for damage-induced intestinal regeneration^{28,119}, the mechanisms that regulate ISC function and induce epithelial regeneration are poorly understood. It has recently been shown that Interleukin-22 (IL22), a cytokine that is upregulated in IBD, promotes proliferation and expansion of ISCs in an *in vitro* organoid model as well as in mouse models of graft-versus-host disease and irradiation^{120,121}. Eventual re-establishment of the crypt-villus architecture and proliferative cell gradient is also essential, as the physical crypt structure protects proliferating cells from microbial metabolites. For example, a microbial metabolite screen revealed that butyrate, a bacterial metabolite that is only exposed to ISCs and TA progenitors during injury, suppresses epithelial cell proliferation¹²².

In both homeostatic and regenerative states of the small intestine, extrinsic components of the ISC niche are integral for ISC survival and proliferation. This dissertation explores the role of two integral extrinsic components, the immune cells and the ECM, on their influence of ISC survival, proliferation and differentiation. First, the influence of Interleukin 22, which is upregulated in patients with IBD and secreted from

immune cells in close proximity to ISCs, is investigated using an *in vitro* model of ileal ISCs (Chapter 2). Methods developed and utilized for assessing intestinal epithelial differentiation and function in response to inflammation using the *in vitro* organoid culture model are outlined in a book chapter (Appendix A). Next, the influence of intestinal ECM is broadly investigated by creating acellular, porcine small intestinal ECM scaffolds and determining its capacity to support mouse ISCs (Chapter 3). Further understanding of how extrinsic factors, and particularly those in close contact with ISCs, can influence ISC function is of central importance when developing therapies for intestinal disease that affect more than just the ISCs themselves. Furthermore, understanding the dynamic communication and interaction between the ISCs and the supportive niche components will also establish key components needed for further developing intestinal tissue engineering strategies.

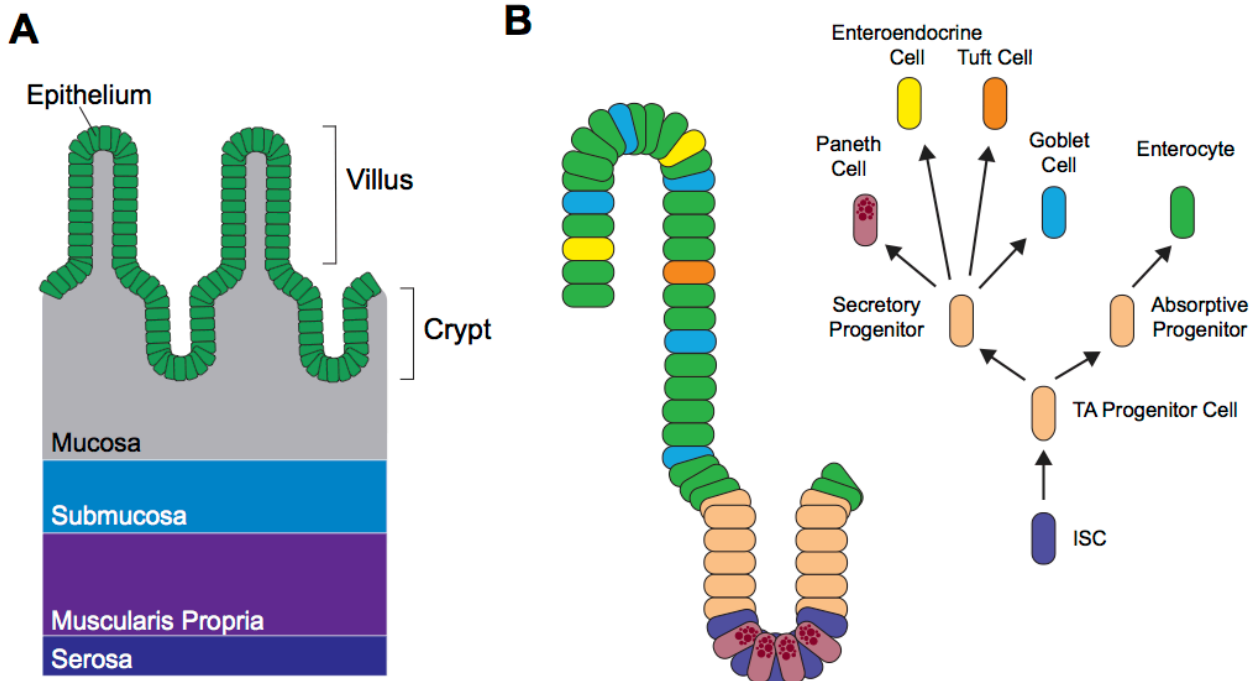


Figure 1.1. Small intestinal anatomy and epithelial cell lineages. (A) The small intestine has four main layers, with the innermost mucosa lined with a single layer of epithelial cells and organized into a villus-crypt architecture. (B) The small intestinal epithelium contains undifferentiated cells in the crypt, including ISCs and TA progenitor cells. TA progenitor cells differentiate into either absorptive or secretory cell types which form the five major differentiated cell types.

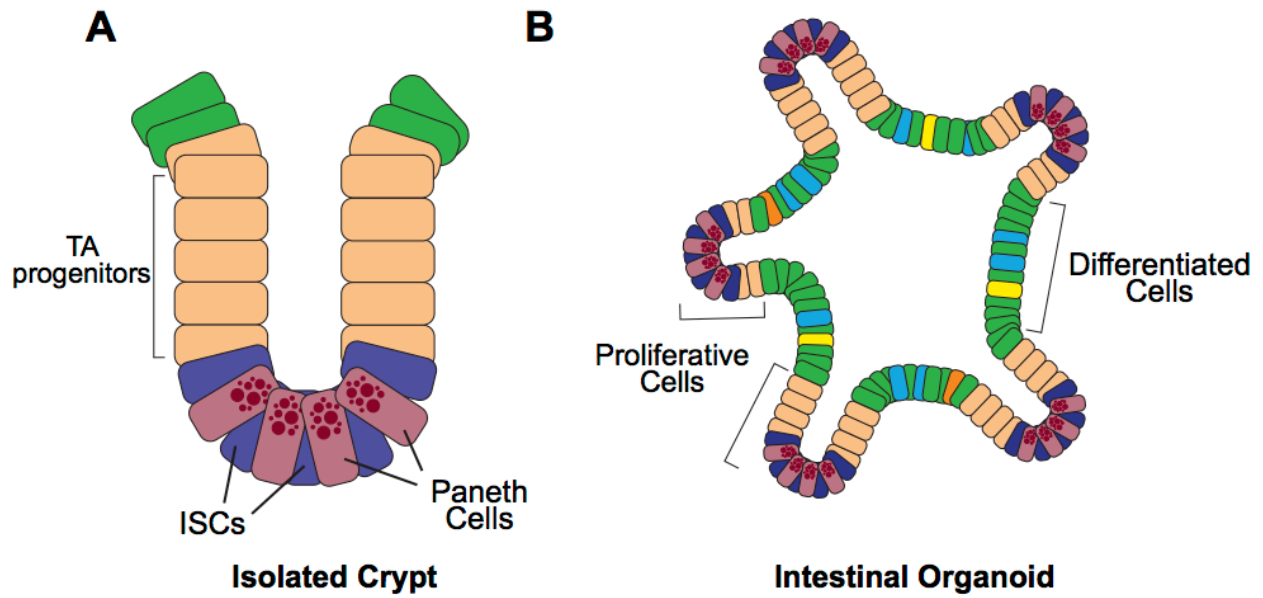


Figure 1.2. ISCs form organoids *in vitro*. (A) Isolated crypts contain ISCs, Paneth cells, and undifferentiated TA progenitor cells. (B) When cultured *in vitro*, isolated crypts and single ISCs form organoids that recapitulate the *in vivo* architecture zones of differentiated and proliferative cells.

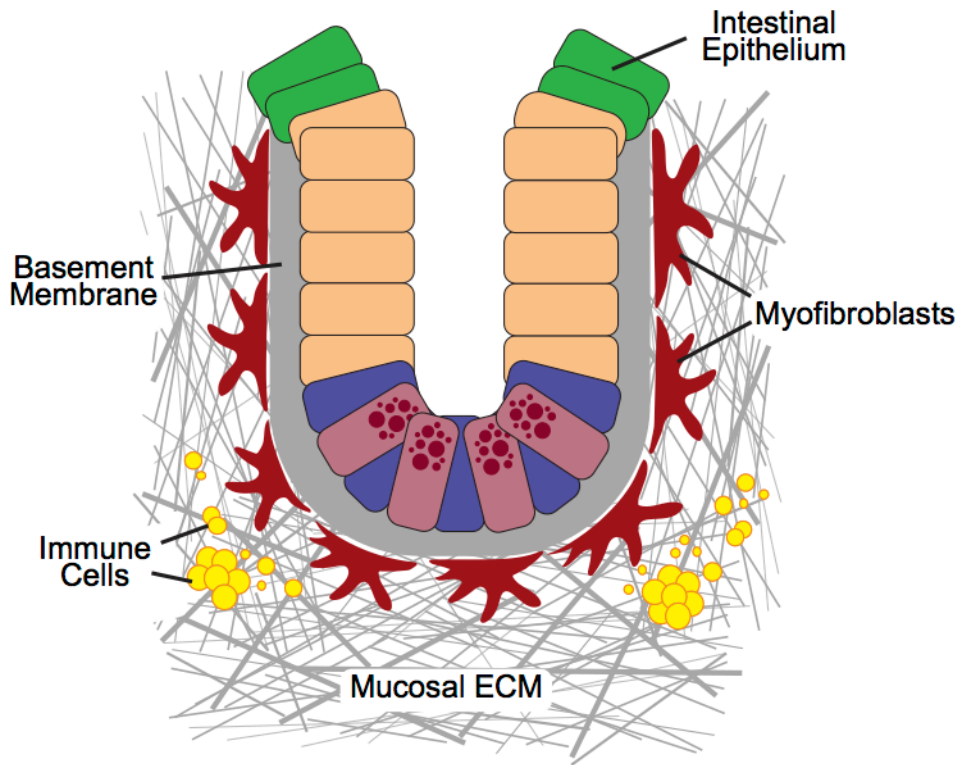


Figure 1.3. The intestinal stem cell niche. *In vivo*, the intestinal epithelium resides on a basement membrane that creates a physical barrier between the epithelium and the underlying lamina propria. The ISC niche is comprised of Paneth cells in the epithelium and myofibroblasts and immune cells in the lamina propria, which are all in close proximity to ISCs.

CHAPTER 2: ELEVATED IL22 INHIBITS EPITHELIAL STEM CELL EXPANSION IN AN ILEAL ORGANOID MODEL^{1,2}

Overview

Background & Aims: Crohn's disease (CD) is an inflammatory bowel disease that affects the ileum and is associated with elevated cytokines. Though Interleukins (IL) IL6, IL17, IL21 and IL22 are elevated in CD and associated with disrupted epithelial regeneration, little is known about their effects on the intestinal stem cells (ISCs) that mediate tissue repair. We hypothesized ILs may target ISCs and reduce ISC-driven epithelial renewal. **Methods:** A screen of IL6, IL17, IL21 or IL22 was performed on ileal mouse organoids. Computational modeling was used to predict microenvironment cytokine concentrations. Organoid size, survival, proliferation, and differentiation were characterized by morphometrics, qRT-PCR, and immunostaining on whole organoids or isolated ISCs. ISC function was assayed using serial passaging to single cells followed by organoid quantification. Single-cell RNAseq was used to assess *Il22ra1* expression patterns in ISCs and Transit-Amplifying (TA) progenitors. An IL22-transgenic mouse was used to confirm the impact of elevated IL22 levels on proliferative cells *in vivo*. **Results:**

¹This chapter has been resubmitted to *Cellular and Molecular Gastroenterology and Hepatology*.

²Full list of contributing authors: Bailey Zwarycz, Adam D. Gracz, Kristina R. Rivera, Ian A. Williamson, Leigh A. Samsa, Josh Starmer, Michael A. Daniele, Luisa Salter-Sid, Qihong Zhao, Scott T. Magness

IL22 demonstrated decreased ileal organoid survival, however, resistant organoids grew larger and exhibited increased proliferation over controls. *Il22ra1* was only expressed on a subset of ISCs and TA progenitors. IL22-treated ISCs did not exhibit appreciable differentiation defects, but ISC biomarker expression and ISC self-renewal-associated pathway activity was reduced by IL22 and was accompanied by an inhibition of ISC expansion. *In vivo*, chronically elevated IL22 levels, similar to predicted microenvironment levels, exhibited increases in proliferative cells in the TA progenitor zone with no increase in ISCs. **Conclusions:** Elevated IL22 limits ISC expansion in favor of increased TA progenitor cell expansion.

Introduction

Inflammatory bowel disease (IBD) features exaggerated immune responses that can affect the small intestine (Crohn's Disease) or colon (Ulcerative Colitis)^{123,124}. Early initiation of inflammation is complex and influenced by a number of contributing factors such as underlying genetics and composition of the gut microbiota; but ultimately, it is chronic inflammation-driven breaches in the epithelial barrier that fuel the continuous cycle of inflammation and impaired epithelial regeneration that culminates in clinical sequelae, such as ulcerated regions of submucosa, pain, and bleeding^{1,3}. Intestinal epithelial stem cells (ISCs) typically regenerate the epithelial lining in a tightly coordinated balance between ISC self-renewal and differentiation into transit-amplifying (TA) progenitor cells and their post-mitotic descendants. How the inflammatory microenvironment in the ISC zone impacts this stereotypical process is poorly understood.

Local immune cells in the gut secrete a wide array of cytokines that mediate initiation, progression, and resolution of inflammation in the small intestine and colon. During an inflammatory response, T cells and innate lymphoid cells (ILCs) secrete a subset of the cytokines called interleukins (ILs) into the ISC microenvironment¹¹². Dysregulated cytokine responses are associated with IBD and are often characterized by chronically elevated serum levels of IL6, IL17, IL21 and IL22 and their associated signaling pathways¹¹². For instance, in healthy individuals serum IL22 levels are reported at ~2pg/mL, while in Crohn's Disease patients those levels are ~12-times higher at ~24 pg/mL¹²⁵. Importantly, these values represent systemic IL22 levels, which may not accurately reflect actual concentrations and the phenotypic consequences close to the mucosal inflammation site. This concept is particularly highlighted in the case of IL23, which at low concentrations promotes proliferation of human lung cancer cells, but inhibits proliferation and at high concentrations¹²⁶. In the case of IBD, it is logical that IL concentrations would be considerably higher in the mucosal microenvironment, where the cytokine is produced by ILCs, and systemic levels would be effectively reduced by systemic diffusion and first pass removal by the liver. While empirical measurements of IL levels in the microenvironment are currently beyond the limits of technology, prediction of microenvironment levels may guide more physiologically relevant dose-response experiments *in vitro* and provide more accurate interpretations related to the mechanisms of action of ILs in the microenvironment.

In this study¹²⁰, we use an ileal organoid model to screen the impact that a subset of IBD-related ILs have on ISCs. Like a recent study, our screen revealed that IL22 has a profound influence on organoid size and survival in a concentration dependent manner,

and confirms that IL22 regulates epithelial proliferation and differentiation. Our study extends this prior work to model and investigate the role of IL22 in the ISC microenvironment, and importantly, draws a distinction between systemic levels of IL22 reported in serum from IBD patients and predicted IL22 concentrations in the ISC microenvironment. Our study offers an alternative interpretation as to how elevated levels of IL22 in the microenvironment affect proliferative epithelial populations in the crypt.

Results

Screening IBD-related cytokines using an ileal organoid model.

Crohn's disease, an IBD, is typically restricted to the ileum in the small intestine. We sought to test the impact of a number of IBD-related cytokines specifically on the ileal epithelium and observe the effects on ISCs *in vitro*. To do this, we used an ileal organoid model in which organoids were derived specifically from the terminal mouse ileum, a region that is involved in a majority of patients with Crohn's disease. Intestinal organoids, also known as enteroids⁵⁶, are spherical, ISC-driven epithelial structures that form *in vitro* when single ISCs or crypts are suspended in extracellular matrix and supplemented with defined growth factors that mimic the *in vivo* stem cell niche⁵⁴. Organoids are comprised of ISCs that differentiate into all the epithelial absorptive and secretory lineages found *in vivo* and self-pattern with crypt buds containing ISCs that differentiate and migrate into intervening villus-like zones⁵⁴. Because of these physiologically relevant properties and functions, organoids represent an excellent model to study the dynamics of ISC-driven regeneration *in vitro*.

Organoids can be used as a rapid and easy screen to visually detect changes in properties that are regulated by ISCs, including growth and longterm self-renewal. We used this ileal organoid model system to test whether a subset of Crohn's disease-related ILs would decrease ISC activity using organoid survival as a proxy for ISC survival and organoid size as a measure of ISC proliferation. IL16, IL1 β , and TNF α levels in patients with IBD average about 100 pM (1,500 pg/mL), a concentration that was used to screen for IL effects on the ileal organoid epithelium¹²⁷. Ileal crypts were allowed to establish *in vitro* for 1 day, then supplemented with 100 pM IL6, IL17, IL21, or IL22 for 6 days (Figure 1A). While there was no significant size increase caused by IL6, IL17, and IL21, organoids treated with 100 pM IL22 grew approximately 3 times larger (Figure 1B,C). IL6, IL17, and IL21 had no significant effect on organoid survival, but IL22 caused an ~72% decrease in organoid survival compared to controls (Figure 1D). In this case, organoid survival is defined by organoid forming efficiency (OFE), which is number of organoids that derive from a single ileal crypt. Although there may have been more subtle effects of IL6, IL17, and IL21 on ISCs, we focused on investigating how IL22 affected ISC self-renewal and differentiation based on the overt organoid growth and death phenotype observed in the screen.

IL22 imparts concentration-dependent effects on ileal organoids

IL22-dependent changes in organoid size and survival have been reported in organoids derived from a mixture of crypts isolated from full-length intestine¹²⁰. It remains to be determined whether IL22 affects ileal specific epithelium in the same way. A dose-response experiment demonstrated that 20 pM of IL22 was the lowest dose that caused

a significant increase in organoid size (Figure 1E). Organoid size continued to increase in a dose-dependent manner at each tested concentration up to 500pM (Figure 1E). Interestingly, while ileal organoid size increased as a function of IL22 concentrations, there was a decrease in OFE from crypts cultured in increasing concentrations of IL22 (up to 500pM) (Figure 1E).

Next we tested whether a reduction in OFE persisted over time. OFE was quantified in ileal organoid cultures exposed to two different IL22 doses: 60pM, a lower dose (60 pM) reported to cause increased organoid size but no decrease in OFE¹²⁰, and 500 pM, a higher dose demonstrated to cause both increased organoid size and decreased OFE (Figure 1F). There was a clear decrease in the ability of crypts to generate organoids at both concentrations and this trend persisted over the two-week time course (Figure 1F). To determine whether these effects were IL22 dependent, ileal organoids were treated with the higher IL22 concentration (500 pM) in the presence or absence of an IL22-neutralizing antibody (Figure 1G,H). The neutralizing antibody blocked IL22-dependent phosphorylation of STAT3¹²⁸, a key downstream signaling mediator of IL22 (Figure 1G). Importantly, the IL22 neutralizing antibody blocked size increases in IL22-treated ileal organoids demonstrating the phenotype was IL22-dependent (Figure 1H). While one study that lower levels of IL22 does not impart a negative effect on organoids derived from a mixture of crypts derived from full-length intestine¹²⁰, our results demonstrate a significant decrease in ileal OFE at both concentrations. Interestingly, while IL22 impaired organoid formation from some ileal crypts, the crypts that survived grew bigger and developed faster than untreated controls crypts.

IL22-receptor is only expressed in subsets of intestinal epithelial ISCs and TA progenitors

The heterogeneous response of some crypts to elevated IL22 levels suggested ISCs in the base of each crypt might have differential responses to elevated IL22. IL22 signals through the receptor IL22RA1 and activates STAT3 signaling¹²⁸, so we reasoned that ISCs might have variable responses to IL22 based on differential expression of its cognate receptor. To test this, the ileal epithelium was dissociated to single cells and populations were differentially FACS-enriched for ISCs, TA progenitors, enteroendocrine/tuft cells, Paneth cells, and Goblet/absorptive cells based on established methods using a Sox9EGFP mouse model⁴¹. Across these populations, *Il22ra1* mRNA was detected at the highest levels in the TA progenitor cells, but was also detected in each of the other populations, albeit at significantly lower levels (Figure 2A). We next investigated *Il22ra1* mRNA expression at cellular resolution using single-cell RNA-sequencing. A previously published dataset that surveyed the full transcriptome of 1,522 single mouse small intestinal cells was interrogated to define the extent of *Il22ra1* expression heterogeneity different lineages (Figure 2B-E). Expression of *Il22ra1* mRNA was quantified in a binary 'on/off' manner for each ISC, progenitor, and differentiated cell population (Figure 2B). Expression of *Il22ra1* was observed only in subsets in each population, and moreover, in those cells that expressed *Il22ra1*, there was a broad range of expression levels (Figure 2C). A higher resolution view of just the ISC and TA progenitor cells further highlights the heterogeneous expression patterns of *Il22ra1* in these populations (Figure 2D,E). We did not observe distinct clustering of *Il22ra1*-positive or *Il22ra1*-negative cells in the t-SNE clustering analysis, suggesting

that while *Il22ra1* expression is heterogeneous, it does not identify discrete sub-populations of ISCs or TA progenitors based on this type of analysis (Figure 2C-E). These data suggest that during homeostasis, only a subset of ISCs and TA progenitor cells are receptive to IL22 stimulation.

To determine if the heterogeneous *Il22ra1* expression extended to the protein level, we immunostained ileal tissue sections to assess IL22RA1 localization, and quantified the number of IL22RA1-expressing cells by flow cytometry (Figure 2F,G). Immunostaining demonstrated broad expression of IL22RA1 in crypt-based epithelial cells with higher levels apparent in the TA progenitor zone¹²⁰ (Figure 2F). Flow cytometry confirmed at the protein level that only sub-populations of epithelial cells express the IL22 receptor (Figure 2G). We attempted to test functional differences between ILR22A1+ and ILR22A1- by FACS-isolation and OFE assays on single ISCs; however, all commercially available antibodies detect cytoplasmic epitopes and were not suitable for isolation of live cells. While technical limitations preclude testing functional differences in ILR22A1+ and ILR22A1- ISCs, the heterogeneous expression of IL22RA1 in ISC and TA progenitors suggest there are mechanistic differences that could impact ISC behavior during an inflammatory response *in vivo*.

Computational modeling predicts higher levels in the ISC microenvironment than in serum

A fundamental question in studies investigating the role of ILs in IBD pathogenesis is, what are the physiologically relevant IL concentrations that contribute to the disease? IL22 levels reported for IBD patients are based on peripheral blood serum levels¹²⁵, which

likely do not accurately reflect the IL22 levels at the site of secretion in the intestinal or colonic mucosa. Currently, there is no accurate method to measure absolute levels of IL22 in the ISC microenvironment, which we define as the distance of IL22-secreting lymphocytes (ILC3s) from the crypt base (~6-17 μm ; Figure 3A). Therefore, we used COMSOL Multiphysics[®] to computationally model and predict IL22 concentrations that ISCs might experience in their microenvironment during an inflammatory episode.

Empirically derived values for factors that could influence IL22 concentrations, such as IL22 secretion rates from ILC3s, distances of ILC3s to ISC, number of ILC3s in a lymphoid follicle, distance of lymphoid follicle to ISCs, and radius of ILC3s were applied to the model (Figure 3A). Previous work established that isolated and induced ILCs can secrete IL22 in culture¹²⁹, and from this study, we calculated that a single ILC can secrete IL22 at an average rate of 4 fg/hr. An estimated diffusion coefficient for IL22 was based on its molecular weight¹³⁰⁻¹³². IL22-secreting ILC3s express ROR γ t¹³³, which was used as marker to measure the distances of ILC3s to the ISCs in the base of the crypt. ILC3s are as close as 6 μm from the base of the crypt (Avg distance ~6.0 μm ; Figure 3A). ILC3s also exist in the mucosal microenvironment localized to innate lymphoid follicles¹⁰, which were measured to be as close as 17 μm from the crypt base (Avg distance ~17 μm ; Figure 3A). These data demonstrate that cells expressing IL22 can be in very close proximity (on the single cell diameter scale) to the ISC zone.

Using these parameters, we first asked how long it would take for a single ILC3 cell to secrete enough IL22 to achieve a concentration of 500 pM at the ISC zone (Figure 3B). The model predicts that IL22 can accumulate to 500 pM within a distance of 0-9 μm within 4 minutes (Figure 3B). In the setting of Crohn's disease and chronic inflammation,

IL22 is upregulated and an influx of IL22-secreting ILC3s is observed¹³⁴; therefore, it is expected that the single-ILC3 model is a conservative estimate and likely under-represents concentrations of IL22 in the inflammatory microenvironment. Since ILC3s also exist in innate lymphoid follicles¹⁰, we next modeled IL22 microenvironment concentrations up to 21 μm , which includes the average distance of a lymphoid follicle from the ISC zone (Figure 3C). We also used secretion values for 67 ILCs, which is the average number of ILC3s in a cross section of a lymphoid follicle (Figure 3A). While the model only takes into consideration the IL22 secretion from the number of ILC3s in a 2-dimensional space, the model effectively approximates the microenvironment concentrations in 3-dimensional space. Using the follicle model prediction, ISC cells in close proximity to the follicle (0-21 μm) would detect 500 pM IL22 within 11 seconds of initiation of secretion (Figure 3C). Although the IL22 concentrations are modeled in a closed system and the rates of IL22 removal and degradation are unknown, the computational models suggest the 500 pM IL22 concentration used in the ileal organoid model are not unreasonable to achieve in the ISC/ILC3 inflammatory microenvironment, therefore this IL22 concentration was used throughout the remainder of the study.

IL22 does not cause appreciable lineage bias of ISCs

While 500 pM of IL22 has a clear impact on ileal organoid survival and size, these metrics do not reflect IL22-dependent influences directly on ISC differentiation. Aberrant differentiation of ISCs caused by elevated levels of IL22 could explain a loss of ISC self-renewal and regenerative capacity of the gut epithelium in inflammatory conditions. We performed a study using isolated ISCs to test whether elevated IL22 influenced early

differentiation programs directly on ISCs. ISCs were FACS-isolated and incubated with 500 pM IL22 for 6 hours followed by gene expression analysis for lineage restricted biomarkers: absorptive enterocyte (*Sl*, *Sucrose Isomaltase*), Paneth (*Lyz2*, *Lysozyme2*), goblet, (*Muc2*, *Mucin2*), and enteroendocrine (*ChgA*, *Chromogranin A*) (Figure 4A). In these studies only lysozyme mRNA, which is associated with Paneth cell lineage, was significantly increased. To determine the impact of elevated IL22 on the tissue level, we tested ileal organoids treated with 500 pM IL22 for expression of all key genes that mark the main differentiated cell types. In this case, elevated IL22 concentrations led to reduced or unchanged levels of all genes except for the Paneth cell biomarker, *Lyz2* (Figure 4B). To determine whether this increase in lysozyme mRNA was associated with increased Paneth cells, IL22-treated ileal organoids were immunostained for Lysozyme and Paneth cell numbers were quantified. While there was a ~2.5-fold increase in intraluminal lysozyme staining, there was a slight reduction in the relative number Paneth cells positioned in the ileal organoid epithelial monolayer (Figure 4C,D). Together these data suggest that IL22 does not cause appreciable differentiation defects of ISCs, but promotes the production and secretion of lysozyme from existing Paneth cells.

IL22 causes a decrease in ISC biomarkers and pathways that maintain ISC self-renewal

We next questioned whether IL22 increased the proliferation and self-renewal properties of ISCs since ileal organoids demonstrated significantly increased size when treated with elevated IL22. Ileal organoids treated with 500 pM of IL22 demonstrated a significantly higher number of KI67+ cells in the epithelial monolayer (Figure 5A). We

evaluated the mRNA levels for ISC biomarkers *Lgr5* and *Olfm4*, and contrary to predictions, found these ISC biomarkers to be significantly down-regulated suggesting there was a decrease in ISC numbers (Figure 5B). Expression of key Wnt- and Notch-pathway genes, which support ISC survival, proliferation and self-renewal¹³⁵⁻¹³⁷, were significantly downregulated in response to IL22 (Figure 5C-D). While *Wnt3* and β -catenin (*Ctnnb1*), which tightly control ISC function and proliferative capacity, were not significantly changed in response to IL22, the Wnt responsive target *Axin2* was downregulated 2-fold in response to IL22 suggesting a reduction of ISC self-renewal pathway inputs (Figure 5C). The *Notch1* receptor ligands *Dll1* and *Dll4* and downstream target *Hes1* were downregulated following exposure to IL22 (Figure 5D); however, there was no significant change in *Atoh1* (Figure 5D), which is directly inhibited by Notch and required for secretory cell differentiation¹³⁸. This result is consistent with no substantial changes in secretory lineage allocation in organoids and single ISCs exposed to IL22. Overall, downregulation of ISCs biomarkers and signaling pathways that regulate and maintain functional ISCs suggests there are lower ISC numbers or impaired ISC self-renewal properties in ileal organoids exposed to elevated IL22.

IL22 limits ISC expansion

Since gene expression studies suggested IL22 caused a reduction in ISCs, we sought to test ISC functional properties when ISCs were exposed to elevated levels of IL22. Serial passaging is used extensively in the hematopoietic stem cell field to assay stem cell function¹³⁹, and here we used this strategy to assay ISC function in the presence of elevated IL22. *In vivo* studies strongly suggest that ISCs primarily divide symmetrically

to generate two ISCs, and thus are able to expand their numbers to maintain the proper balance of ISCs in the crypt base³. With this mechanism in mind, every passage of organoids to single cells should produce a clonal organoid derived from the number of ISCs found in the original organoid. During organoid ontogeny from a single ISC, ISCs undergo symmetric expansion to produce more ISCs/organoid; and conceptually, upon each passage the extent of the symmetric ISC expansion is measured by the increase in organoid numbers. Ileal organoids were allowed to establish in culture for 1 day, then were exposed to IL22 for 6 days followed by dissociation to single cells and re-plating (defined as passaging). Organoids were passaged 4 times over ~4 weeks. In untreated controls, organoid numbers increased with each passage, indicating symmetric division and expansion of ISCs (Figure 5E). By contrast, treatment with IL22 suppressed the ability for organoid numbers to increase with passage (Figure 5E). Although IL22 limited ISC expansion, it did not completely ablate ISCs, as a similar number of organoids were observed throughout all 4 passages in response to IL22. These data suggest that IL22 is not explicitly toxic to ISCs, but rather is limiting expansion by regulating symmetric division.

Elevated IL22 *in vivo* causes an increase in proliferative cells in the TA progenitor zone

While there is a significant increase in proliferating cells in ileal organoids treated with elevated levels of IL22, there was no increase in functional ISCs based on organoid passaging experiments. Based on this, we hypothesized that the increase in proliferating cells observed in IL22-treated organoids was due to an increase in TA progenitors, not

ISCs. We identified an IL22 transgenic mouse model (IL-22TG) that was used to study the role of IL22 in liver disease¹⁴⁰. These mice express high levels of IL22 from an albumin-promoter, and IL22 serum levels reach ~4-7 ng/ml, which is in the range of ~8 ng/ml IL22 used in our ileal organoid studies¹⁴⁰. Intestines from these mice were obtained and the number of proliferating cells, their location in the crypt, and the number of ISCs was quantified (Figure 6).

In the IL-22TG mice, the number of cells per crypt and crypt height increased (Figure 6A,B). The TA progenitor cell zone increased 2-fold (Figure 6C), and the number of KI67+ proliferating cells increased 1.4-fold (Figure 6D,E). To determine if this increase in proliferating cells was due to an increase in ISC numbers, intestinal sections were stained with the ISC marker OLFM4. No difference was observed in the number of OLFM4+ cells per crypt between control and IL-22TG mice (Figure 6F,G), suggesting that IL22 does not expand ISC numbers, but rather acts to expand the progenitor cell population.

Discussion

Defining how inflammation of the GI tract impairs ISC driven epithelial renewal could have profound impacts on understanding the mechanisms regulating initiation, progression, and resolution of IBD. Since inflammation-induced cytokines that mediate the immune response are found in close proximity to the ISC *niche*, we used an ileal organoid model to screen a subset of IBD-related interleukins for their impact on ISCs. The screen revealed that IL22 in particular decreased OFE, however, the organoids that survived were substantially larger and had more proliferating cells compared to controls.

These observations served as a foundation to test the hypothesis that IL22 was regulating ISC survival and proliferation.

The IL22-dependent increase in growth was observed at levels ~14 times those found in the serum of patients with IBD, but interestingly the reduced OFE was only observed at levels ~340 times those measured in serum¹²⁵. While the serum levels of cytokines are commonly used as a guide for 'physiologic levels', we questioned this assumption and reasoned that IL22 levels might be substantially higher in the ISC microenvironment. Supporting this concept, Crohn's disease patients have an influx of IL22-secreting ILC3 lymphocytes in inflamed lesions¹³⁴ and in colitis ILC3s increase IL22 production in response to inflammatory stimuli¹⁴¹. These studies suggest there could be much higher IL22 concentrations in the ISC *niche* compared to serum IL22 levels, which would likely be effectively reduced due to systemic dilution and first-pass liver effects. Direct measurement of IL22 in the ISC microenvironment is currently not technically possible; however, computational modeling of IL22 concentrations in the ISC *niche* indicated that IL22 could achieve the highest levels used in this study within seconds to minutes after an inflammatory stimulus. Together these findings indicated that pathophysiologic IL22 concentrations could be much higher at the site of secretion compared to those measured in the peripheral circulation. These results challenge conventional assumptions regarding the definition of 'physiologically relevant' levels based on serum cytokine concentrations and provide a method to predict microenvironment concentrations, which can guide experimental design for testing IL doses in organoid culture systems.

A recently study concluded that lower levels of IL22 promoted ISC mediated epithelial regeneration in a mouse model of graft-versus-host disease¹²⁰. Our study demonstrated that IL22 concentrations ~1.7 times higher inhibited ISC expansion in ileal organoids. Down-regulation of ISC-associated biomarkers and a decrease in ISC self-renewal pathway gene expression also supported the interpretation of an IL22-dependent loss of ISC expansion, which was functionally confirmed in organoid passaging experiments. Yet, surviving ileal organoids exhibited a seemingly contradictory, but clear, increase in organoid size and number of proliferating cells. In an attempt to reconcile the results, we explored whether high IL22 levels had a similar effect *in vivo*. Consistent with interpretations from ileal organoid passaging experiments, high levels of IL22 in an IL-22TG mouse showed no ISC expansion based on OLFM4 ISC biomarker expression. However, the mice demonstrated a substantial and significant increase in proliferating cells in the TA progenitor zone. Together our results suggest that high IL22 levels might selectively increase expansion of proliferative TA progenitor cells at the expense of ISCs expansion.

Serial organoid passaging assays, in which new organoids are clonally derived after passaging organoids to single cells, indicated there was no ISC expansion in the presence of high IL22 levels. These assays also demonstrated that the number of organoids remained constant over time and multiple passages, suggesting that ISC numbers were not reduced but remained constant. *In vivo* studies indicate that ISCs expand primarily by symmetric self-renewal³. In this case ISC commitment is driven not by asymmetric division dynamics, but rather by migration of ISCs out of a self-renewal *niche* supporting high Wnt- and Notch-signaling⁷. A potential explanation for an IL22-

dependent increase in proliferating cells with no increase in ISCs is that IL22 shifts the balance of symmetric self-renewal to asymmetric division where ISC division produces one ISC and one TA progenitor. In this case, a cellular mechanism would produce equivalent numbers of ISCs and TA progenitor cells after division. Our *in vitro* and *in vivo* results indicate that elevated IL22 levels primarily expand TA progenitor cells, which is a reasonable conclusion considering that the highest *Il22ra1* expression was found in TA progenitor cell population. Increasing the pool of cells that will soon become differentiated epithelium may be an IL22-dependent cellular mechanism for producing the epithelial tissue bulk necessary to maintain barrier function in the face of chronic inflammation.

Interestingly, inactivation of STAT3 in cochlear hair cell differentiation results in a shift from asymmetric to symmetric divisions of immature cells that give rise to hair cells, thus, activation of STAT3 signaling preserves the asymmetric division mode in this particular context¹⁴². In the intestinal epithelium, IL22 signals through its cognate receptor, IL22ra1, and activates STAT3 signaling¹²⁸. It is possible that in the context of ISCs, IL22 signals through STAT3 to promote asymmetric division of ISCs resulting in the loss of ISC expansion properties. We show that IL22ra1 is expressed in the majority of ISCs, however, there is a small subset of IL22RA1-negative ISCs (23%). This could produce a scenario where IL22ra1-negative ISCs regenerate the epithelium through symmetric self-renewal, while the IL22 receptor-positive ISCs would be influenced to undergo asymmetric division to increase the TA progenitor pool, and ultimately the number of differentiated epithelial cells. This mechanism is consistent with altered stem cell division observed in psoriasis, where IL22 levels are elevated¹⁴³, the percentage of stem cells decreases, and the TA progenitor cell compartment becomes enlarged¹⁴⁴. This would

also explain the increased TA progenitor cell zone in IL-22TG mice and mice injected with IL22 to enhance epithelial repair during graft-versus-host disease¹²⁰.

While IL22-induced epithelial repair was enhanced in mouse model of graft-versus-host disease¹²⁰, studies demonstrate that elevated levels of *IL22* mRNA in inflamed lesions of patients with Crohn's disease correlate with impaired regeneration^{145,146}. These reports indicate that IL22 alone is insufficient to resolve impaired epithelial renewal in chronic inflammatory conditions and may point to a more complex and deleterious role for high IL22 levels in IBD. High IL22 failed to support organoid development in ~43% of ileal crypts put into culture, possibly indicating that IL22-responsive ISCs in the crypt base become incompetent to drive ISC self-renewal, and thus organoid development. We attempted to test this hypothesis by FACS-isolation of IL22ra1-positive ISCs and single cell organoid assays, however, there are no commercially available antibodies that facilitate FACS-isolation of IL22RA1-expressing cells. Since elevated IL22 impairs ISC expansion in ileal organoids, chronically elevated IL22 may actually inhibit ISC-driven epithelial repair because of reduced expansion capabilities of ISCs in a high IL22 environment. This potential mechanism has important implications for establishing a role of IL22 in acute versus chronic inflammation, where IL22 in acute inflammation enhances epithelial repair and rapidly replaces lost tissue through expansion and differentiation of the TA progenitors, while in chronic inflammation epithelial repair is inhibited by the loss of ISC expansion and perhaps even loss of crypts due to IL22-induced commitment to TA progenitors over time. Since IL22 therapies have been proposed as a therapy to enhance epithelial repair of the intestinal epithelium¹⁴⁷, it is important to take the potentially negative IL22-dependent effects on ISC expansion under consideration.

Methods

Mice

All organoid experiments were conducted on C57Bl6 mice obtained from Jackson Laboratory (stock number: 000664). Sox9-EGFP mice, which were originally generated by the GENSAT Brain Atlas Project¹⁴⁸ and have been previously characterized^{41,149}, were maintained on an outbred C57Bl/6 background. All mice used in these studies were 8-12 weeks old. All animal use was reviewed and approved by the Institutional Animal Care and Use Committee (IACUC) of the University of North Carolina at Chapel Hill.

Crypt isolation, organoid culture and quantification

The distal 8cm of mouse small intestine (ileum) was isolated, fileted open and rinsed in ice cold DPBS. The intestine was placed in 3 mM EDTA in DPBS for 15 minutes at 4°C with gentle agitation, then villi were gently scraped off using a pipette tip. The intestine was cut into 2-3 cm pieces and placed into fresh 3 mM EDTA in DPBS with 10 mM Y27632 (Selleck Chemicals, Cat#S1049) for 30 minutes at 4°C with gentle agitation. Intestinal pieces were transferred to fresh DPBS with 10 μM Y27632 and shaken by hand for 3 minutes at 2 shakes/second to release crypts. Isolated crypts were filtered through 100 and 70 μm filters to remove villus fragments and rinsed once with DPBS. Approximately 100-200 crypts were plated per 10 uL of Growth Factor Reduced Corning Matrigel Matrix (Corning, Cat#354230), which was polymerized for 30 minutes at 37°C in a tissue culture incubator before addition of overlay media. Overlay media consisted of: Advanced DMEM (Gibco, Cat# 12634-028), 1X N2 (Gibco, Cat#17502-048), 1X B27 without Vitamin A (Gibco, Cat#16704-044), 1 mM HEPES (Gibco, Cat#15630-056), 1X

Glutamax (Gibco, Cat# 35050-079), 100 U/mL Penicillin/Streptomycin (Gibco, Cat#15140-122), 500 mM *N*-acetyl-cysteine (Sigma, Cat#A9165), 50 ng/mL recombinant murine EGF (Invitrogen, PMGG8043), 100 ng/mL recombinant murine Noggin (Peprotech, Cat#250-38), 250 µg/mL recombinant mouse R-spondin1 (R&D Systems, Cat#4645RS025/CF), and 10 µM Y-27632. Y-27632 was only present in the first 24-48 hours of cell culture and was not added to subsequent media changes. Organoids were allowed to establish in culture for 1 day before addition of IL6, IL17, IL21 or IL22 (R&D, Cat#'s 406-ML, 421-ML, 594-ML, 582-ML) to cultures. Media was then changed every 2 days after plating and cytokines were added to overlay media after each media change (Figure 1A). To determine organoid efficiency, the number of living organoids were manually counted on days 0 (before cytokine addition), 6, 9, 12 and 14 post-plating. To determine organoid area, 10+ organoids were chosen and imaged before cytokine addition on day 1 and stage positions were saved to image the same organoid on day 6. Organoids were randomly chosen throughout the culture simply based on organoid morphology (spherical shape with clearly defined borders) to determine that the organoid was alive and its proximity to other organoids as to be able to determine Day 6 individual organoid size. Organoid area was measured from images using Image J Software¹⁵⁰ and day 6 measurements were compared to day 0 to determine percent area increase.

For serial passaging, organoids were allowed to establish in culture for 1 day before addition of 60 or 500 pM IL22. Media was then changed every 2 days after plating and cytokines were added to overlay media after each media change. The number of living organoids was recorded before passage and each well of organoids was passaged every 6 days for 4 passages. To passage, organoids and Matrigel were scraped up in

250 μ L TrypLE Express (Gibco, Cat#12605-036) with 10 μ M Y-27632 and triturated with a p1000 pipette tip 75 times to dissociate Matrigel and organoids. Organoids were then transferred to a 1.7mL microcentrifuge tube containing 250uL TrypLE Express with 10 μ M Y-27632 and incubated at 37°C for 2.5 minutes. Cells were then triturated using a p1000 20 times to further dissociate Matrigel and organoids, then incubated at 37°C for another 2.5 minutes. Cells were then pelleted, re-suspended in appropriate amount of Matrigel for calculated passage ratio, and plated. Cells were re-plated at a similar density to previous passage. Matrigel was allowed to polymerize for 30 minutes at 37°C in a tissue culture incubator before overlay media and IL22 was added.

Western Blot

Organoids were rinsed three times with sterile DPBS. Cell Recovery Solution (Corning, Cat#354253) supplemented with 10 μ M Y-27632 was then added to each well and organoids and Matrigel were gently scraped from bottom of tissue culture plate. Organoids were incubated with end-over-end rotation for 45 minutes at 4°C, then pelleted and re-suspended in 2X RIPA buffer with 1% protease inhibitor cocktail (Sigma, Cat#P8340), 1% phosphatase inhibitor cocktail (Sigma, Cat#P2850), and 1 μ M phenylmethylsulfonyl fluoride (PMSF; Sigma, P7626). Samples were homogenized by passing through a 21-gauge needle 10 times. Protein concentration was determined using Bradford Protein Assay Kit (BioBasic, Cat# SK3031). Proteins were separated using electrophoresis in a 10% acrylamide gel and transferred to GE Healthcare Amersham Hybond P 0.45 μ m PVDF membrane (Fisher, Cat#45-004-110). Membrane was blocked with 5% BSA in 1XTBS with 0.1% Tween-20 for 1 hour at room temperature,

then incubated overnight with rotation at 4°C with pSTAT3 primary antibody (1:500, Cell Signaling Technology, Cat#9145) in 5% BSA in 1X TBS with 0.1% Tween-20. The membrane was rinsed with 1X TBS with 0.1% Tween-20, then incubated with the secondary antibody anti-rabbit HRP (1:1000, Jackson ImmunoResearch, Cat#111-035-003) for 2 hours at room temperature. Clarity Western ECL Substrate (BioRad) was used to visualize protein bands. Western blots were imaged using FluorChem E system (Protein Simple). After pSTAT3 bands were imaged, membrane was re-blotted with β -actin primary antibody (1:1,000, Abcam, Cat# ab8225) and anti-rabbit HRP secondary antibody. Western blot images were quantified using Image J Software¹⁵⁰.

Computational Modeling

IL22 cytokine diffuses from ILC3 cells to influence the intestinal crypt. Estimated IL22 concentration used in this model was derived from literature values describing IL22 secretion from human ILC cells¹²⁹. Briefly, ELISA was used to measure secreted IL22 in supernatant derived from co-cultures of LPS-stimulated macrophages and a population of ILCs composed of 22-35% ILC3 cells, as determined by positive staining for IL22. From ELISA measurements obtained with a detection limit of 15.6 pg/mL, a single ILC3 cell determined to secrete IL22 at an average rate of 4 fg/hr. Using Fick's first law at steady-state, diffusion flux from a single ILC3 was modeled. Flux was calculated using the surface area occupied by a single ILC3 cell ($19.635 \mu\text{m}^2$), the diffusion of a single molecule of IL22 ($1 \times 10^{-11} \text{ m}^2/\text{s}$), and the average secretion rate of IL22 ($6.94 \times 10^{-17} \text{ g/hr}$), assuming uniform secretion across the entire surface area and constant secretion over time. The flux of IL22 produced by a single ILC3 cell represented in the first model

as a circle with a radius of $2.5\mu\text{m}$ was calculated as $5.78 \times 10^{-14} \text{ mol/m}^2/\text{s}$. The flux of IL22 produced by 67 cells in a lymphoid follicle represented in the second model as a circle with radius of $20 \mu\text{m}$ was calculated as $3.87 \times 10^{-12} \text{ mol/m}^2/\text{s}$.

Finite-element analysis software COMSOL Multiphysics® (Burlington, MA) was used to simulate the secretion rate and concentration of IL22 generated from a single ILC3 cell near the intestinal crypt and a lymphoid follicle containing 67 ILC3 cells. With previously reported values of human IL22 levels generated from patient-derived ILC3 cells¹²⁹, the Transport of Dilute Species Interface was used to generate a model of IL22 diffusion. The model includes two simulations: 1. a single ILC3 cell with a radius of $2.5 \mu\text{m}$ secreting IL22, and 2. a circular lymphoid follicle with a radius of $20 \mu\text{m}$ containing 67 tightly packed ILC3 cells secreting IL22 from each cell. Both simulations model cell secretion as isotropic diffusion without convective mixing. The diffusion coefficient of IL22 ($1 \times 10^{-11} \text{ m}^2/\text{s}$) in liquid solution was conservatively estimated based upon its molecular weight (17 kDa) from a range of diffusion rates (from $1 \times 10^{-10} \text{ m}^2/\text{s}$ to $1 \times 10^{-11} \text{ m}^2/\text{s}$) of signaling molecules in the 10 to 100 kDa range. IL22 has a small M. W. of 17 kDa in this range, and, therefore, its diffusion coefficient is expected to be toward the lower end of the numerical range reported^{131,132}.

In a previous computational model used to predict the spatial distribution of IL-4, the authors of this study found that IL-4 secreting cells communicate with possible target cells within a range of approximately $100\mu\text{m}$ ¹⁵¹. The authors included local molecular processes of diffusion, degradation, internalization, and dissociation to determine that communication distance from a cytokine-producing cell to a target cell depends on several parameters but only a few variables. Parameters of low ligand diffusion, long half-

life of the ligand, and high affinity of the target cell's receptors can contribute to an increased effective communication distance, but these are biophysical properties that the target cell cannot regulate. Variables of the source cell, such as rate of internalization and dissociation, have little effect on the local cytokine distribution even when set to extremely fast levels. The major variable responsible for effective communication distance is the rate of secretion. These previous findings support the model presented here to simulate diffusion-dominant secretion of IL22 with parameter exclusions. The model presented does have its limitations, including a simplification of a closed system, despite a lymphoid follicle existing in an open system with continual inflow and outflow of cells. The flow of liquid through the modeling space was not considered, but, as liquid flow would likely reduce the effective concentration of the cytokine, we present a conservative model of IL22 diffusion and concentration dynamics.

Immunohistochemistry

Organoids in Matrigel were rinsed once with DPBS and fixed with room temperature 4% paraformaldehyde (PFA) for 20 minutes at room temperature. Organoids were then rinsed three times with 30% sucrose and incubated overnight at 4°C in 30% sucrose. Organoids were embedded into cryomolds with O.C.T. Compound (Tissue-Tek, Cat#4583), 8µm sections were cut using an OTF5000 Cryostat Microtome (Bright Instruments) and placed onto positively charged microscope slides and stored at -80°C. For immunostaining, slides were rinsed with PBS to remove O.C.T. Antigen retrieval, incubation in pressure cooker for 30 seconds at 120°C and 10 seconds at 95°C, was performed only on slides being stained for KI67 and IL22RA1. Slides were blocked with

protein block (DAKO, Cat#X090930-2, or Cell Signaling Technologies, Cat#15019S) for 1 hour at room temperature. Primary antibodies were diluted in antibody diluent (DAKO, Cat#S080981-2 or Cell Signaling Technologies, Cat#15019S) and incubated overnight at 4°C. Primary antibodies and dilutions used were: KI67 (rabbit, 1:100, Dako, Cat#M7249), LYZ (goat, 1:500, Santa Cruz, Cat#sc-12091), CD326 (rat, 1:500, Biolegend, Cat#H8201, Clone#G8.8), IL22RA1 (rat, 1:50, R&D, Cat#FAB42941P), OLFM4 (rabbit, 1:250, Cell Signaling, Cat#39141). Secondary antibodies were diluted in antibody diluent and incubated on slides for 2 hours at room temperature. Secondary antibodies and dilutions used were: anti-rabbit Cy3 (sheep, 1:1,000, Sigma, Cat#C2306), anti-goat Cy3 (donkey, 1:1,000, Jackson ImmunoResearch, Cat#705-165-003), anti-rat Alexa Flour 488 (Donkey, 1:1,000, Jackson ImmunoResearch, Cat#712-546-153), anti-rat Cy3 (Goat, 1:1,000, Jackson ImmunoResearch, Cat#112-165-003). Nuclei were stained with bis-benzamide (1:1,000) diluted in PBS. Slides were mounted using Hydromount (National Diagnostics, Cat#HS-106). Images were collected using Olympus IX81 or Zeiss LSM 700 confocal microscope. Images were analyzed in Metamorph Basic (Molecular Devices) and Image J¹⁵⁰.

Intraluminal lysozyme content was quantified using the open-source image analysis platform CellProfiler¹⁵². Images of sectioned organoids were taken marking the epithelial monolayer (CD326), the epithelial nuclei (DAPI), and Lysozyme protein after immunohistochemical staining as previously described. Images of each organoid were loaded into CellProfiler in sequence and pixel intensity of each image was rescaled. Binary images of each marker were formed by applying an intensity threshold using a three class Otsu's method with the mid-level class considered background¹⁵³.

Thresholded DAPI and CD326 images were combined to create binary images with the foreground depicting the entire epithelial signal. Gaps in the foreground of the combined images were closed using a 10 pixel top-hat transformation resulting in a binary image with the epithelial element represented as a smoothed foreground¹⁵⁴. The lysozyme binary image was masked by the epithelial element to remove intracellular lysozyme signal. The foreground area of the masked image was quantified and categorized by organoid treatment.

Gene Expression

Wells with organoids were rinsed once with DPBS and 200 μ L RNA Lysis buffer (from RNAqueous-Micro Total RNA Isolation Kit, ThermoFisher, Cat#AM1931) was added to each well containing 50-200 organoid or 10,000 single ISCs. RNA was extracted from samples using RNAqueous-Micro Total RNA Isolation Kit (ThermoFisher, Cat#AM1931) according to manufacturer's protocols and stored at -80°C . cDNA was created using iScript Reverse Transcription Supermix for RT-qPCR (BioRad, Cat#170-8891) according to manufacturer's protocols. cDNA was diluted 1:20 and 1 μ L of diluted cDNA was used for Real-Time PCR using Taqman probes (see Table 1) and SsoAdvanced Universal Probes Supermix (BioRad, Cat#1725281) according to manufacturer's protocols.

Single Cell Isolation and FACS

For Sox9-EGFP cell isolation, crypts were isolated from whole small intestine from Sox9-EGFP^{+/-} mice and single cells were isolated by FACS by established

methods^{41,48,155}. For wildtype cell isolation for IL22RA1 expression, crypts were isolated from distal half of small intestine from C57Bl6 mice. After crypt isolation, crypts were pelleted and re-suspended in 9 mL calcium and magnesium-free HBSS with 0.6 U/mL Dispase (Corning, Cat#354235), 120 U/mL DNase (Sigma, Cat#DN25), and 10 μ M Y-27632. Cells were then vigorously shaken for 30 seconds every 2 minutes for 10-15 minutes until a majority of the cells were single, filtered through a 40 μ m filter into ice cold DPBS, and washed twice with DPBS. Cells were re-suspended in ISC Basal Media (Advanced DMEM/F12, 1X N2, 1X B27 without Vitamin A, 1mM HEPES, 1X Glutamax, 100 U/mL Penicillin/Streptomycin) and stained with FACS antibodies on ice for 1 hour protected from light.

For intracellular staining, cells were re-suspended in room temperature 4% paraformaldehyde, mixed thoroughly, and incubated for 15 minutes at room temperature. Cells were washed with 1% BSA in 1XPBS and intracellular antibodies were added to cells in 1X saponin permeabilization buffer in 1% BSA in 1XPBS, mixed and incubated for 30 minutes at room temperature protected from light. Cells were then rinsed with permeabilization buffer and re-suspended in 1% BSA in 1XPBS for FACS analysis. Extracellular antibody staining was done for APC-conjugated anti-CD326 (1:250, Biolegend, Cat#118218, Clone#G8.8). Intracellular antibody staining was done for PE-conjugated anti-IL22RA1 (1:100, R&D, Cat#FAB4291P). Immediately before FACS analysis of live cells, AnnexinV Pac-Blue (1:100, Biolegend, Cat#640918) was used for live/dead discrimination. All FACS and flow cytometry experiments were performed using a SH800Z Cell Sorter (Sony Biotechnology). For RNA isolation, 50,000 cells were sorted directly into 250 μ L RNA Lysis buffer (from RNAqueous-Micro Total RNA Isolation Kit).

Statistical Analysis

All data are mean and standard error of the mean for the various groups. Statistics are based on 'n=3' biological replicates. For comparison of one group to a reference value (Western blot) a one-sample t-test was performed. For the comparison of two groups, an unpaired t-test with Bonferroni correction was performed. For the comparison of multiple groups, a one-way ANOVA followed by Tukey's multiple comparisons test or a Bonferroni correction was performed. All analyses of statistical significance were calculated and displayed in reference with the control group unless otherwise stated. All graphs were made and statistics were performed using Graphpad Prism version 7.0b for Mac, (GraphPad Software).

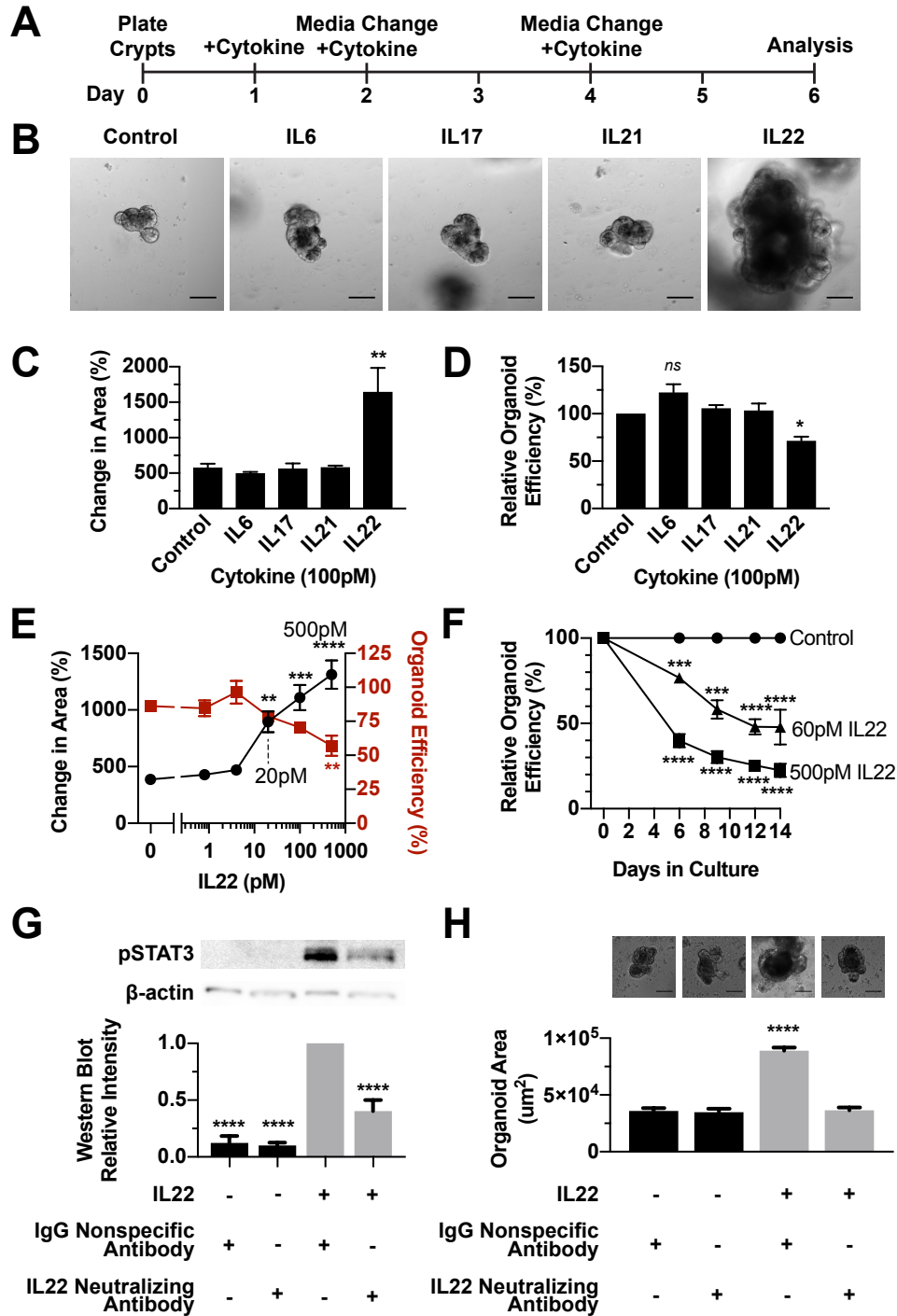


Figure 2.1. A focused screen of IBD-related cytokines reveals that IL22 causes a dose-dependent decrease in organoid survival and increase in organoid size. (A-D) Ileal organoid screen for cytokine effects on intestinal epithelium. (A) Schematic of experimental design where ileal organoids were treated for 6 days with 100 pM IL6, IL17, IL21 or IL22. (B) Representative images of treated organoids after 6 days. Scale bar=100 μm. (C) Percent change in area of organoids comparing day 0 to day 6. Technical n=10+

organoids; biological n=3; significance is relative to untreated control. **(D)** Organoid efficiency relative to control organoids. Technical n=3 wells; biological n=3 mice; significance is relative to untreated control. **(E)** Organoid response to a range of concentrations of IL22 (0, 0.8, 4, 20, 100, and 500 pM), measured by change in organoid area (left Y axis, black lines, technical n=10+ organoids) and organoid survival (right Y axis, red lines, technical n=3+ wells) after 6 days. Biological n=3 mice/treatment; significance is in relation to 0pM IL22. **(F)** Organoid survival with 0, 60, or 500 pM IL22 treatment. Technical n=3 wells; biological n=3; asterisks denote significance between treatment group and control at the designated time point. **(G-H)** Organoids were treated with 500 pM IL22 in the presence of 206 ng/mL IL22 neutralizing antibody or 206 ng/mL IgG of the same species. **(G)** *Top*. Representative images of treated organoids. *Bottom*. Quantification of organoid area. Technical n=10+ organoids; biological n=3; significance is relative to IgG-only control. Scale bar=100 μ m. **(H)** *Top*. Representative Western blot images for pSTAT3 and β -actin. *Bottom*. Quantification of intensity of Western blot bands normalized within each blot to the band with the highest intensity. Technical n=3 blots, biological n=3 mice. Significance was calculated by one-way ANOVA with a Bonferroni correction for multiple comparisons. ns=not significant; *p<0.05, **p<0.01, ***p<0.001, ****p<0.0001.

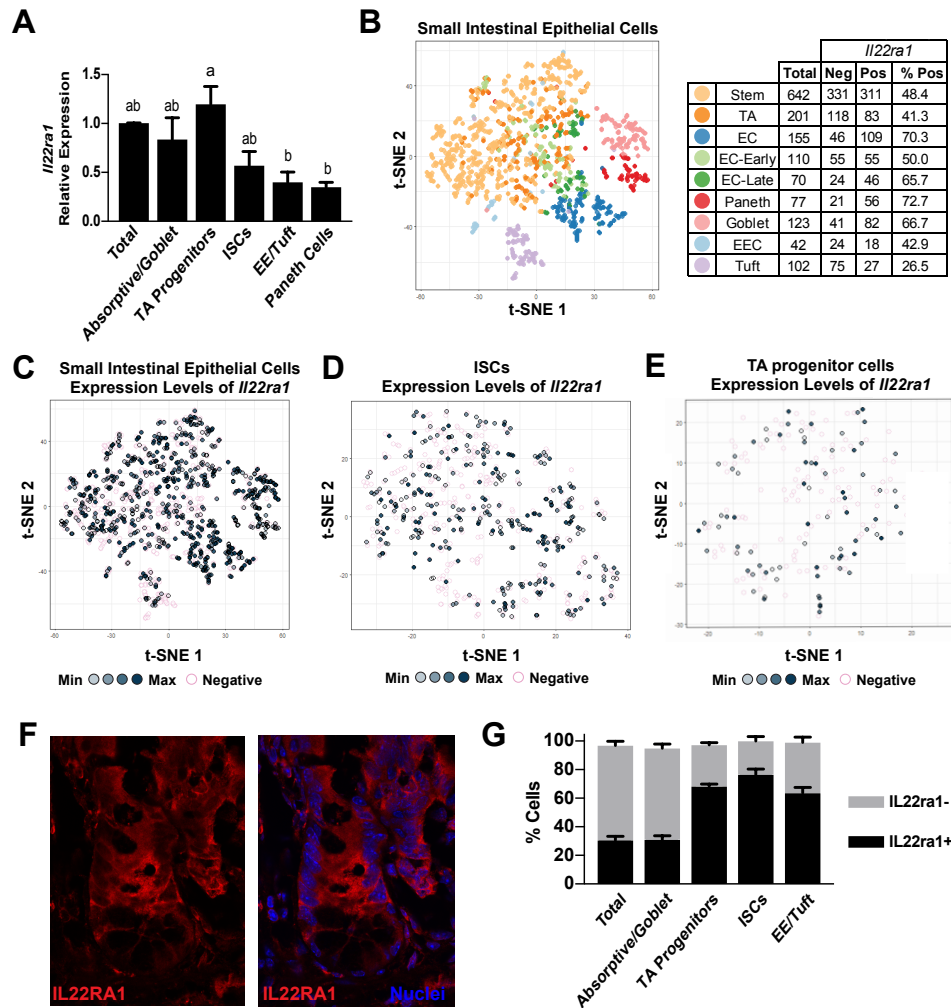


Figure 2.2. IL22ra1 is heterogeneously expressed throughout the crypt(A) IL22ra1 gene expression profile characterized in FACS-isolated Total epithelium (CD326+), Absorptive/Goblet differentiated cells (Sox9-EGFP^{neg}), TA progenitor cells (Sox9-EGFP^{sublow}), ISCs (Sox9-EGFP^{low}), Enteroendocrine/Tuft cells (Sox9-EGFP^{high}), and Paneth cells (Sox9-EGFP^{high}, CD24^{high}). n=3; biological n=3, Significance calculated by one-way ANOVA with Tukey's multiple comparisons; bars not connected by the same letter are statistically significant (p<0.05). (B) *Left.* t-SNE analysis of single cell RNAseq analysis of mouse small intestinal epithelium. Each color represents a different population defined in the original analysis based on lineage-specific transcriptomic signatures. *Right.* Table depicts the number of cells in each lineage category expressing IL22ra1. (C) Cells from the t-SNE profiles in graph 'B' highlighted specifically for expression of IL22ra1 levels in all epithelial cells. Darker shades of grey represent higher expression levels. Pink circles represent no expression. (D) The same analysis in 'C' except only ISCs are depicted. (E) The same analysis in 'C' except only TA progenitors are depicted. (F) Representative immunohistochemistry of Interleukin 22 Receptor A1 (IL22RA1) (red) and cell nuclei (blue) in a mouse ileal crypt. (G) FACS analysis of fixed cell populations

described in (A) stained for IL22RA1. Technical n=3; biological n=3. Bars represent parts of whole.

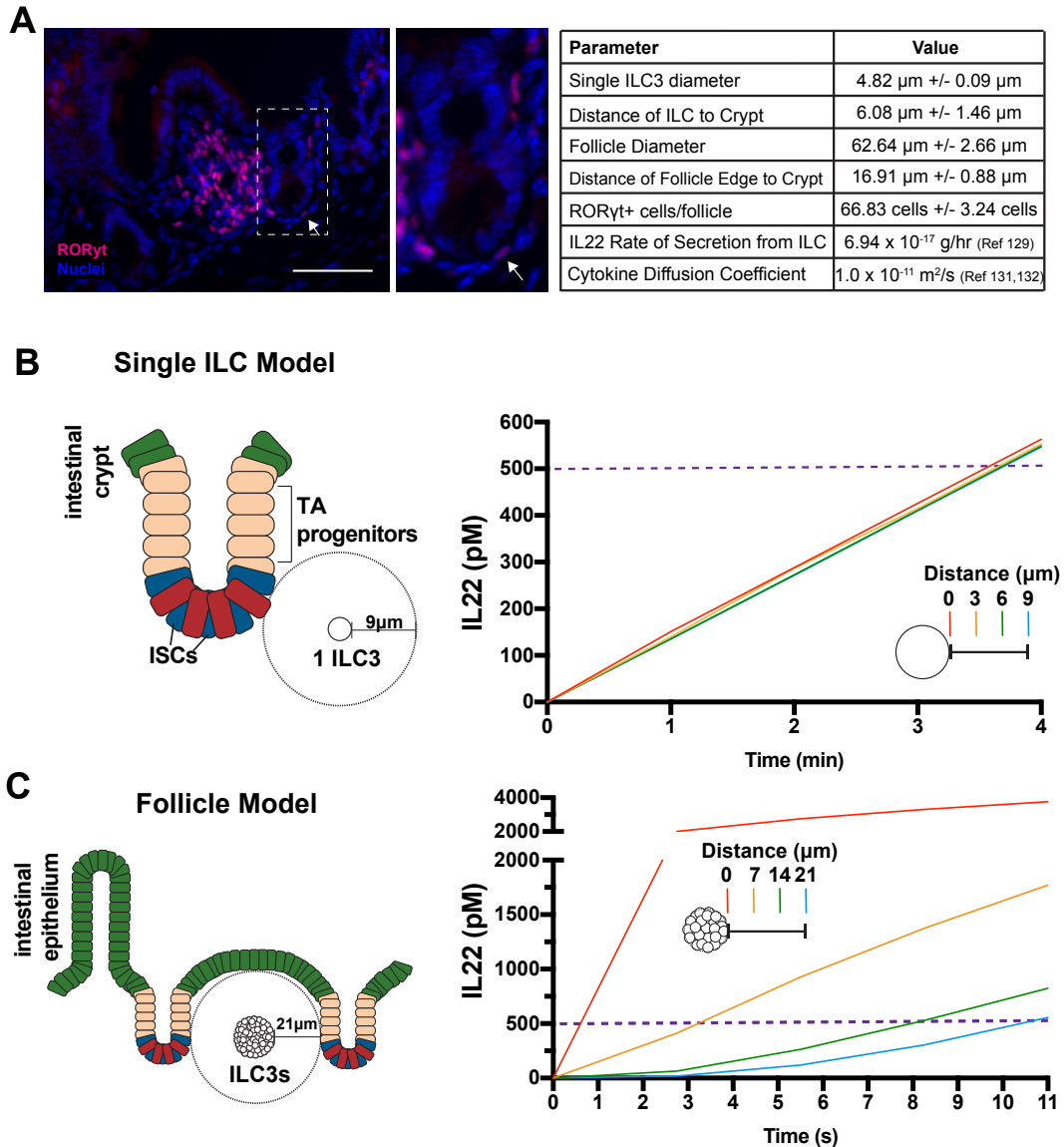


Figure 2.3. COMSOL Multiphysics simulation of IL22 diffusion. (A) Representative *in vivo* image of mouse ILC3 follicle with ROR γ t+ ILC3 immune cells (pink) and cell nuclei (blue). Parameters in table were empirically determined, n=10+ measured values/mouse, n = 3 mice. Scale bar = 100 μm . **(B) Left.** Single ILC3 IL22 secretion model where values of IL22 concentration were calculated by computational model along a line segment with length of 9 μm surrounding one ILC3 cell. **Right.** Concentration of IL22 over time at 4 points at 3 μm increments. **(C) Left.** Follicle model where values of IL22 concentration were calculated along a line segment with length of 21 μm . **Right.** Concentration of IL22 from a lymphoid follicle over time at 4 points at 7 μm increments.

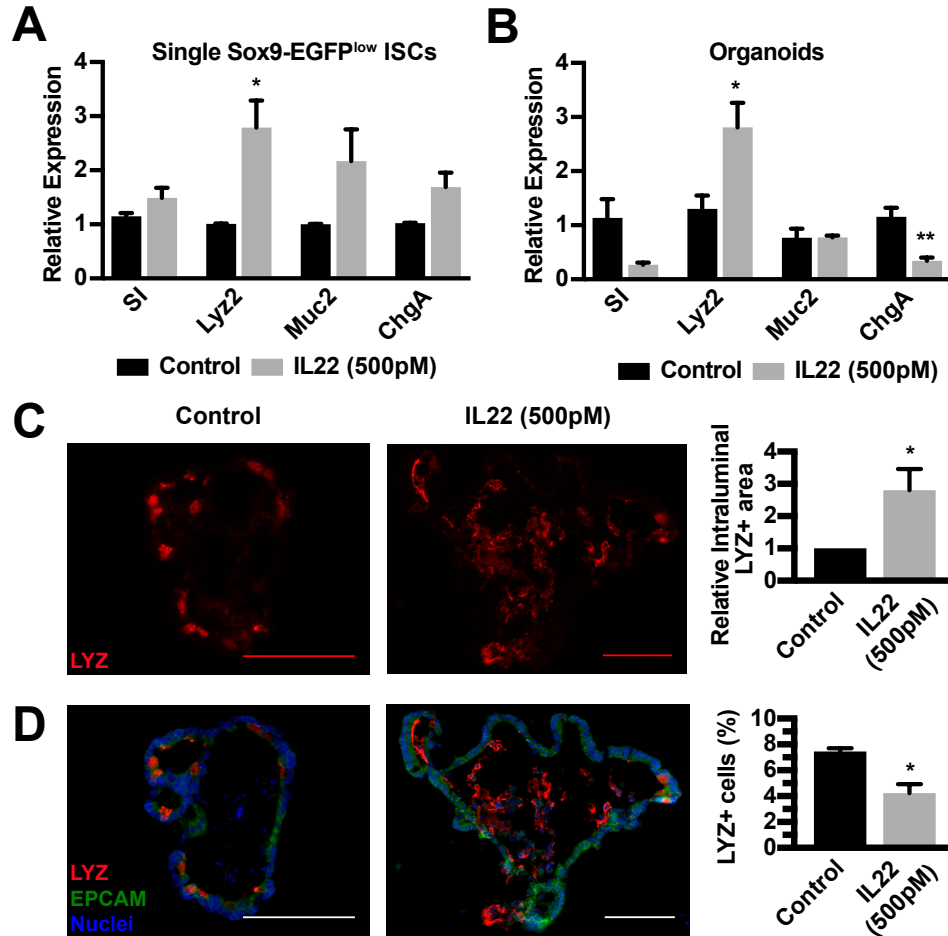


Figure 2.4. Cell lineage analysis in single ISCs and ileal organoids treated with IL22. (A) Gene expression analysis of single Sox9-EGFP^{low} single ISCs after 6 hours with or without 500 pM IL22 examining expression of differentiated cell genes. Technical n=3, biological n=3. (B) Gene expression analysis of organoids after 6 days with or without 500 pM IL22 examining expression of differentiated cell genes including *Sl* (enterocytes), *Lyz2* (Paneth cells), *Muc2* (goblet cells), and *ChgA* (enteroendocrine cells). (C-D) Immunohistochemistry staining and quantification of organoids treated for 6 days with IL22 then stained for Lysozyme (LYZ, red), EPCAM (green), and nuclei (blue). Technical n=10+ organoids; biological n=3;. (C) *Left*. Representative intraluminal LYZ staining (red). *Right*. Quantification of intraluminal stain. (D) *Left*. Representative organoid staining. *Right*. Quantification of total number of LYZ+ cells relative to total nuclei per organoid. Significance was calculated using an unpaired t-test relative to the untreated control. Scale bar=100 μ M; *p<0.05, **p<0.01, ***p<0.001, ****p<0.0001.

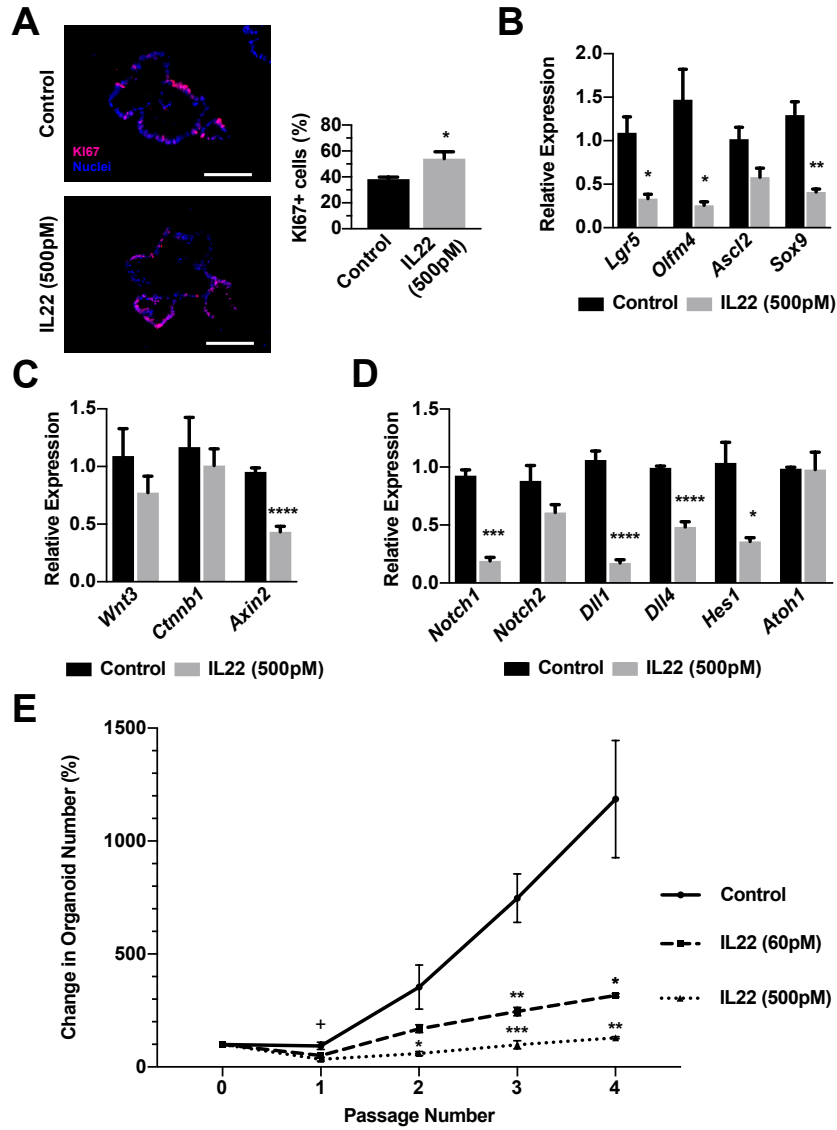


Figure 2.5. IL22 limits ISC expansion. (A) Representative immunohistochemistry for the proliferation marker KI67 (red) and nuclei (blue) with quantification of the proportion of KI67+ nuclei. Technical n=10+ organoids; biological n=3. Scale bar=100uM. (B-D) Gene expression analysis of organoids after 6 days with or without 500 pM IL22 for (B) ISC-associated genes including *Lgr5*, *Olfm4*, *Ascl2* and *Sox9*, (C) Wnt signaling pathway-associated genes including *Wnt3*, *Ctnnb1*, and *Axin2*, and (D) Notch signaling pathway-associated genes including *Notch1*, *Notch2*, *Dll1*, *Dll4*, *Hes1* and *Atoh1*. Technical n=3, biological n=3 mice. Significance was calculated using an unpaired t-test relative to the untreated control. (E) Percent organoid increase in response to 0, 60, or 500 pM IL22 at each passage compared to number of organoids at initial plating at p0. Technical n=3; biological n=3 mice. Significance was calculated using one-way ANOVA with Bonferroni correction at each time point in comparison to control. + = p<0.05 for 500pM IL22 compared to control at Passage 1. *p<0.05, **p<0.01, ***p<0.001, ****p<0.0001.

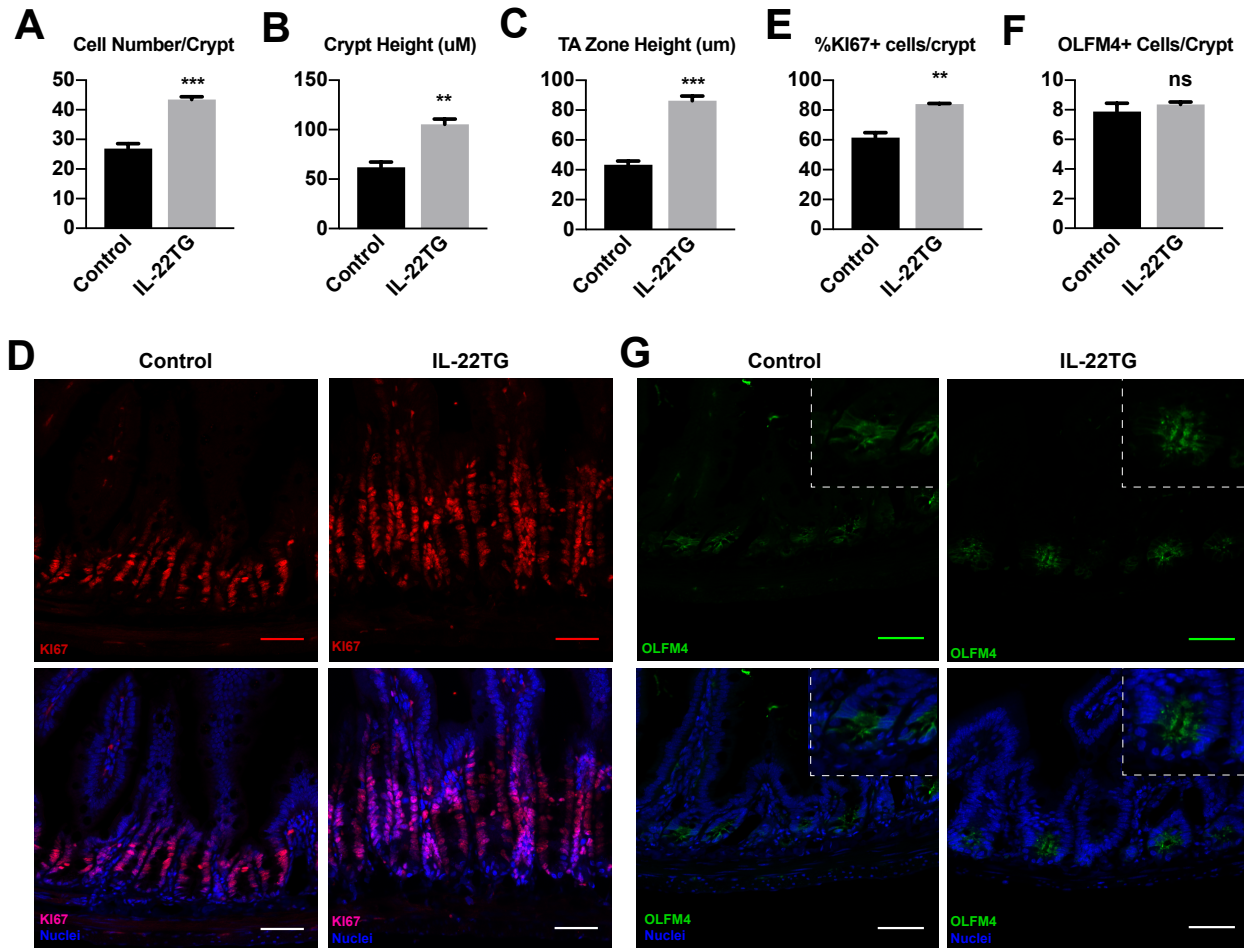


Figure 2.6. Elevated IL22 causes an increase in TA progenitors. Quantification of (A) total number of cells/crypt, (B) total crypt height, and (C) height of TA zone in control and IL-22TG mice. (D) Representative immunohistochemistry for the proliferation marker KI67 (red) and nuclei (blue). Quantification of (E) percent positive KI67 cells/crypt and (F) total number of OLFM4+ cells/crypt. (G) Representative immunohistochemistry for the ISC marker OLFM4 (green) and nuclei (blue). All quantification: n = 10+ crypts/mouse, n = 3 mice/treatment. Scale bar = 100 μ m. Ns = not significant, **p<0.01, ***p<0.001. Significance was calculated using an unpaired t-test relative to the untreated control.

Gene Symbol	Gene Name	Life Technologies assay ID
<i>18S</i>	Eukaryotic 18S rRNA	Hs99999901_s1
<i>SI</i>	sucrase isomaltase (alpha-glucosidase)	Mm01210305_m1
<i>ChgA</i>	chromogranin A	Mm00514341_m1
<i>Muc2</i>	mucin 2	Mm00458299_m1
<i>Lyz2</i>	lysozyme 2	Mm00727183_s1
<i>Lgr5</i>	leucine rich repeat containing G protein-coupled receptor 5	Mm00438890_m1
<i>Olfm4</i>	olfactomedin 4	Mm01320260_m1
<i>Ascl2</i>	achaete-scute family bHLH transcription factor 2	Mm01268891_g1
<i>Sox9</i>	SRY-box 9	Mm00448840_m1
<i>Wnt3</i>	Wnt family member 3	Mm00437336_m1
<i>Ctnnb1</i>	catenin beta 1	Mm00483039_m1
<i>Axin2</i>	axin 2	Mm00443610_m1
<i>Notch1</i>	notch 1	Mm00435245_m1
<i>Notch2</i>	notch 2	Mm00803077_m1
<i>Dll1</i>	delta like canonical Notch ligand 1	Mm01279269_m1
<i>Dll4</i>	delta like canonical Notch ligand 4	Mm00444619_m1
<i>Hes1</i>	hes family bHLH transcription factor 1	Mm00468601_m1
<i>Atoh1</i>	atonal bHLH transcription factor 1	Mm00476035_s1

Table 2.1. List of Taqman probes for qRT-PCR

CHAPTER 3: DEVELOPMENT OF EXTRACELLULAR MATRIX SCAFFOLDS FROM PORCINE SMALL INTESTINE THAT SUPPORT THE PROLIFERATION AND DIFFERENTIATION OF INTESTINAL EPITHELIAL CELLS

Overview

Loss of any part of the intestine due to surgical resection or congenital abnormality can be devastating to a patient. Resection, leading to a severely shortened bowel, may end up being the only option for patients who experience trauma or ischemia to the intestine or who suffer from disease such as necrotizing enterocolitis or inflammatory bowel disease. Although intestinal transplants can be performed when parenteral nutrition and traditional bowel lengthening strategies fail to improve patient health, transplantation can be problematic due to low donor availability and complications from immunosuppressive therapy. An engineered intestine comprised of autologous cells would circumvent the complications associated with intestinal transplant, including the need for a donor and tissue rejection. However, the architecture of the small intestine is complex and difficult to synthetically recapitulate. An acellular intestinal ECM would be the ideal natural scaffold to create an intestine *ex vivo*, considering that a scaffold can retain all ECM proteins and associated growth factors and cytokines in the same pattern as found *in vivo* depending on the isolation technique¹⁵⁶. Creation of decellularized scaffolds have been successful in other organs including the heart, liver, and lung. Here, I have optimized a procedure to decellularize porcine small intestine that retains integral

anatomical structures, preserves key extracellular matrix components including Collagen Type I and Elastin, and supports mouse epithelial proliferation and differentiation.

Introduction

When the intestine fails, no digestion of food or absorption of nutrients, electrolytes or fluids occurs, creating a life-threatening condition^{157,158}. The major cause of intestinal failure is short bowel syndrome (SBS), defined as having less than 200 centimeters (or about 30%) of functional intestine, and can result from surgical resection due trauma or disease¹⁵⁸. Intravenous parenteral nutrition (PN) is required for SBS patients¹⁵⁹. While this alleviates the need for digestion and absorption in the intestine in the short-term while the intestine adapts, up to 25% of patients continue to permanently depend on parenteral nutrition leading to a 5-year survival of just 63% and a range of other negative effects, often including liver failure^{159,160}. When PN is no longer effective, patients need to undergo surgery to increase the length of the intestine or receive an intestinal transplant^{158,159}. Intestinal transplants are complex due to tissue rejection, high cost of transplantation, and lack of viable donors¹⁵⁷. Even with transplant, prognosis is very poor, with up to 40% of patients experiencing rejection within the first year and ten-year patient survival at only 29%¹⁶¹. A possible alternative treatment option for SBS patients is to lengthen the intestine by surgical implantation of a piece of engineered tissue created from autologous cells. This approach has the advantage of limiting tissue rejection and negating the need for a healthy intestinal donor¹⁶².

When growing patient cells *ex vivo*, an acellular scaffold or matrix is needed to support cell growth¹⁶². Decellularized matrices are attractive as a scaffold since they

preserve the native architecture and extracellular matrix (ECM) components, but lack immunogenic host cells¹⁶³. Native ECM is a complicated, intertwining mix of collagens, fibronectins, laminins, proteoglycans, and glycosaminoglycans that are present throughout a tissue in 3-dimensional patterns and gradients⁷⁵. The ECM provides structure and aids in attachment, migration, and proliferation of resident cells and is integral for the function of each tissue^{75,79}. Currently, decellularized scaffolds are being created from whole organs such as skin, heart, liver, lung, kidney, and intestine as well as other tissues such as blood vessels, heart valves, adipose tissue, and cartilage¹⁶⁴. Since the native ECM and associated proteins are preserved, many of these decellularized organs have been able to be recellularized with native cell types or used to treat human disease¹⁶⁴.

As surplus human intestine is not available, porcine intestine is an attractive source for creating decellularized scaffolds due to its accessibility as an unused by-product of the meat industry and its similarity in overall size and macro (small intestine and colon) and micro (crypt and villus) anatomy to human intestine¹⁶⁵. Additionally, using intestinal tissue as a scaffold allows for all native ECM components to be present and in the proper orientation and concentration found in the native intestine¹⁵⁶. Here, I have developed a protocol to efficiently decellularize full-thickness porcine small intestine and demonstrate its ability to support mouse small intestinal epithelial cells. Creation of an acellular small intestinal scaffold will create the basis for future tissue engineering of the small intestine¹¹⁷.

Results

Decellularization of Porcine Intestine

While the overall approach to perfusion decellularization is conceptually similar across tissues and species, optimization is essential for every application^{156,164}. Essentially, cells are removed by exposing them to detergents and enzymes, while still preserving the underlying ECM scaffold¹⁶⁶. I modified a previously established protocol that has been particularly successful in decellularizing rat liver¹⁶⁷. This strategy is focused on collagen chemistry and allowed for the resulting liver scaffold to maintain native histology, patent vasculature, >95% of its collagens, and physiologic levels of ECM-bound growth factors and cytokines¹⁶⁷. Successful modification of this protocol involved modifying all stages of the decellularization process. Integral modifications included the luminal perfusion of N-acetylcysteine (NAC) to remove mucus from the intestinal lumen, luminal perfusion of decellularization reagents to aid in the removal of cellular debris, increasing the salt concentration to account for collagens found in the intestine, and increasing all solution volumes and perfusion times to account for the increased size of the tissue.

Porcine small intestine was obtained from a meat processing facility and transferred back to the lab where it was trimmed to a smaller 6-8-inch piece of intestine with attached mesentery and vasculature in order to easily process (Figure 3.1A). Since all cells are in close proximity to a vascular network (most within 50-100um of a capillary), vascular perfusion was an efficient method for reaching all cells and is used in most decellularization protocols¹⁶⁸. However, I found that luminal perfusion was necessary to remove mucus and cellular debris that remained in the intestinal lumen during and after

luminal perfusion (data not shown). To enhance luminal perfusion, the lumen was first rinsed with 100mM NAC to remove intestinal mucus by a modified catheter placed into one end of the intestine lumen (Figure 3.1B,C). In order to perfuse through the vasculature and lumen, another catheter was placed into the mesenteric vasculature (Figure 3.1C). After vascular and luminal rinse of blood and luminal contents, the intestinal vasculature is no longer marked by dark blood, suggesting a patent vasculature system for perfusion (Figure 3.1C).

A 4-step protocol was then followed to perfuse solutions through both the vasculature and luminal catheters. First, gentle delipidation was performed with phospholipase A2 (PLA2) and sodium deoxycholate (SDC). These solutions degrade the phosphoglyceride found on the cell and mitochondrial membranes to induce necrosis and cytolysis¹⁶⁷. Importantly, soybean trypsin inhibitor was also added to these perfusion solutions to limit protease activity from dying cells. After perfusion, the perfused intestine appeared pale and begins to look translucent (Figure 3.1D).

Next, a high salt solution was perfused to retain collagens and keep them insoluble. The most abundant type of collagen in the intestine is Type I^{169,170}. Collagen Type IV, which is found in most basement membranes surrounding cells¹⁷¹, is also found throughout all layers of the small intestine¹⁷². To a lesser extent, Collagen Types II¹⁷³, III, V, VI¹⁷⁰, and VII¹⁷⁴ are also present in the small intestine, further demonstrating the complex mix of collagens required for intestinal homeostasis. To keep all of these collagens insoluble during perfusion, a high salt concentration of 4.2M was used for perfusion¹⁷⁵. After perfusion of the high salt solution, the perfused intestine appeared translucent/white in color (Figure 3.1E).

To remove any residual nucleic acids in the scaffolds, nuclease treatment was performed by perfusion of DNase and RNase. A final perfusion with basal media removed any remaining prior perfusion solutions. The resulting intestinal scaffold was translucent and appears pink after final perfusion with basal media (Figure 3.1F).

Intestinal scaffolds were successfully decellularized

Acellular scaffolds were sectioned and their histology analyzed. First, intestinal scaffolds were stained with bisBenzimide, which marks DNA and nuclei, to determine if any cells remained after the decellularization procedure. Compared with native porcine intestine, the intestinal scaffolds did not contain punctate nuclei, suggesting no intact cells remained in the scaffolds (Figure 3.2A). Minimal diffuse staining was observed, particularly at the villus tips, suggesting that further rinsing of the intestinal scaffold may be necessary to remove all traces of native nucleic acids. Co-staining with Collagen Type 1 (Col1a1) outlined the protruding villi, allowing for a clearer visualization of the underlying mucosal architecture (Figure 3.2B).

Intestinal Scaffolds maintain mucosal architecture and ECM patterning

To determine if the intestinal scaffolds retain micro architecture and ECM composition, scaffold histology was examined. Col1a1 and Elastin were detected by immunohistochemistry to visualize the overall scaffold microarchitecture. *In vivo*, the mucosal layer is organized into crypts, which invaginate into the lamina propria and contain mostly undifferentiated cells, and villi, that protrude into the intestinal lumen to increase surface area and contain mostly differentiated cells⁷. Immunostaining of native

porcine small intestine revealed that Col1a1 was mainly observed in the villi (Figure 3.2B,C). After the decellularization procedure, a similar pattern of Col1a1 was observed in the preserved villi, suggesting preservation of both the micro-architecture and Col1a1 composition of the villi (Figure 3.2B, right). Col1a1 was also observed in the outermost layer of the intestine, the serosa, in both native and scaffold sections (Figure 3.2C).

Elastin was found predominantly surrounding the crypts, between the Col1a1 staining in the villi and the serosal layer (Figure 3.2C). Similar patterns of Elastin were observed between the native intestine and the intestinal scaffold (Figure 3.2C), suggesting retention of Elastin throughout the decellularization procedure. Importantly, preservation of spatial location of both of these ECMs was observed. The locations of porcine Col1a1 and Elastin were similar to those found in human small intestine (Figure 3.2D), suggesting the translational applicability for porcine decellularized scaffolds.

Intestinal Scaffolds support mouse epithelium

In order to determine if the scaffolds could support epithelial cells *in vitro*, I next cultured mouse small intestinal epithelium on the scaffolds and examined cell expansion, proliferation, and differentiation. The culture of small intestinal crypts, which contain intestinal epithelial stem cells, in an ECM-rich hydrogel results in a high survival of the epithelial cells and subsequent proliferation and differentiation of the epithelium³². To provide sterile culture conditions for the epithelial cells to interact with the scaffold, 60 μ m sections of the decellularized intestinal scaffold were placed on the bottom of a tissue culture plate. Mouse small intestinal crypts were isolated from Ubq-GFP mice, which ubiquitously express green fluorescent protein (GFP) in all cells, allowing the visualization

of live epithelium over time. Crypts were overlaid onto the scaffolds with supportive media and growth factors. Importantly, no other ECM substrate was supplemented in the culture wells. GFP+ epithelial cells were observed on the scaffolds at Day 2 and expanded in area through Day 10 (Figure 3.3A). No epithelial growth was observed in wells with the scaffold without crypts or without the scaffold with crypts (data not shown).

The decellularized scaffold supported epithelial growth for 21 days post-plating (Figure 3.3B). To confirm that the cells were epithelial, the scaffolds were fixed and immunostained for the epithelial cell marker CD326 (epithelial cell adhesion molecule, Epcam)¹⁷⁶. Qualitatively, all nuclei on the scaffold co-localized with Epcam, suggesting epithelial cell expansion on the intestinal scaffolds. To determine if the cells on the scaffold were proliferating, cultures were pulsed with 5-ethynyl-2'-deoxyuridine (EdU), which incorporates into DNA during active DNA synthesis¹⁷⁷, for 2 hours prior to fixation of the scaffolds. *In vivo*, intestinal stem cells divide approximately once every 24 hours, giving rise to proliferating TA progenitor cells that divide more frequently^{3,7}. Since one type gives rise to the other, proliferative cells are in close proximity to each other in the crypt *in vivo*⁷. Clusters of proliferative Edu+ cells were observed throughout the Epcam+ epithelium on the scaffold (Figure 3.3C), suggesting that the intestinal scaffold is supportive of ISC and TA progenitor cell proliferation.

Intestinal Scaffolds support differentiation of mouse small intestinal epithelial cells

I next wanted to determine if the epithelium was differentiating into cell types found in the intestinal epithelium *in vivo*. TA progenitor cells differentiate as they move out of the crypt and onto the villi, and give rise to either secretory or absorptive cell types⁷. The

more abundant secretory cell type in the villus is the mucus-secreting goblet cell, marked by *Muc2*¹⁷⁸. Immunostaining for *Muc2* showed *Muc2*⁺ cells in the epithelium on the scaffold (Figure 3.4A). A less abundant secretory cell type in the villus epithelium is the hormone-secreting enteroendocrine cell, marked by *ChgA*¹⁷⁹. Immunostaining for *ChgA* showed rare *ChgA*⁺ cells in the epithelium on the scaffold (Figure 3.4B). Qualitatively, these differentiated cell types do not co-localize in areas of cell proliferation (*Edu*⁺ cell clusters), suggesting zones of proliferation and differentiation in the scaffold. Importantly, presence of goblet and enteroendocrine cell types suggest that the scaffold supports differentiation of epithelial cells found on the villus *in vivo*.

The only differentiated cell type that does not migrate out of the crypt is the Paneth cell, which remains at the base of the crypt to support ISCs²³. Paneth cells secrete growth factors, create antimicrobial proteins, and are marked by *Lyz*²⁵. Immunostaining for Lysozyme showed clusters of *Lyz2*⁺ cells in the epithelium on the scaffold (Figure 3.4C). *Lyz2*⁺ cells were found in close proximity and intercalated among proliferative *EdU*⁺ cells, similar to their pattern *in vivo*. Phenotypically, the Lysozyme staining of scaffold epithelial cells was granulated, suggesting that these Paneth cells are making Lysozyme granules and functioning similarly to how they do *in vivo*.

Discussion

Current intestinal engineering approaches expand a small piece of patient intestine approximately 3-fold by mincing and reorganizing it on a scaffold¹⁸⁰, which does not allow for consistently functional or therapeutic levels of tissue to be generated and relies upon availability of a significant amount of initial patient tissue. Alternative approaches to

creating autologous patient tissue lie in expanding cell types from a small patient biopsy¹⁸¹ or use of induced pluripotent stem cells¹⁸² from a more abundant cell source from the patient. Methods have been developed to isolate and expand many of the cell types of the intestine *in vitro*; however, re-creating a patient scaffold that adequately supports all intestinal cell types and is large enough to substantially improve patient health is challenging. The use of a decellularized porcine intestine provides a scalable scaffold that is both similar in size to the human intestine and maintains ECM architecture and composition to support all intestinal cell types.

ECM is a requirement for intestinal epithelial cell survival *in vivo* and *in vitro*^{32,65}. Currently, most *in vitro* culture systems use Matrigel³², ECM derived from an Engelbreth-Holm-Swarm mouse sarcoma that is not well defined and is not FDA-approved for use in humans. More recently, epithelial cells have also been cultured on more defined ECMs, including Collagen Type I⁶⁶ or combinations of isolated and synthetic ECMs⁶⁷ with success; however, these sources do not provide all the ECM found in the native small intestine in the proper concentration and 3-dimensional location. Our results suggest that an intestinal scaffold is a promising ECM source for reconstruction of the human small intestine *ex vivo*, as the architecture and organization of Col1a1 and Elastin are retained post-decellularization and found in similar patterns as in the human small intestine.

A biologically relevant ECM is integral for proper cell function, as ECM has been shown to influence cell behavior^{75,183}. Specifically, ECM isolated from cancerous patient tissue has been shown to influence niche cells differently than ECM isolated from healthy patient tissue¹⁸⁴. I demonstrated that decellularized intestine can support the proliferation and differentiation of mouse intestinal epithelium. Although further studies need to be

performed characterizing the performance of the intestinal scaffold compared to other ECMs, our data suggest a broad use of the scaffold for the *in vitro* culture of epithelial cells in an environment that more accurately recapitulates the *in vivo* environment. Other groups have shown that acellular ECM scaffolds can be ground up and coated on plates¹⁶⁷ or made into a hydrogel to suspend cells in 3-dimensional culture^{117,185}, both of which may be translational to support the growth of and expand isolated human intestinal epithelium. Although I demonstrated the use of the procedure on a small piece of intestine, methods can be scaled up to decellularize more therapeutically-relevant pieces of intestine and associated vasculature.

Our protocol utilizes an otherwise discarded part of the pig that is widely available at most meat processing plants. In 2016, 118 million pigs were slaughtered for meat¹⁸⁶, highlighting the availability and ease of obtaining porcine intestines to create scaffolds for intestinal tissue engineering. A porcine ECM scaffold is attractive for human clinical use due to the minimal immunogenic response caused by scaffold placement, demonstrated by clinical studies using commercially available porcine SIS grafts^{187,188}. Acellular SIS have been harvested by many commercial companies¹⁸³ to effectively treat many health problems including hernias¹⁸⁹, vaginal prolapse¹⁹⁰, venous ulcers¹⁹¹, cranial and spinal dural defects¹⁹², and a variety of foot and ankle disorders¹⁹³. The difference between commercially available SIS and the acellular scaffold described in this chapter is that the acellular scaffold maintains the ECM and architecture of all intestinal layers, which are integral in the recellularization process for tissue engineering applications.

Creation of decellularized porcine small intestine opens many avenues for future intestinal tissue engineering. For example, ground ECM can be suspended in solution

and sprayed onto the luminal surface of the intestine through an endoscope or ECM scaffolds can be placed placed onto the intestinal surface as intestinal “band-aids”¹¹⁷. These scaffolds could even be supplemented with ISCs or antibiotics to encourage epithelial regeneration. The native ECM scaffold is an integral component of the ISC niche and therefore an invaluable component for small intestinal tissue engineering, as it would be void of host cells, retain its native architecture, and promote intestinal cell growth. Eventually, human intestinal cells could be seeded on the scaffold and grown into all layers of the small intestine, opening many new doors for autologous transplant and grafting strategies.

Methods

Pig Intestinal Tissue

Adult, market-weight female pig intestinal tissue was obtained from City Packing Company (Burlington, North Carolina). Eighteen to twenty-four inch pieces of jejunum were dissected at the processing plant. Intestinal pieces were placed in ice cold DMEM/F:12 (Gibco) and transported on ice back to the lab. Before decellularization, intestine and attached mesentery was trimmed to approximately 6-8 inches in length and placed a glass tray on ice for the decellularization procedure (Figure 3.1A).

Decellularization Procedure

A 20G X 1” catheter (Exel International) was placed centrally in mesenteric vasculature pointing towards the intestine and secured with suture string for vascular

perfusion (Figure 3.2B). Vascular perfusion of DMEM/F12 (Gibco) was performed for 10 minutes to confirm catheter placement and to remove blood from the vasculature.

A 14G X 1¼" catheter (Exel International) was tightly fit into the smaller end of a 1mL pipette tip, place into one end of the small intestine, and secured with suture string for luminal perfusion. To remove intestinal contents, the intestinal lumen was filled with 40mL of DMEM/F:12, and the other end of the intestine was clamped with a binder clip (Figure 3.2B). The piece of intestine was rocked back and forth on the glass tray at 1 cycle/second by hand for 1 minute. Luminal contents and media were discarded by removal of the binder clip. Luminal washing was performed again with 50mL of 100mM N-acetyl-L-cystine (NAC, Sigma) in DMEM/F:12. A final wash of the intestinal lumen was performed with 20mL DMEM/F12 to remove residual NAC and intestinal contents.

Clear silicone tubing (L/S 13, Cole Parmer, Cat#SK-96410-13), was attached to each catheter with a male luer lock ring x 1/16" hose barb (Cole Parmer, Cat#SK-45505-00). Both vascular and luminal perfusion was performed simultaneously for the remainder of the procedure at a rate of 5mL/minute using a Masterflex L/S pump (Cole Parmer). First, DMEM/F12 was perfused for 10 minutes total. Next, two rounds of 66ml of DMEM/F:12 and 6 units of Phospholipase A2 (PLA₂) from porcine intestine (Sigma-Aldrich) was perfused. The PLA₂ solution was made twice for this step to limit the amount of PLA₂ degradation during perfusion. Next, 25mL 1% Sodium Deoxycholate (SDC) (Sigma) in 1X PBS, 0.025g Ca²⁺Cl⁻, and 2 units of PLA₂ was perfused ten times. This solution was also made fresh 10 times to limit the amount of PLA₂ degradation during perfusion. The intestine was then perfused with DMEM/F:12 for 30 minutes. Next, 500mL of 4.2M NaCl in sterile water was perfused. The intestine was then perfused again with

DMEM/F:12 for 30 minutes. Next, 100mL DMEM/F:12, 0.001g DNase, 5mg RNase, and 0.01g Trypsin inhibitor from Glycine max (Sigma) was perfused. A final perfusion of DMEM/F12 was performed for 30 minutes.

Sectioning Intestinal Scaffolds

The resulting intestinal scaffold was embedded either fixed or fresh. If fixed, the scaffold was placed in ice cold 4% paraformaldehyde overnight at 4°C, rinsed with 30% sucrose, and stored in 30% sucrose overnight at 4°C. If fresh, intestinal scaffolds were placed in 30% sucrose for 2 hours at 4°C. All scaffolds were then embedded into cryomolds with O.C.T. Compound (Tissue-Tek, Cat#4583). For immunohistochemistry experiments, 8µm sections of fixed scaffolds were cut using an OTF5000 Cryostat Microtome (Bright Instruments), placed onto positively charged microscope slides, and stored at -80°C until use. For culture experiments, 60µm sections of fresh scaffolds were cut and placed in the bottom of wells in a 12-well tissue culture plate. Sections were dried in a sterile tissue culture hood for one hour at room temperature. Each scaffold was rinsed five times with 1X DPBS (Gibco) supplemented with 100U/mL Penicillin/Streptomycin (Gibco) for 5 minutes. Scaffolds were overlaid with Advanced DMEM/F:12 with 100U/mL Penicillin/Streptomycin until cell seeding.

Human Intestinal Tissue

Human intestine was obtained from deceased organ donor patients from Carolina Donor Services. Human tissue used in this study qualified as exempt after full Institutional Review Board review (approval #14-1750). Full-thickness jejunum was isolated from the

small intestine and fixed in cold 4% paraformaldehyde overnight at 4°C. Jejunum was rinsed with 30% sucrose and stored in 30% sucrose overnight at 4°C. Small, full-thickness pieces of jejunum were embedded into cryomolds with O.C.T. Compound (Tissue-Tek, Cat#4583). Sections (8µm) were cut using an OTF5000 Cryostat Microtome (Bright Instruments), placed onto positively charged microscope slides and stored at -80°C.

Mice

Mice expressed enhanced green fluorescent protein (GFP) under the direction of the human ubiquitin C promoter (Ubq-GFP). Mice were originally purchased from Jackson Labs (Strain Name: C57BL/6-Tg(UBC-GFP)30Scha/J, Stock Number: 004353) and were maintained as homozygotes. All mice used in these studies were 8-12 weeks old. All animal use was reviewed and approved by the Institutional Animal Care and Use Committee of the University of North Carolina at Chapel Hill.

Mouse Intestinal Crypt Isolation, Plating, and Culture

The jejunum (middle 1/3 of small intestine) of the mouse was isolated, flushed, fileted open and rinsed in ice cold 1XDPBS. The intestine was cut into 3-5cm pieces and placed in 3 mM EDTA in 1XDPBS for 45 minutes at 4°C on an orbital rocking platform. Intestinal pieces were then transferred to 1X DPBS with 10 µM Y-27632 (Selleck Chemicals) and shaken by hand for 2 minutes at 3 shakes/second to release crypts. Isolated crypts were filtered through 100 and 70 µm filters to remove villus fragments and rinsed once with DPBS.

One thousand isolated crypts were plated in each well of 6-well plate (with or without a scaffold) with 250uL Overlay media/well. Overlay media consisted of 50% Advanced DMEM/F12, 50% RSPO2 conditioned media (made in-house), 100ng/mL recombinant murine Noggin (Peprotech), 50ng/mL recombinant murine EGF (Invitrogen), 100X Glutamax (Gibco), 100X N2 Supplement (Gibco), 50X B27 Supplement (Gibco), 1mM HEPES (Gibco), 500mM N-acetylcystine (NAC, Sigma), 100U/mL Penicillin/Streptomycin (Gibco), and 50g/mL Gentamicin. Media was changed every other day, being careful not to disturb underlying scaffold.

Stage positions within wells were saved on Day 2 and imaged on Days 2, 6 and 10 post-cell plating using an Olympus IX81 microscope to serially observe the same scaffold section over time. Mouse epithelial cells expressed GFP and were able to be visualized by excitation at 488 nm. To mark proliferating cells, epithelium on scaffolds were pulsed with 20uM 5-ethynyl-2'-deoxyuridine (EdU) for 2 hours after 21 days in culture. Cells were rinsed with 1DPBS and fixed for at room temperature for 20 minutes with room temperature 4% paraformaldehyde. Wells were then rinsed 3 times with 3% BSA in 1XDPBS and stored in 3% BSA in 1XDPBS until whole mount staining.

Immunohistochemistry

For immunostaining sections, slides were rinsed with PBS to remove O.C.T. Slides were blocked with Protein Block (DAKO) for 1 hour at room temperature. Primary antibodies were diluted in Antibody Diluent (DAKO) and incubated overnight at 4°C. Primary antibodies and dilutions used were: CD326 (Epcam; anti-mouse, primary conjugated to Alexa647, 1:250, Biolegend, Cat#118211, Lot#B15046), Anti-Collagen

Type I (mouse, 1:300, Sigma-Aldrich, Cat#C2456), and Anti-Elastin (rabbit, 1:100, Abcam, Cat#21610). Secondary antibodies were diluted in antibody diluent and incubated on slides for 2 hours at room temperature. Secondary antibodies were all diluted 1:1,000 in antibody diluent and were: Goat anti-mouse, Cy3, Jackson ImmunoResearch, Cat#115-166-003; and Goat anti-rabbit, 488 AlexaFluor, Jackson ImmunoResearch, Cat#111-545-144). Nuclei were stained with bisBenzamide (1:1,000) diluted in PBS for 10 minutes at room temperature. Slides were mounted using Hydromount (National Diagnostics, Cat#HS-106). Images were collected using an Olympus IX81 microscope.

For whole mount immunohistochemistry, the Click-iT EdU Imaging kit with Alexa Fluor 555 (Invitrogen) was used to visualize EdU labeling. Protocol was followed per manufacturer's instructions. Further antibody staining was performed after EdU detection. Primary antibodies were diluted in antibody diluent and incubated overnight at 4°C. Primary antibodies and dilutions used were: CD326 (Epcam; anti-mouse, primary conjugated to Alexa647, 1:250, Biolegend, Cat#118211, Lot#B15046), Lyz2 (rabbit, 1:500, Diagnostic Biosystems, Cat# RP028), Muc2 (rabbit, 1:500, Santa Cruz, Cat# sc-15334), and ChgA (goat, 1:100, Santa Cruz, Cat# sc-1488). Secondary antibodies were diluted in antibody diluent and incubated on slides for 2 hours at room temperature protected from light. Secondary antibodies were all diluted 1:1,000 in antibody diluent and were: Donkey anti-goat Alexaflour 488 (Jackson ImmunoResearch, Cat#705-475-147), Goat anti-rabbit Alexaflour 488 (Jackson ImmunoResearch, Cat#111-545-144), Donkey anti-rabbit Alexaflour 647 (Jackson ImmunoResearch, Cat# 711-605-152). Nuclei were stained with bisBenzamide (1:1,000) diluted in PBS for 10 minutes at room temperature. Scaffolds were stored in 1XDPBS at 4°C until imaging.

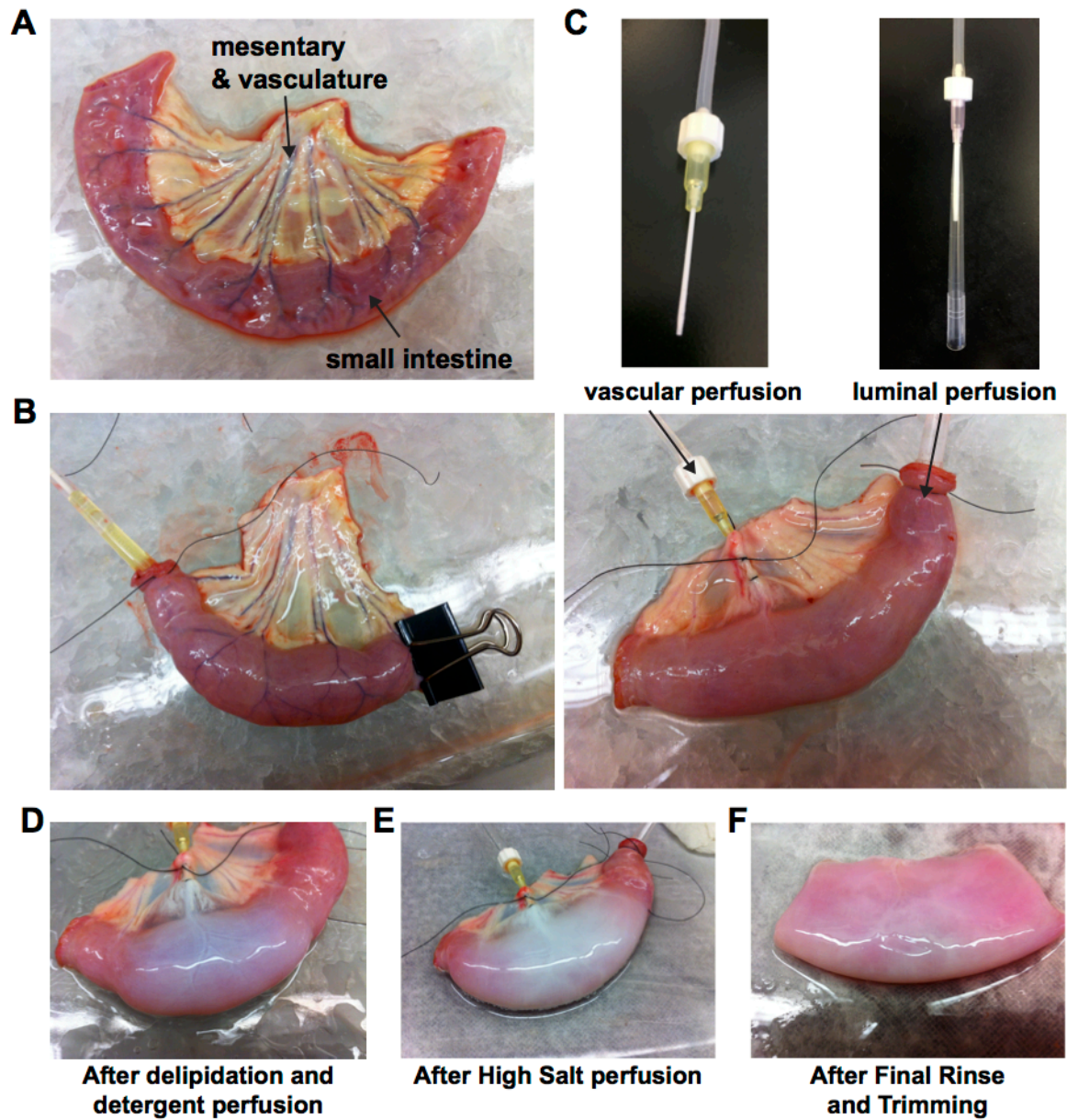


Figure 3.1. Porcine intestine throughout the decellularization process. (A) Vasculature (dark blue) is found in both the mesentery (yellow) and throughout the small intestine. (B) Luminal rinsing is achieved by placing a catheter into one end of the intestinal lumen and clamping off the other end with a binder clip. (C) Vascular and luminal perfusion is achieved by a catheter (top left) placed into the vasculature and a modified catheter (top right) placed the intestinal lumen. (D-F) A gross color change of the intestinal tissue from opaque to white/translucent throughout the decellularization procedure.

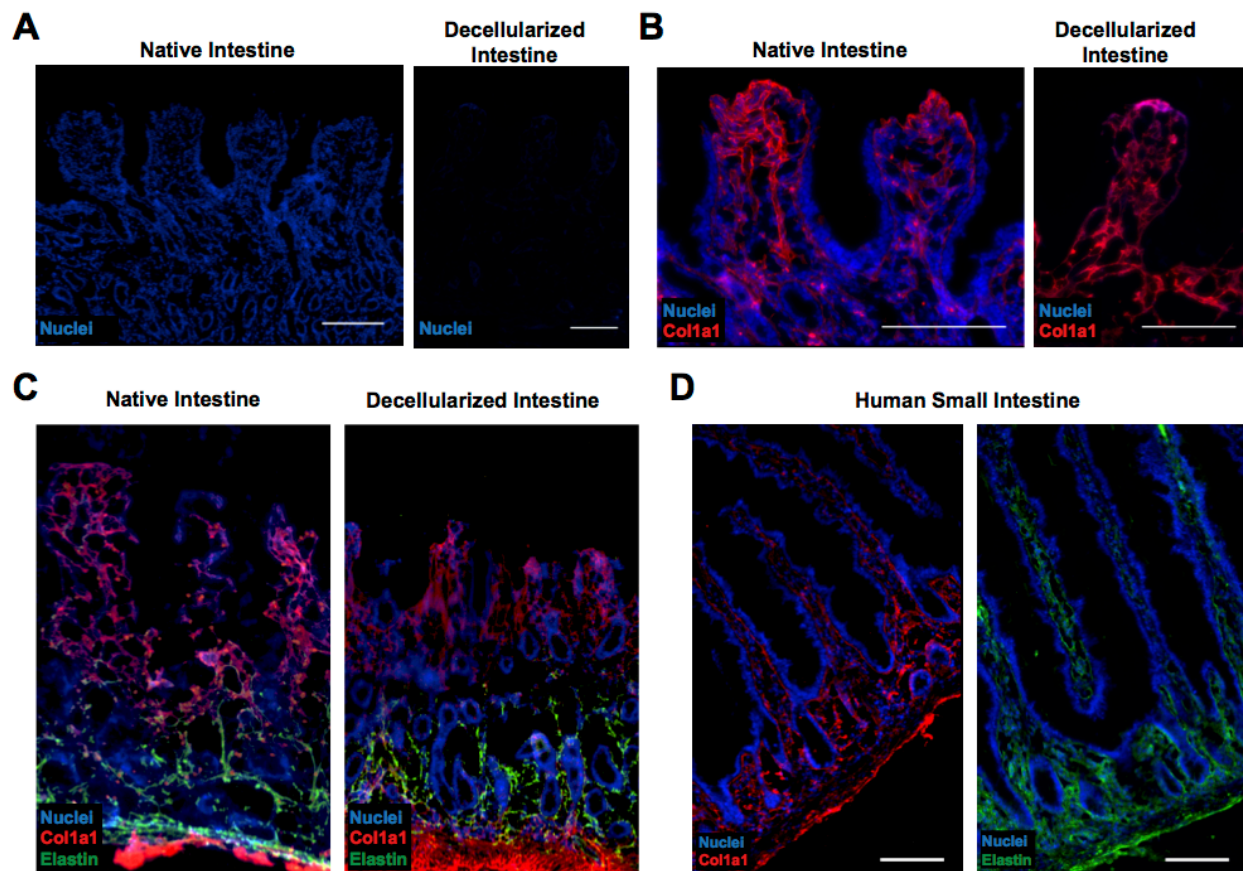


Figure 3.2. Intestinal scaffolds retain architecture and ECM composition. (A) Native porcine small intestine (left) and decellularized intestinal scaffold immunostained for nucleic acid (blue). (B) Mucosa of native intestine (left) and intestinal scaffold (right) immunostained for Col1a1 (red) and nuclei (blue), highlighting the intact villus architecture of the small intestine. (C) Full-thickness native intestine (left) and intestinal scaffold (right) immunostained for Col1a1 (red), Elastin (green) and nuclei (blue) demonstrating retention of ECM. (D) Human small intestine immunostained for Col1a1 (red), Elastin (green) and nuclei (blue) demonstrating similar ECM patterning to porcine intestine. Scale bar = 100µM.

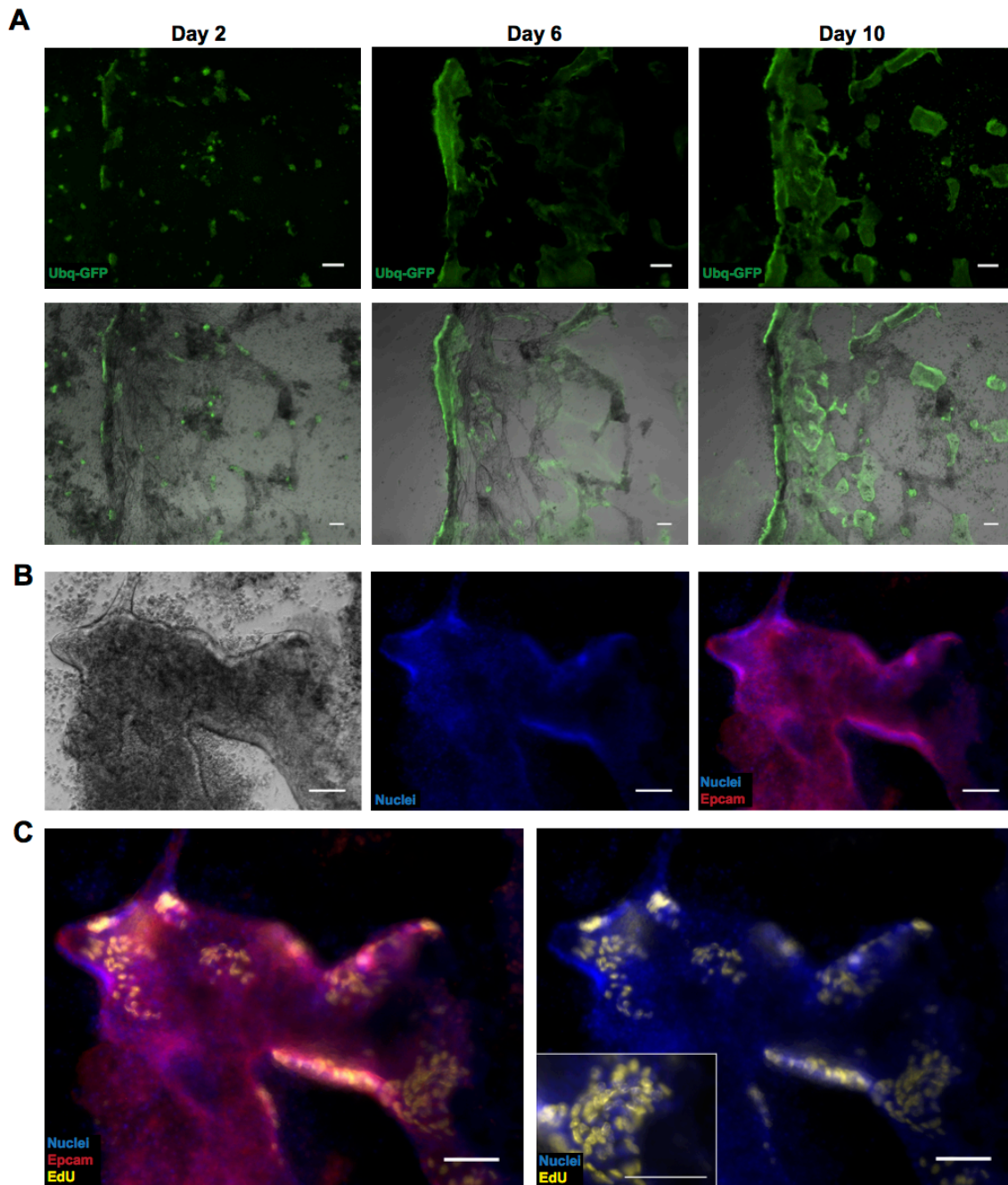


Figure 3.3. Intestinal scaffolds support intestinal epithelial cell proliferation. (A) Representative images of sixty micron sections of intestinal scaffold and Ubq-GFP intestinal epithelium (green, top) 2, 6, and 10 days post-epithelial seeding. Bright field images (bottom) show cell seeding on scaffolds. (B) Cells on scaffolds are marked by nuclei (blue) and the epithelial cell marker Epcam (red). (C) Edu+ proliferating cells (yellow) are marked by nuclei (blue) and Epcam (red). Edu+ cells (yellow) are found in small clusters, similar to spatial organization in crypts *in vivo*. Scale bar = 100µM

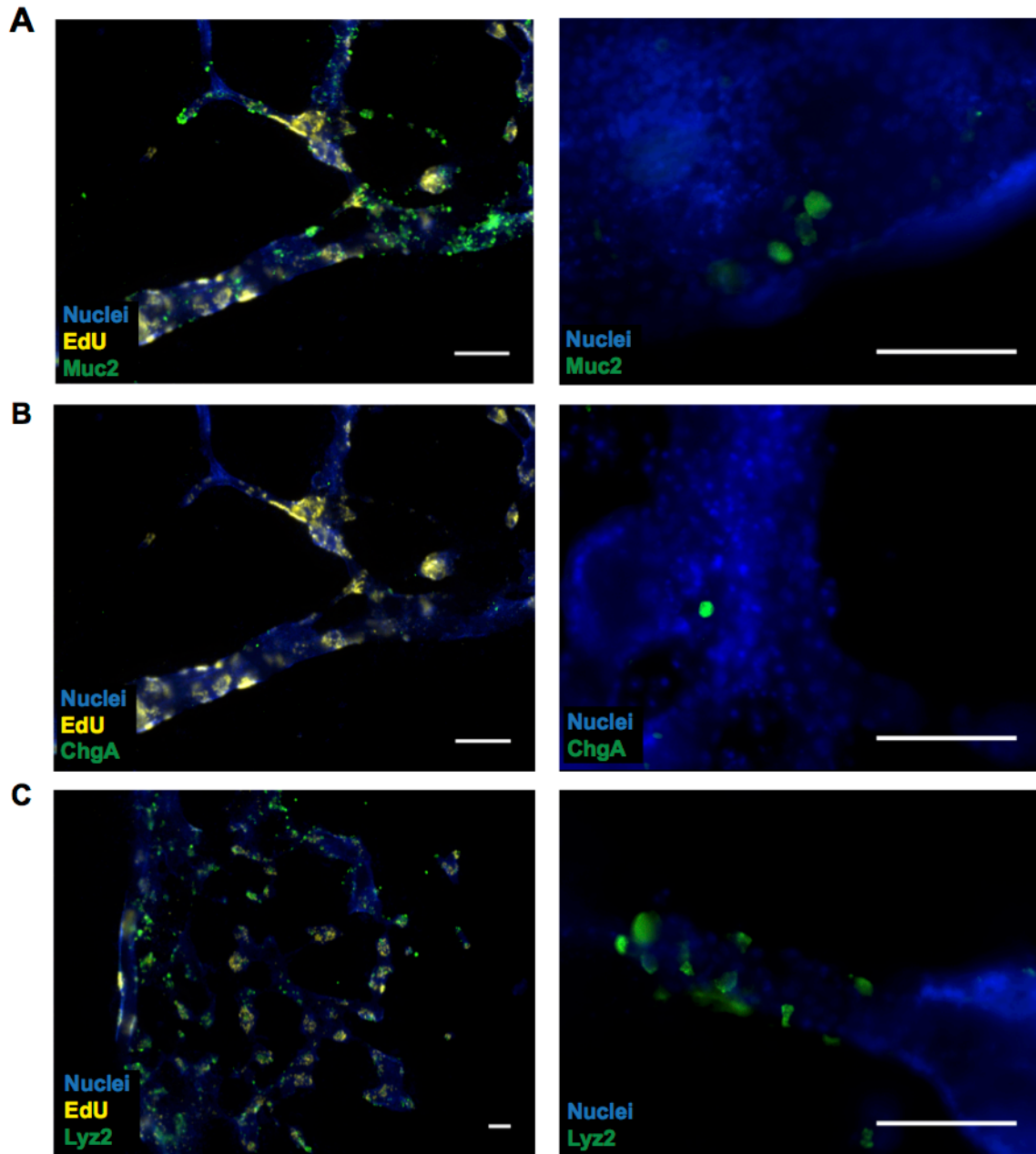


Figure 3.4. Intestinal scaffolds support intestinal epithelial cell differentiation. (A) Immunostaining for Muc2⁺ goblet cells (green), Edu⁺ proliferating cells (yellow), and nuclei (blue). (B) Immunostaining for ChgA⁺ enteroendocrine cells (green), Edu⁺ proliferating cells (yellow), and nuclei (blue). (C) Immunostaining for Lyz2⁺ Paneth cells (green), Edu⁺ proliferating cells (yellow), and nuclei (blue). Scale bar = 100 μ M

CHAPTER 4: SCOPE OF WORK, SIGNIFICANCE, AND IMPLICATIONS FOR FUTURE STUDIES

IL22 levels are physiologically important

Interaction between the local and recruited immune cells in the intestine has been studied in the context of interaction with the epithelium as a whole⁸⁴; however, few studies specifically investigate the effect that immune cells have on the ISC. In Chapter 2, an *in vitro* model of ileal ISCs was utilized to determine the specific effect that recombinant IBD-related cytokines played on ISC dynamics. This screening approach is attractive to identify ISCs reactions to exogenous factors and recent technological advances have made this type of assay even more specific and high-throughput⁴⁸. The approach of the *in vitro* model system allowed for the specific interaction of IL22 and ileal ISCs, which interact *in vivo* during inflammation, to be studied in a controlled, reproducible environment, which is a strength of the study as a whole. Ultimately, these studies revealed a dose-dependent effect of IL22 on ISCs isolated from the ileum, suggesting a novel, dual role of IL22 in the small intestine where low levels encourage ISC regeneration and high levels promote TA progenitor cell proliferation and differentiation. This anti-inflammatory role of IL22 at low levels is supported by clinical data from patients with mild to moderate Crohn's disease being treated with Ustekinumab (Stelara), which blocks Interleukin 23, and in turn lowers IL22 levels^{194,195}. Use of Ustekinumab in Crohn's disease patients that did not respond to TNF-alpha therapy has showed great promise

with a majority of patients showing clinical response¹⁹⁴, suggesting that lowering levels of IL22 may lead to disease remission.

IL22 has also recently been the direct focus of therapeutics for the treatment of intestinal epithelial wound healing, as IL22 has been suggested to directly promote ISC regeneration¹²⁰. In mouse models of graft-versus-host disease, the use of an IL22 fusion protein that stabilizes IL22, increased survival and decreased disease pathology¹²⁰. Since then, a human IL22 fusion protein, known as “IL22-Fc” or “UTTR1147A”, has been developed by Genentech and is currently in Phase I clinical trials for patients with ulcerative colitis. The implications of increasing IL22 in a human patient is more complex than an *in vitro* model system, considering the diffusion rates of IL22 throughout the body, supplemental IL22 degradation, and the presence of IL22BP and its ability to sequester IL22 before it interacts with epithelial cells. Measurement of IL22 that actually reaches the intestinal epithelium and interacts with the ISCs during therapy is challenging; however, it may be indirectly estimated by intestinal mucosal biopsy, where the regenerative capacity of ISCs can also be assessed in response to elevated IL22 levels. Nevertheless, the clinical consequence of elevated levels of IL22 should be closely monitored in light of the data presented in Chapter 2. The long-term use of IL22 supplementation should also be carefully examined as accumulation of IL22 may also lead to prolonged inflammation.

The data presented are limited in their applicability to intestinal inflammation in the intestine as a whole, as they focus on one cytokine in one region of the small intestine. However, the intestine is dynamic and each region has a specialized epithelium and immune system¹⁰, so investigation into segment response is needed to fully understand how regional populations ISCs respond to inflammation. Previous investigation into the

influence of IL22 on ISCs isolated ISCs from the whole small intestine¹²⁰, which limits the physiological relevance of the findings since IL22-secreting cells, inflammation, and Crohn's disease are all less abundant in the proximal small intestine. However, the described *in vitro* assay, as well as the methods of investigation outlined in Chapter 2 can be easily translated to other cytokines, other regions of the gastrointestinal tract, or other species of ISCs.

The work presented in Chapter 2 has been reviewed at *Cellular and Molecular Gastroenterology and Hepatology* and is currently in revision. In order to strengthen the revised manuscript, I plan to further characterize the organoids after IL22 exposure and more precisely characterize the spatial location of ILC3s within the mouse ileum. Reviewers were interested in the mechanism for increased Reg family gene expression, with the suggestion that it may be in part due to upregulation of *NOD2*. I will investigate the effect that *NOD2* has on the expression of the Reg family of antimicrobials by treating *NOD2*-knockout organoids with IL22 and it is expected that IL22 will not be able to upregulate *Reg3b* and *Reg3g* without *NOD2* present. Additionally, the concept of autophagy was briefly discussed in the manuscript, as autophagy in response to bacterial sensing has been shown to be *NOD2*-dependent and *NOD2* was found to be upregulated with IL22 treatment. I will measure autophagy by Western blot analysis for Microtubule-associated protein 1A/1B-light chain 3 (LC3), which is recruited to autophagosomal membranes. It is expected that IL22-treated organoids will have an increased expression of LC3-II, suggesting increased autophagy as well as an explanation for the decrease in Paneth cell numbers. Finally, we will provide a more accurate computational model of ILC3 secretion of IL22 by defining parameters associated with ILC3s *in vivo*. I will perform

immunohistochemistry on sections of mouse ileum for ROR γ t, which marks IL22-producing ILC3s in the intestine, to determine the distance between ILC3s and ISCs, innate lymphoid follicle size, and the number of ILC3s per follicle.

Acellular porcine intestine is an attractive scaffold for intestinal tissue engineering

Underlying the epithelium and supporting all cell types in the intestine, the ECM is integral to ISC survival both *in vivo* and *in vitro*. The mesenchyme of each tissue is specifically tailored to promote the attachment, migration, and proliferation of resident cells^{75,79}. Use of this naturally occurring scaffold for tissue engineering gives a distinct advantage over synthetic scaffolds as it retains the architecture and protein composition in the proper 3-dimensional gradients and patterns⁷⁵. Decellularized scaffolds have also been shown to retain ECM-associated glycosaminoglycans as well as bound growth factors and cytokines, allowing for other organs to be successfully de- and re-cellularized, including the liver, heart, lung, and kidney¹⁹⁶.

The data presented in Chapter 3 is only the start of the process of creating the optimal acellular intestinal scaffold. Current defined criteria for effective decellularization include: removal of cells and DNA content, quantification of residual detergents, preservation of ECM components, maintenance of 3D architecture and vascular integrity, and biomechanical performance¹⁹⁶. The lack of nuclei present and retention of two major ECM proteins post-decellularization are promising for the future translational use of the described intestinal scaffolds. Most importantly, the intestinal scaffold supports the growth, proliferation and differentiation of mouse ISCs without the need for exogenous

ECM, such as the previously required Matrigel or Collagen Type I substrates. This suggests that the acellular scaffold has all ECM components necessary to support epithelial cell growth and highlights its translational potential as a scaffold to support human cell growth. However, extrapolation of the abilities of the scaffold are limited as only mouse primary epithelial cells were tested for their compatibility with the scaffold in a 2-dimensional assay using thin sections of the acellular scaffold. The next steps in intestinal scaffold development include confirming that acellular scaffolds met established decellularization criteria, decellularizing larger pieces of intestine, and reperfusing intestinal cell types through the patent vasculature.

Development of an acellular intestinal scaffold will be useful in many future applications. As previously discussed, porcine intestinal tissue is a by-product of the agriculture industry; therefore, the starting material for large pieces of intestine are readily available and decellularization techniques can be scaled up to incorporate physiologically-relevant sized pieces of intestine. Although the completion of a full-thickness bioengineered intestine is still far off, the use acellular intestinal scaffolds can have a more immediate use. For intestinal-specific therapies, acellular intestinal ECM could be used as a “band aid” to patch ulcers associated with IBD by providing a substrate for epithelial and mesenchymal cells to interact with. Furthermore, this “band aid” could be enhanced with antimicrobials to help limit invasion of microbes and/or growth factors to help promote epithelial regeneration. More specific decellularization of ECM found surrounding the crypts versus villi may also differentially influence intestinal cell proliferation and differentiation, providing a more specific ECM substrate to promote epithelial regeneration. Isolated ECM from other tissue sources has been ground up into

a powder or made into a hydrogel, further displaying the potential therapeutic benefits of acellular ECM¹¹⁷. An intestinal ECM hydrogel could coat tissue culture plates as a more physiologically relevant substrate for *in vitro* intestinal cell culture or be sprayed on ulcers through a colonoscope¹¹⁷.

The research and development of this project highlights the complexity of the intestinal ECM and its integral influence on both intestinal homeostasis and recovery from damage. The requirement of a specific ECM for the proper proliferation and differentiation of ISCs and other cell types suggests the idea of dynamic reciprocity in the intestine. Dynamic reciprocity is a long-standing theory and explains the ongoing, bidirectional interaction between cells and ECM and has been thoroughly investigated in regenerative models including wound healing and tumorigenesis where resident cells and ECM are being remodeled¹⁹⁷. However, little is known about the concept of dynamic reciprocity in the intestine between the ECM and the many cell types in is in contact with. To further investigate this concept, the interaction between the ECM, myofibroblasts, and ISCs was the focus of my Ruth L. Kirschstein Predoctoral Individual National Research Service Award (F31DK107137). The focus of this fellowship was to investigate the role of Collagen XVIII (Col18a1), which found in the basement membrane in the ISC niche and able to sequester Wnts. Although initially thought to be made in epithelial cells, single cell RNA-seq and immunohistochemistry revealed that Col18a1 was not of epithelial origin. Col18a1 was found to be expressed in myofibroblasts within the lamina propria surrounding the crypts. Interestingly, single cell RNA-seq revealed an increased number of colonic myofibroblasts expressed *Col18a1* during colitis, suggesting a role for Col18a1 during intestinal damage and regeneration. Although the data were not presented in this

dissertation, these findings have led to interesting insights into how the supportive ECM created by surrounding myofibroblasts is dynamic and heterogeneous, suggesting that the ECM in the niche is complex and may influence ISC proliferation and differentiation. These findings provide even more support towards using a native ECM scaffold for intestinal engineering, as recapitulating the complex microenvironment will be challenging using individual or synthetic scaffolding materials.

Extrinsic niche factors influence ISC proliferation and differentiation

The data presented in this dissertation adds to an ever-expanding field of gastrointestinal research by: 1. Identifying a dose-dependent role for IL22, where elevated levels of IL22 limit ISC expansion, and 2. Developing a small intestinal acellular scaffold that supports ISC proliferation and differentiation. Together, these findings underscore the importance of extrinsic niche signaling on ISC proliferation and differentiation. Niche factors are integral for the survival and proliferation of ISCs; therefore, understanding the ISC environment during homeostatic, damage, and regenerative responses is important for the development of therapeutics for patient health. The scope of work presented here is limited to the small intestine; however, it provides the basis and rationale to continue investigation into ISC niche interactions to further understand human health.

APPENDIX A: ORGANOID CULTURES FOR ASSESSING INTESTINAL EPITHELIAL DIFFERENTIATION AND FUNCTION IN RESPONSE TO TYPE-2 INFLAMMATION¹

Overview

During helminth infection of the gastrointestinal tract, a complex Type-2 inflammatory response involving immunological and mucosal components is mounted to clear the infection and re-establish a physiologically normal state. This response is characterized by the secretion of key interleukins, which impact epithelial lineage allocation and drive tuft and goblet cell hyperplasia to lead to eventual clearance of parasitic organisms. While there have been advances towards understanding Type-2 inflammatory responses in the intestine, detailed cellular and molecular mechanisms of epithelial responses to general inflammation and specific inflammatory cytokines remain to be explored. Intestinal organoids represent a physiologically relevant *in vitro* model to study how Type-2 inflammation impacts stem cell maintenance and differentiation, and offer a new approach for investigators to test compounds that modulate mechanisms involved in worm clearance. The methods described in this chapter include: (1) intestinal crypt and single cell isolation, (2) organoid culture and cytokine treatment, as well as methods for downstream organoid analyses: (3) gene expression analysis by qRT-PCR, (4) protein analysis by western blot, immunohistochemistry, and florescent-activated cell sorting, and (5) organoid self-renewal by serial passaging.

¹This chapter will appear as a book chapter in *Type 2 Immunity: Methods and Protocols* (Methods in Molecular Biology), “Organoid cultures for assessing intestinal epithelial differentiation and function in response to Type-2 inflammation”, 2018, Bailey Zwarycz, Adam D. Gracz, Scott T. Magness. ©Springer Science+Buisness Media LLC. With permission of Springer Nature.

Introduction

The gastrointestinal tract is a complex organ that functions as the site of nutrient and water absorption at the interface of the lumen and the epithelial monolayer. The lumen is home to a vast number of commensal microbiota that exist in a symbiotic relationship with the host organism, and while these microbiota play a critical role in health, it is essential that they are restricted to the luminal compartment by an uncompromised epithelial monolayer. The epithelial barrier can be compromised by physical injury or by pathogenic microbiota that are ingested by the host. When this occurs acutely on a large scale the host may succumb to sepsis, but at the chronic small scale the host may develop conditions associated with inflammatory bowel disease (IBD). A host infected with pathogenic microbes may not present with clinical symptoms because of an insufficient inoculum, inability of pathogenic strains to outcompete the commensal communities, or because of efficient physiologic clearance by the host immune system. Surveillance of pathogenic microorganisms by the intestinal epithelium requires complex coordination between the epithelial cells that serve as the primary barrier to luminal contents and other submucosal cell types that actuate the immune response. Epithelial Tuft cells have an essential role in monitoring the luminal environment for parasitic infection and communicating this information to the underlying immune cell compartment that responds to the infection¹⁹⁸⁻²⁰².

Tuft cells are one of six primary differentiated lineages found in the intestinal epithelium, and until recently, their function remained unknown. Decades ago, tuft cells were first described as 'Brush cells' based on the presence of apical tufts of stiff microvilli²⁰². In homeostasis, Tuft cells are considered a very rare epithelial cell (~0.4% -

1.0%), however, following infection of the host by helminths, a type of microscopic worm, the intestinal epithelium undergoes tuft cell hyperplasia (~7.2%) in an effort to clear the worms¹⁹⁹. Aside from morphological identification, a number of biomarkers are now associated with the tuft cell lineage including: *Dclk1*, *Cox1*, *Plcγ2*, *Gfi1b*, *Trpm5*, and high levels of *Sox9*^{21,28,199,200}. At a transcriptomic level, tuft cells demonstrate a Th2 gene expression signature suggesting that they have the capacity to respond to infection through a specific interleukin response²⁰³. Recent studies confirm this prediction by showing that tuft cells are involved in a positive feedback circuit initiating a Type-2 immune response to helminth infection¹⁹⁸⁻²⁰⁰.

In the intestine, Type-2 immune responses are commonly associated with helminth parasitic infection, but also participate in IBD²⁰⁴. CD4⁺ lymphocytes are classically known as a mediator for Th2 immunity, but a subset of innate lymphoid cells known as ILC2 cells in the submucosa are now recognized as key mediators of Th2 responses in the intestine. ILC2 cells are characterized by expression of IL-4, IL-5, and IL-13 which in turn activate other immune cell types (basophils, mast cells, and eosinophils) that assist in clearing the infection²⁰⁵. Tuft cell function involves a sophisticated positive feedback loop between helminths, the differentiated epithelium, ILC2s, and the undifferentiated stem/progenitor cell compartment (Figure 5.1)¹⁹⁸⁻²⁰⁰. Upon parasitic infection, tuft cells detect the presence of helminths or protozoa through a *Trmp5*-dependent chemosensory pathway¹⁹⁹. This causes tuft cells to secrete IL-25 that in turn acts on submucosal ILC2 cells (Figure 5.1A), which secrete IL-13 (Figure 5.1B). ILC2 cells are in close proximity to the stem/progenitor cell compartment and the IL-13 secreted by ILC2 cells promotes lineage bias toward tuft and goblet cells (Figure 5.1C, D). Goblet cell hyperplasia has a

dual function to increase mucous to protect the epithelium and aid in worm clearance, while tuft cell hyperplasia serves to increase sentinels to monitor and respond to the worm infection. Increases in tuft cell numbers continue to fuel the IL-25 positive feedback during infection (Figure 5.1E). Reduction in worm burden serves as a break to tuft and goblet cell hyperplasia and the epithelium returns to homeostasis (Figure 5.1F). While significant strides have been made to understand the cellular mechanisms regulated by the tuft cell-ILC2 axis, much remains to be investigated related to the impact of other Th2 cytokines on ISC differentiation, the specificity of tuft cell responses to different helminth species, and additional roles that tuft cells may play in regulating the microbiome in health and disease.

Animal models have served a critical role in moving the Th2-field forward; however, there is substantial merit for using culture models to address questions that are not feasible in animal models, and to develop *ex vivo* platforms that are useful for screening compounds that are capable of enhancing or abrogating Th2 responses. Intestinal organoid technology has revolutionized *in vitro* study of gastrointestinal epithelial biology and has recently been applied to investigate Type-2 immune responses^{199,200}. Intestinal organoids are stem cell driven structures derived from whole isolated crypts or single ISCs that can be spherical or budding in nature, depending on proliferation status⁴⁸. They are non-transformed and are capable of growing indefinitely in a three-dimensional extra cellular matrix (typically Matrigel) with a defined media consisting of essential growth factors found in the ISC *niche in vivo*^{32,54}. Nomenclature for organoids has been further refined as 'enteroids' when derived from small intestinal tissue, or 'colonoids' when derived from colonic tissue⁵⁶. Organoids represent a powerful tool to study Type-2

immune responses due to their ability to: (1) generate all the differentiated lineages found in the gastrointestinal tract and (2) maintain an ISC compartment that is able to respond to extrinsic signals that influence ISC proliferation and differentiation. While organoids are comprised exclusively of epithelial cells, the cytokine environment produced by a Th2 response can be recreated in culture media, and organoids are capable of being co-cultured with other cell types that impact Type-2 immunity. The properties render organoid cultures highly adaptable and amenable to detailed mechanistic analysis.

Organoids generated from normal mouse strains typically used in research settings can be readily evaluated for proliferation and differentiation by immunostaining, and gene expression can be interrogated by qPCR or RNA-seq analysis. While these standard methods are useful, a number of transgenic mouse lines that express fluorescent reporter gene associated with secretory lineages involved in Type-2 immunity enable detection and isolation of live cells for analysis. *Dclk1*, *Gfi1b*, *Il25*, and *Trpm5* represent biomarkers highly restricted to the tuft cell lineage^{21,198,199,201}. A *Dclk1*-CreERT2 transgenic mouse line has been developed that enables identification, isolation by fluorescent-activated cell sorting (FACS), and evaluation of tuft cells when crossed to a mouse line harboring conditional fluorescent reporter allele like ROSA-flox-STOP-flox-EGFP. Additionally, *Gfi1b*-EGFP, *IL25*-RFP, and *Trpm5*-EGFP transgenic mouse lines have likewise demonstrated restricted expression to tuft cells and do not require a separate fluorescent reporter allele^{198,199,206}.

The focus of this chapter is to provide step-by-step methods for: 1) producing conditioned media that supplies the necessary growth factors for organoid culture, 2) isolation of crypts from mouse small intestine, 3) culturing crypts in ECM and conditioned

medial to generate organoids, 4) splitting organoids for continual maintenance in culture, and 5) analyzing organoids by immunostaining, qPCR, flow cytometry, and western blot for responses to Type-2 immune responses.

Materials

Generating Conditioned Media

1. Cultrex R-spondin1 293T cells (Trevigen)
2. Tissue Culture Treated Dishes 150 x 20mm (Genesee)
3. Dulbecco's Phosphate Buffered Saline (DPBS (1X), Gibco)
4. Selection Media: Dulbecco's Modified Eagle Medium (DMEM, Gibco), 10% Fetal Bovine Serum (Gemini), 100 U/mL Penicillin/Streptomycin (Invitrogen), 2mM GlutaMax (Gibco), 300 µg/mL Zeocin (Thermo Fisher)
4. Culture Media: Dulbecco's Modified Eagle Medium (DMEM, Gibco), 10% Fetal Bovine Serum (FBS), 100 U/mL Penicillin/Streptomycin (Invitrogen), 2mM GlutaMax (Gibco)
5. Harvest Media: Advanced Dulbecco's Modified Eagle Medium/F12 (DMEM/F12, Gibco), 100 U/mL Penicillin/Streptomycin (Invitrogen)
6. 0.22 µm bottle top filter
7. Freezing Media: DMEM, 20% FBS, 10% Dimethyl sulfoxide (DMSO)

Crypt-enriched intestinal epithelial isolation

1. Dulbecco's Phosphate Buffered Saline (DPBS): 1X DPBS
2. 0.5 M EDTA, pH 8.0

3. 3 mM EDTA
4. 10 cm petri dishes
5. 70% Ethanol
6. Dissection tools: surgical scissors, dissection forceps
7. Glass plate
8. 100 μ m cell strainer
9. 2X ISC Medium: Advanced DMEM/F12, 200X N2 (Invitrogen), 100X B27 without Vitamin A (Gibco), 2 mM HEPES (Gibco), 4mM Glutamax (Gibco), 200 U/mL Penicillin/Streptomycin (Gibco) (See Note 1)

Organoid culture and cytokine treatment

1. Tissue culture plate (Genessee) (See Note 2)
1. Extracellular Matrix: Growth Factor Reduced Matrigel (Corning) or Cultrex (Trevigen) (See Note 3)
2. Recombinant Interleukin 4 (IL-4)
3. Recombinant Interleukin 13 (IL-13)
4. 2X ISC Medium (See Note 1)
5. ENR (EGF/Noggin/R-spondin 1) medium: 50% 2X ISC media (see above), 40% Advanced DMEM/F12, 10% RSPO1-conditioned media (see Section 2.1 above for creation of this conditioned media), 50 ng/mL recombinant murine EGF, 100 ng/mL recombinant murine Noggin, 10 μ M Y-27632 (Selleck Chemicals) (See Notes 4-6)

RNA lysis and gene expression analysis

1. RNAqueous Micro Kit (Ambion)
2. Dulbecco's Phosphate Buffered Saline
3. 1.7 mL microcentrifuge tubes
4. iScript cDNA Synthesis kit (BioRad)
5. Taqman Probes (see Table 1)

Protein lysis for western blot

1. Cell Recovery Solution (Corning)
2. 1.7 mL microcentrifuge tubes
3. Dulbecco's Phosphate Buffered Saline
4. 2X RIPA buffer: 0.3M NaCl, 0.1M Tris-HCl, 0.05% Sodium Azide, 2% Triton X-100, 2% Sodium Deoxycholate (w/v), 0.2% Sodium dodecyl sulfate in H₂O
5. Protease Inhibitor Cocktail (Sigma)
6. Phosphatase Inhibitor Cocktail (Sigma)
6. Phenylmethylsulfonyl fluoride (PMSF)
7. 2X RIPA inhibitor buffer: 1% protease inhibitor cocktail, 1% phosphatase inhibitor cocktail, and 1 μ M PMSF in 2X RIPA buffer

Immunofluorescence analysis – sections

1. 4% Paraformaldehyde (PFA) in H₂O
2. 30% Sucrose in H₂O
3. Parafilm

4. 15 mm x 15 mm x 5 mm Cryomold
5. Optimal Cutting Temperature (OCT) Compound
6. Dry Ice
7. Charged Glass Slides (Superfrost Plus)

Immunofluorescence analysis – whole mount

1. 4% Paraformaldehyde (PFA)
2. Dulbecco's Phosphate Buffered Saline (DPBS)
3. 0.5% Triton X-100 in PBS
4. 100 mM glycine in PBS
5. Normal goat serum (NGS)
6. Immunofluorescence (IF) Buffer: 0.1% BSA, 0.2% Triton X-100, 0.05% Tween-20 in PBS
7. Primary and secondary antibodies (end user determined targets)
8. Parafilm
9. Optional: Bisbenzimidazole
10. Optional: Antifade Media

Preparation of cells for staining and analysis of intracellular markers by flow cytometry/FACS

For crypt dissociation flow cytometry/FACS:

1. Hanks Balanced Salt Solution (HBSS) (Gibco)

2. 50 U/mL Dispase
3. 20,000 U/mL Deoxyribonuclease I (DNase I) from bovine pancreas
4. Y-27632 (Selleck Chemical)
5. Disassociation solution: 0.6 U/mL Dispase, and 120 U/mL DNase I, and 10 μ M Y-27632 in HBSS
6. Fetal Bovine Serum (FBS)
7. 40 μ m cell strainer (Falcon)
8. Dulbecco's Phosphate Buffered Saline (DPBS)
9. 2X ISC Medium (See Note 1)

For *Dissociation of organoids for flow cytometry/FACS*:

1. TrypLE Express (Gibco)
2. Y-27632 (Selleck Chemical)
3. Water bath set to 37°C
4. Dulbecco's Phosphate Buffered Saline (DPBS (1X), Gibco)
5. 40 μ m cell strainer (Falcon)
6. Dulbecco's Phosphate Buffered Saline (DPBS (1X), Gibco)
7. 2X ISC Medium (See Note 1)

For *Intracellular staining for flow cytometry/FACS*:

1. 1% Bovine Serum Albumin (BSA) in 1X DPBS
2. 4% Paraformaldehyde (PFA) in H₂O
3. Permeabilization buffer: Permeabilization Buffer (10X) (eBioscience) diluted to 1X in 1% BSA in PBS

Serial passaging for functional analysis

1. TrypLE-Express (Gibco)
2. Y-27632 (Selleck Chemical)
3. 1.7 mL microfuge tubes
4. Advanced DMEM/F12
5. Extracellular Matrix: Growth Factor Reduced Matrigel or Cultrex
6. ENR (EGF/Noggin/R-spondin 1) medium (See Note 7)

Methods

Generating Conditioned Media

1. Plate Cultrex R-spondin1 293T cells in 15cm tissue culture plate with 20 mL Selection media
2. Allow cells to grow to ~95% confluency, changing media every 2 days
3. Split cells 1:25 into 25 15cm tissue culture plates with 20 mL Culture media
4. Allow plates to grow to approximately 50% confluency. Remove Culture media. Rinse plates twice with room temperature 1X DPBS. Add 20 mL Harvest media to plates.
5. After ~24 hours, collect media from plates. This is the “first harvest” of conditioned media. Filter through 0.22 μ m filter into sterile container and store at 4°C until second harvest.
6. Add 20 mL Culture media to each plate and allow cells to grow to 80-90% confluency. Again, remove culture media. Rinse plates twice with 1XDPBS. Add 20 mL Harvest media to plates.

7. After ~24 hours, collect media from plates. This is the “second harvest” of conditioned media. Filter through 0.22 µm filter into sterile container and store at 4°C. (See Note 8)
8. After both collections are obtained, combine harvests in a sterile container and thoroughly mix.
9. Aliquot media into 40mL aliquots and store frozen at -80°C. (See Note 9)

Crypt-enriched intestinal epithelial isolation

1. Prepare and label the following 50 mL conical tubes, one set (a-d) per mouse. All tubes should be pre-chilled on ice or at 4°C prior to crypt isolation:
 - a. Tube “P”: 10 mL DPBS
 - b. Tube “E1”: 10 mL 3 mM EDTA in DPBS
 - c. Tube “E2”: 10 mL 3 mM EDTA in DPBS
 - d. Tube “S”: 10 mL DPBS
2. Prepare and label two 10 cm petri dishes containing 10 mL DPBS each, per mouse
3. Euthanize mouse in accordance with institutionally approved humane practices
4. Clean mouse abdomen around planned incision area using 70% EtOH
5. Open abdomen with surgical scissors and dissect desired length of intestine (See Note 10)
6. Place dissected intestine in first of two DPBS-containing 10 cm petri dishes
7. Open intestine longitudinally by cutting down the length of the lumen with sharp surgical scissors (See Note 11)

8. Rinse opened intestine by gripping tissue with forceps and gently swirling in DPBS-containing petri dish to remove fecal matter
9. Transfer intestinal tissue to Tube "P" using forceps and invert gently 5-10 times to remove remaining fecal matter
10. Transfer intestinal tissue to Tube "E1" and incubate for 15 minutes at 4°C, with gentle agitation (See Note 12)
11. While tissue is incubating in "E1", prepare a glass plate or dish by cleaning with 70% EtOH followed by sterile DPBS
12. Remove tissue from "E1" and transfer to prepared glass plate, positioned so that luminal side is facing up
13. Using a sterile pipette tip, gently "brush" the full length of intestinal tissue, first in one direction, then in the opposite direction. This step will remove a majority of villus tissue, leaving crypts intact. Avoid brushing too forcefully or for an extended period of time in order to preserve crypts (see Figure 5.2B vs Figure 5.2C)
14. Transfer brushed intestine to second DPBS-containing 10 cm petri dish and rinse off remaining villi by gripping tissue with forceps and gently swirling, as in step 8.
15. Transfer tissue to lid of second DPBS-containing petri dish (lid should not contain any buffer) and cut into 2-3 cm pieces using surgical scissors
16. Transfer intestinal pieces into Tube "E2" and incubate for 35 minutes at 4°C, with gentle agitation, as in step 10.
17. Transfer intestinal pieces into Tube "S" and shake gently for 2-5 minutes to remove epithelium (including crypts) (Figure 5.2D). (See Note 13)

18. Add 10 mL DPBS to Tube “S” and filter crypt epithelial slurry through 100 μ m cell strainer into new 50 mL conical to enrich epithelial suspension for crypts (Figure 5.2E)
19. Pellet crypts at 500 x g-force, 4°C for 5 minutes
20. Discard supernatant and resuspend crypt pellet in 250-500 μ L 1X ISC media
21. Prepare three 1:10 dilutions of concentrated crypt slurry and determine average number of crypts per 1 μ L volume by counting on inverted light microscope (See Note 14)

Organoid culture and cytokine treatment

1. Pre-chill all tubes and tips to be used for handling 3D extracellular matrix (ECM) reagent (See Note 15)
2. Depending on experimental needs, place a 48 well or 96 well plate(s) in cell culture incubator to pre-warm to 37°C prior to plating ECM
3. Prepare the total volume of ECM needed per crypt sample by transferring to a 1.7 mL conical on ice. (See Notes 16 and 17)
4. Using crypt concentration previously determined in Section 3.2 Step 21, add desired number of crypts to be plated to ECM and mix by gently pipetting to disperse crypt slurry evenly in ECM (See Notes 18-20)
5. Create “bubbles” of crypt-containing ECM by pipetting appropriate volume (10 μ L for 96 well plate; 20-50 μ L for 48 well plate) directly in the center of each well of the plate (Figure 5.3A-D)

6. Taking care to avoid disturbing freshly-plated “bubbles”, transfer well plate to 37°C cell culture incubator and allow to polymerize for 15-20 minutes (See Note 21)
7. While ECM is polymerizing, prepare ENR media: 250 µL per well of 48 well plate; 100 µL per well of 96 well plate (See Note 22)
8. Following polymerization, overlay ECM “bubbles” with appropriate volume of media. To avoid damaging ECM, pipet media down the side of each well. Avoid pipetting media directly into ECM “bubble” (Figure 5.3E-G)
9. Complete ENR media should be changed every 48 hours throughout duration of organoid cultures
10. Following organoid establishment, Type-2 epithelial responses (e.g.: goblet and tuft cell differentiation) can be induced by the addition of cytokines IL-4 and IL-13. We have noted strongest induction of goblet/tuft cell hyperplasia in jejunal organoids treated with 100 ng/mL IL-13 (Biolegend), but optimal cytokine concentrations should be determined per intestinal segment studied and by manufacturer source of recombinant protein. (See Note 23)

RNA lysis and gene expression analysis

1. To lyse and isolate total RNA from organoid cultures which consist of low numbers of cells, we recommend the RNAqueous Micro Kit (Ambion)
2. Aspirate full volume of media from wells to be lysed using P200 (96 well plate) or P1000 (48 well plate) pipette tip. Take care to avoid disturbing ECM bubble (Figure 5.3E-G)

3. Rinse wells once by adding and aspirating 100 μ L (96 well plate) or 250 μ L (48 well plate) 1X DPBS
4. Lyse organoids in ECM bubbles by adding 200 μ L (96 well plate) or 500 μ L (48 well plate) Lysis Buffer (Ambion) directly to center of each well. Allow Lysis Buffer to incubate with 3D ECM/organoids for ~5-10 seconds at RT, then collect lysate while scraping bottom of well with pipette tip to break up and dissolve any remaining solid ECM.
5. Transfer lysates to 1.7 mL microcentrifuge tubes and prepare RNA as per manufacturer instructions, or store at -80°C until RNA isolation
6. Prepare cDNA and conduct qRT-PCR as per standard laboratory protocols. We recommend the iScript cDNA Synthesis kit (BioRad) and Taqman probes for cDNA synthesis and gene expression analysis, respectively. (See Note 24) Table 1 includes the gene names and catalog numbers of Taqman probes recommended for validation of Type-2 response in epithelial organoid cultures. (See Note 25)

Protein lysis for western blot

1. Due to the number of crypts required for protein analysis by western blot, we recommend using cultures in 48-well plates (250-500 crypts per well) for these assays
2. Aspirate full volume of media from wells to be lysed using P200 (96 well plate) or P1000 (48 well plate) pipette tip. Take care to avoid disturbing ECM bubble (Figure 5.3E-G)

3. Add 500 μ L Cell Recovery Solution (Corning) to each well and break up ECM patty into recovery solution by scraping bottom of well and pipetting vigorously (See Note 26)
4. Incubate organoids in Cell Recovery Solution with end-over-end rotation for 45 minutes at 4°C
5. Pellet organoids at 5,000 x g-force for 5 minutes at 4°C
6. Aspirate and discard supernatant and rinse organoid pellet twice with 500 μ L of ice cold DPBS
7. Lyse organoids in 30 μ L 2X RIPA inhibitor buffer
8. Proceed with western blot analysis as per standard protocol

Immunofluorescence analysis – sections

1. Aspirate full volume of media from wells to be lysed using P200 (96-well plate) or P1000 (48 well plate) pipette tip. Take care to avoid disturbing ECM bubble (Figure 5.3E-G)
2. To fix organoids in ECM, add 100 μ L (96-well plate) or 250 μ L (48-well plate) freshly-prepared, room temperature 4% paraformaldehyde (PFA) and incubate at room temperature for 20 minutes (See Note 27)
3. Aspirate and discard PFA in accordance with chemical safety standards
4. Rinse each well with 100 μ L 30% Sucrose three times to remove any residual PFA
5. Add 100 μ L 30% sucrose to each well, wrap well plate in Parafilm to prevent evaporation, and store samples for at least 24 hours at 4°C

6. Take p200 tip and bend tip to use as a scraping tool. Gently scrape up organoids with bent P200 and transfer organoids and sucrose to 1.7mL microfuge tube using P200 tip attached to pipette with tip cut to create a larger bore as to not break up organoids
7. Centrifuge at 200 x g for 5 minutes at room temperature to gently pellet organoids. Remove as much 30% sucrose as possible without disturbing organoids
8. Fill a cryomold with OCT
9. Add organoids and sucrose to top left region of OCT in the cryomold, making sure not to touch the edges. To evenly distribute organoids within OCT, gently swirl the organoids and sucrose in a figure-8 shape to mix the sucrose and OCT. (See Note 28)
10. Freeze organoids in OCT on dry ice and store at -80°C
11. To section organoids: take a series of ten 8-10 µm serial sections on separate slides, then check for sectioned organoids by light microscopy (Figure 5.5). When organoid sections are located, take serial sections until full thickness of organoid has been sectioned. Repeat until desired number of sections is procured. (See Note 29)
12. Proceed with standard immunohistochemical or immunofluorescent analysis, or store slides at -80°C until use. Examples of immunofluorescent staining for DCLK1 (Tuft cells,), MUC2 (Goblet cells, Santa Cruz, Cat#sc-15334, 1:500), and LYZ (Paneth cells, Diagnostic Biosystems, Cat#RP028, 1:500), are in Figure 5.6.

Immunofluorescence analysis – whole mount

1. Aspirate full volume of media from wells to be lysed using P200 (96 well plate) or P1000 (48 well plate) pipette tip. Take care to avoid disturbing 3D ECM bubble (Figure 5.3E-G)
2. Fix organoids in ECM by adding 100 μ L (96 well plate) or 250 μ L (48 well plate) freshly-prepared, room temperature 4% PFA and incubating at room temperature for 20 minutes.
3. Aspirate and discard PFA in accordance with chemical safety standards
4. Rinse fixed wells three times with 100 μ L PBS
5. Add 100 μ L 0.5% Triton X-100 in PBS to permeabilize organoids and incubate at RT for 20 minutes
6. Aspirate permeabilization buffer and rinse wells twice with 100 mM glycine in PBS, 15 minutes at RT for each wash
7. Add 100 μ L of 10% NGS in IF Buffer to each well and incubate at RT for 90 minutes to block nonspecific antigen binding
8. Add 100 μ L of primary antibody diluted in 10% NGS in IF Buffer, wrap plate in Parafilm to prevent evaporation, and incubate overnight at 4°C
9. Aspirate primary antibody and wash each well three times in IF Buffer at RT, 20 minutes per wash
10. Add 100 μ L of secondary antibody diluted in 10% NGS in IF Buffer, incubate at RT for 2 hours
11. Aspirate secondary antibody and wash each well three times in IF Buffer at RT, 20 minutes per wash

12. OPTIONAL: To detect nuclei, dilute bisbenzimidazole 1:1000 in 1X DPBS and add to wells for 20 minutes at RT
13. Wash wells three times with an excess of 1X DPBS
14. Add 1X DPBS or antifade media to wells and image samples immediately

Analysis by flow cytometry

If analyzing primary intestinal crypts, follow methods in Methods Section 3.1 to isolate crypts, then proceed to: *Dissociation of crypts for flow cytometry/FACS* (3.8.1) . If analyzing organoid cultures, proceed to: *Dissociation of organoids for flow cytometry/FACS* (3.8.2) . If analyzing with intracellular antibodies and fixation is necessary for analysis, proceed to *Intracellular staining for flow cytometry/FACS* (3.8.3) after isolating single cells from either described method.

Dissociation of crypts for flow cytometry/FACS:

1. Pellet crypts at 1,800 x g-force for 5 minutes at 4°C
2. Resuspend crypt pellet in 1 mL HBSS, then add to 9 mL of Dissociation solution
3. Place tube in 37°C water bath for 10-15 minutes, shaking vigorously for 30 seconds every 2 minutes
4. After each shake, observe 10 µL aliquot of solution to assess extent of dissociation to single cells (See Note 30)
5. Once dissociation is complete, add 1 mL FBS to tube and place on ice
6. Filter cells through 40 µm cell strainer directly into 50 mL conical containing 5 mL ice cold sterile 1X DPBS

7. Pellet cells at 1,800 x g-force for 5 minutes at 4°C
8. Wash three times with 15 mL ice cold sterile DPBS
9. Resuspend in 1X ISC media with 10 µM Y-27632
10. Stain cells with antibodies at proper concentration for 1 hour on ice with gentle agitation 2-3 times/hour (See Notes 31 and 32)
11. Rinse twice with ice cold 1X DPBS, centrifuge at 1,800 x g-force for 5 minutes at 4°C
12. Resuspend in 1X ISC media with 10 µM Y-27632 and perform *flow cytometry/FACS*

Dissociation of organoids for flow cytometry/FACS:

1. Remove media from each well and add 100 µL (for 96 well plate well) of TrypLE Express with 10 µM Y-27632.
2. Break up enteroids and ECM with P200 tip by scraping bottom of well and pipetting up and down 30 times
3. Pool all wells of cells in 5 mL of pre-warmed TrypLE Express buffer with 10 µM Y-27632
4. Place tube in 37°C water bath for 10-15 minutes. Shake tube every 1-2 minutes for 30 seconds. After each shake, observe 10 µL aliquot of solution to judge dissociation of crypts to single cells.
5. Filter cells through 40 µm cell strainer directly into 50 mL conical containing 5 mL ice cold sterile 1X DPBS.
6. Pellet cells at 1,800 x g-force for 5 minutes at 4°C

9. Wash three times with 15 mL ice cold sterile 1X DPBS
10. Resuspend in 1X ISC media with 10 μ M Y-27632
11. Stain cells with antibodies at proper concentration for 1 hour on ice with gentle agitation 2-3 times/hour (See Notes 31 and 32)
12. Rinse 2 times with ice cold 1X DPBS, centrifuge at 1,800 x g-force for 5 minutes at 4°C
13. Resuspend in 1X ISC media with 10 μ M Y-27632 and perform flow cytometric analysis

Intracellular staining for flow cytometry/FACS:

1. Bring single cells to concentration of 10 million cells/mL in 1% BSA in PBS
2. If using a surface antibody, apply now and incubate for the appropriate time and temperature for your antibody (See Note 32)
3. Wash cells with 3 mL 1% BSA in PBS, spin down, aspirate supernatant
4. Place 100 μ L of RT 4% PFA on pellet and gently pipette up and down 10X to mix. Incubate for 15 minutes at RT
5. Wash cells with 3 mL 1% BSA in PBS, spin down, aspirate supernatant
6. Add optimized concentration of intracellular antibody to 100 μ L of Permeabilization buffer and place on cell pellet, pipette up and down to mix, incubate for 30 minutes at RT protected from light
7. Wash cells twice in 3 mL Permeabilization buffer, spin down, aspirate supernatant
8. Resuspend in 500 μ L 1% BSA in PBS for analysis by flow cytometry/FACS

Serial Passaging for functional analysis

1. Count number of living organoids in each well, record
2. Remove media from each well
3. Add 250 μ L TrypLE Express with 10 μ M Y-27632 to each well of 48 well plate
4. Scrape up each ECM bubble, pipette up and down 75 times to dissociate ECM and organoids, and transfer to 1.7mL tube containing 250 μ L TrypLE Express with 10 μ M Y-27632
5. Place in 37°C water bath for 2.5 minutes
6. Pipette cells up and down 20 times
7. Place in 37°C water bath for 2.5 minutes
8. Add 1 mL ice cold Advanced DMEM/F12 and place tube on ice
9. Centrifuge at 2,000 x g-force for 5 minutes to pellet cells
10. Carefully remove supernatant and add appropriate amount of ECM to each tube on ice (See Note 33)
11. Pipette up and down at least 50 times to resuspend cells within ECM and plate as directed in Section 3.3 (*Organoid culture and cytokine treatment*)
12. Allow ECM bubbles to polymerize for 15-20 minutes in 37°C incubator
13. Overlay ECM bubbles with 250 μ L ENR media (See Note 34)
14. Allow organoids to grow in culture for 7-10 days, then record number of living organoids present in each well. This number reflects the increase in organoid number after passaging. If necessary, repeat passaging procedure until number of required serial passages is completed. (See Note 35)

Notes

1. Media can be made 1X by adding equal volume of Advanced DMEM/F12 to 2X ISC media.
2. Other tissue culture plates may be incompatible with Matrigel/Cultrex due to the surface charge after plastic treatment.
3. Both commercially available matrices have been used to successfully grow intestinal organoids. To our knowledge and at the time of this publication, no studies quantifying differences in organoid performance using each matrix exist.
4. Recombinant Mouse R-spondin1 (250 $\mu\text{g}/\text{mL}$, R&D Systems) can be used instead of conditioned media, but conditioned media is thought to be more biologically active.
5. Y-27632 is included for first 48 hours of culture only.
6. 50 $\mu\text{g}/\text{mL}$ Primocin (Invivogen, 1,000X of 50 mg/mL stock) can be added to media if concerned about contamination at time of crypt isolation and organoid establishment. Primocin is included for first 48 hours of culture ONLY. Primocin can also be used at 100 $\mu\text{g}/\text{mL}$ (500X) if contamination persists with 50 $\mu\text{g}/\text{mL}$ concentration.
7. Optional: To encourage single cell growth, cultures receive 0.3 nM CHIR-99021 and 100 nM Valproic Acid for the first two days in culture only.
8. Cells can be discarded or frozen back down for storage in Freezing media and subsequently used to make additional batches of conditioned media.
9. Protein activity in conditioned media can be determined by commercially available ELISA or protein activity assays, as desired.

10. Regional differences in gene expression, morphology, and performance in epithelial prep and crypt culture have been noted between duodenum, jejunum, and ileum. It is important to control for portion of intestine used when planning crypt isolation and culture experiments.
11. Fine iris scissors produce best results when opening intestines.
12. Agitation on a rocking platform is recommended.
13. Shaking force and time will affect quality and extent of crypt yield and must be determined empirically by each user. We recommend examining progress of crypt isolation from intestinal tissue by removing 10 μ L aliquots from Tube “S” at 1min intervals to check for the presence of intact, well-separated crypts. If crypt yield is especially low, remnant intestinal tissue can be fixed and examined by histology for the presence of un-released crypts.
14. To prevent drying of aliquots while counting, we recommend pipetting each 1:10 dilution into a separate region of a 10 cm petri or cell culture dish.
15. Pre-chilling tubes and tips is optional, but recommended for users who are new to Matrigel or Cultrex. Both reagents have been used successfully by a number of groups; this protocol will refer to Matrigel and Cultrex collectively as “ECM”. End users are encouraged to test reagents empirically and decide which is best for their projects.
16. For experiments in 48 well plates, we recommend 20-50 μ L of ECM per well (depending on number of crypts plated); for experiments in 96 well plates, we recommend 10 μ L of ECM per well.
17. We recommend plating crypts at a density of 5-10 crypts/ μ L of ECM.

18. Take care to avoid introducing bubbles in ECM; never pipet past first stop on pipette.
19. Addition of crypt slurry will dilute ECM, so using a very concentrated crypt sample will reduce the amount by which ECM is diluted. We strongly recommend avoiding dilution of ECM past 50%.
20. We recommend a crypt density of ~50-100 crypts per 10 μ L droplet in 96 well plate and 250-500 crypts per 50 μ L droplet in 48 well plate. Plating crypts too densely will result in poor survival of organoid cultures.
21. Polymerization may take longer than 15min depending on dilution factor of ECM. In our experience, crypts can be left in polymerized ECM at 37°C for up to 45 min without any notable loss in organoid-forming ability.
22. To account for pipetting error, we recommend preparing 0.5 well volume more than needed.
23. Organoids are considered “established” when they start developing well-defined crypt-like buds (Figure 5.4). The appropriate culture timepoints for organoid establishment, expansion, and cytokine treatment should be determined empirically based on the needs of the experiment. We recommend allowing organoids to establish in culture for at least 48 hours prior to treatment, to allow for removal of anoikis inhibitor Y-27632.
24. cDNA prepared from RNA lysates of 50-100 organoids per 96 well plate performs well in qRT-PCR assays when diluted in a range of 1:5-1:10.
25. We recommend using *Muc2* and *Dclk1* as controls for goblet and tuft cell hyperplasia, respectively, and *Lyz2*, *Chga*, and *Sl* to validate that Paneth,

enteroendocrine, and absorptive enterocyte lineages remain unaffected by cytokine treatment.

26. Cell Recovery Solution is critical to eliminate as much ECM as possible prior to crypt lysis. Residual ECM will affect total protein assays and may affect western blot results, depending on proteins of interest.

27. Avoid adding cold PFA to plates, as this can compromise integrity of ECM and result in loss of organoids.

28. Evenly mixing fixed organoids into OCT is important for downstream sectioning; if organoids are not evenly distributed within the cyromold, it will be more difficult to acquire high quality sections.

29. Organoid sections are not visible by naked eye unless organoids are very large at time of processing. Examining serial sections by microscopy is essential for obtaining sectioned tissue.

30. Many factors can cause differences in the length of time it takes for crypt dissociation, including mouse age/genotype, intestinal region, or treatment. We recommend constantly checking each sample for single cell dissociation.

31. If staining for live/dead discrimination, vital dyes should be added immediately before running samples on flow cytometer/FACS instrument.

32. Antibodies and antibody concentrations must be empirically determined by end user.

33. The amount of ECM to cells is dependent on experimental conditions and size of plate; we recommend 20-25 μ L for each well of a 48 well plate and 8-10 μ L for 96 well plate.

34. To encourage single cell growth, cultures receive 0.3 nM CHIR-99021 and 100 nM Valproic Acid for the first two days in culture only.
35. Organoids will eventually become very crowded within each well, so we suggest keeping organoid concentration similar across treatments and passages by increasing the passaging ratio (1:2, 1:4, etc) as cultures become crowded. It is important to record this passaging ratio to accurately reflect number of organoids resulting from serial passaging even if all organoids are not plated/counted.

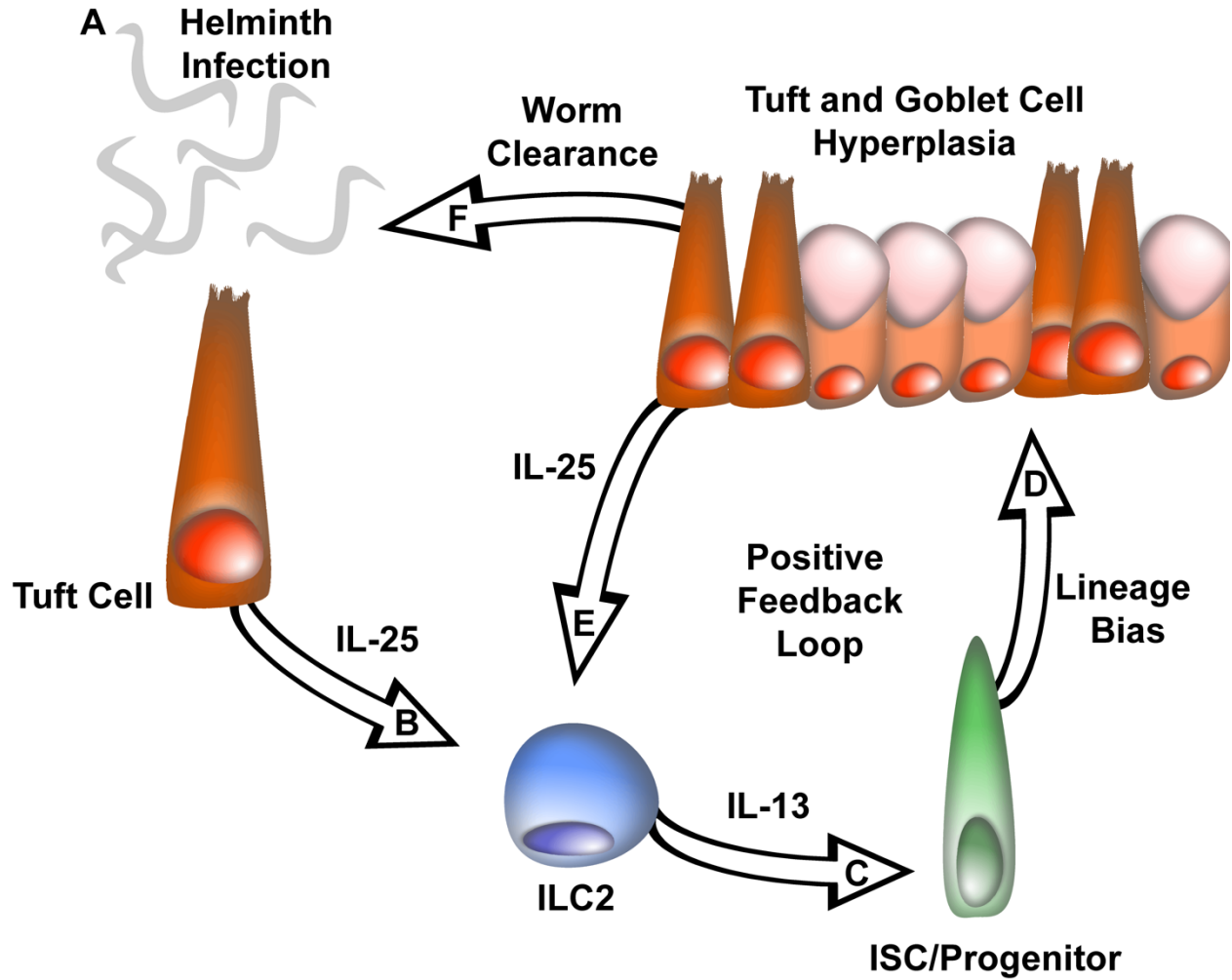


Figure 5.1 A cellular mechanism to resolve helminth infections in the gastrointestinal tract. Upon parasitic infection, Tuft cells detect the presence of helminths or protozoa chemosensory pathway. Tuft cells respond by secreting IL-25 that in turn acts on submucosal ILC2 cells (A), which secrete IL-13 (B). ILC2 cells are in close proximity to the stem/progenitor cell compartment and the IL-13 secreted by ILC2 cells promotes lineage bias toward Tuft and Goblet cells (C, D). Goblet cell hyperplasia has a dual function to increase mucous to protect the epithelium and aid in worm clearance, while Tuft cell hyperplasia serves to increase sentinels to monitor and respond to the worm infection. Increases in Tuft cell numbers continue to fuel the IL-25 positive feedback during infection (E). Reduction in worm burden serves as a break to Tuft and Goblet cell hyperplasia and the epithelium returns to homeostasis (F).

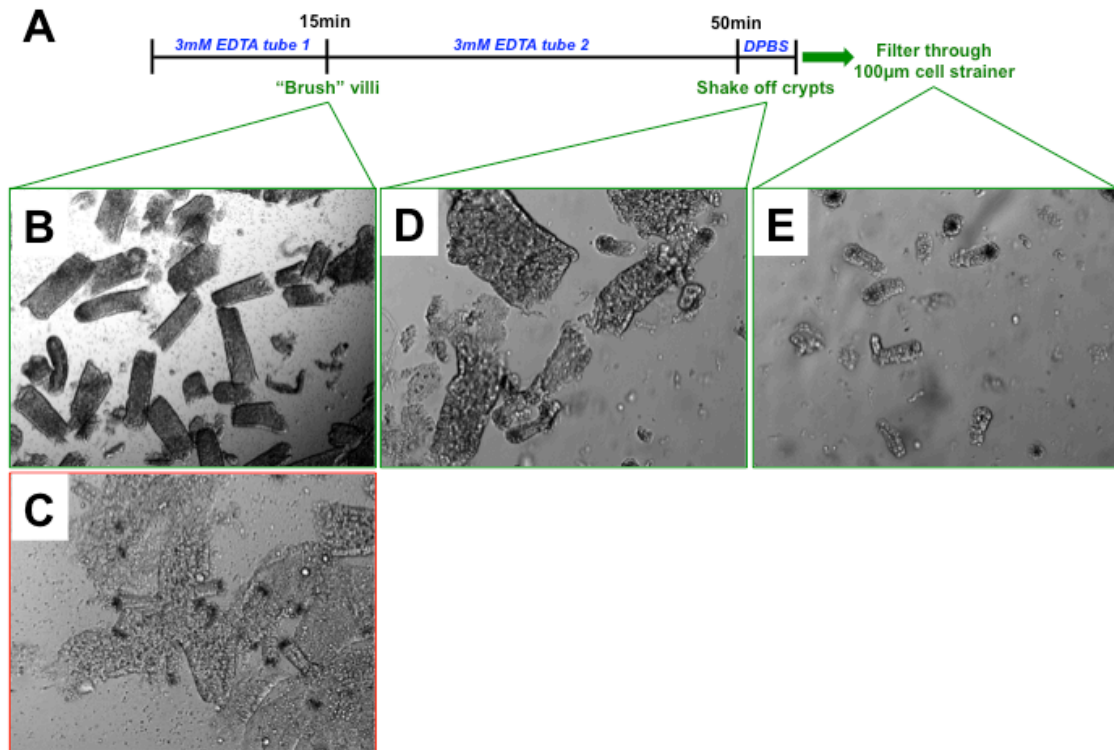


Figure 5.2 Quality control steps in intestinal crypt isolation. Crypt-enriched epithelial preparations should be monitored by light microscopy at several critical steps in order to ensure high quality isolation (A). First, gentle “brushing” of intestinal tissue following an initial 15 minutes incubation in 3mM EDTA removes a majority of villi (B). Care should be taken to avoid over brushing or applying too much force while removing villi, as this will displace crypts as well (C). Further incubation in 3mM EDTA for 35 minutes, followed by shaking of intestinal tissue in DPBS yields a mixed fraction of crypts and villi (D). Finally, filtering the mixed crypt/villus epithelial “slurry” through a 100 µm cell strainer enriches for the crypt fraction, which can be used for crypt culture or further dissociated to single cells for analysis by flow cytometry (E).

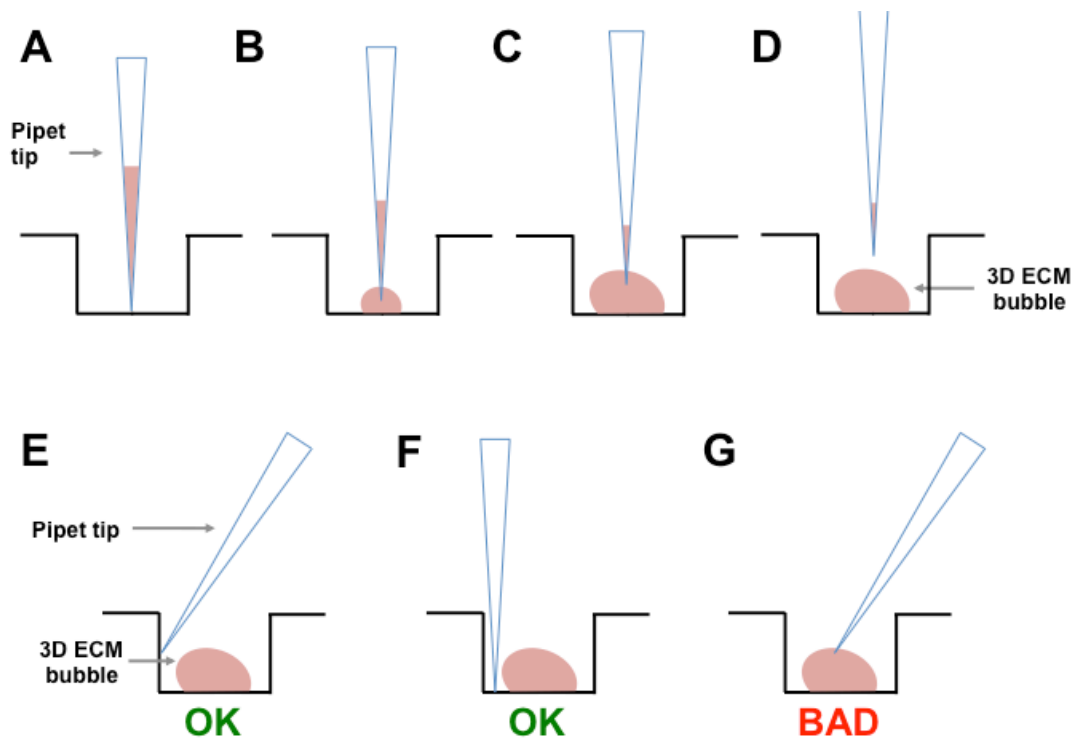


Figure 5.3 Best practices for placing ECM, and adding/removing media from ECM-based cultures. ECM plating technique and media change instructions. (A) Start with the pipette tip touching center of the well base. (B) While gently ejecting the ECM, slowly raise the pipette tip from the well base. (C & D) Leaving a small amount of ECM in the pipette tip to not introduce bubbles, remove the pipette tip straight up out of the ECM patty. (E) We recommend adding media by gently pipetting down the side of the well plate, to avoid direct contact with the ECM. (F) To aspirate media prior to media changes, pipet tips can be placed in contact with the base of the well, adjacent to the ECM. (G) Care should be taken to avoid making direct contact with the ECM either by pipet tip or forceful ejection of media, as this can compromise the structure of the ECM and result in loss of organoids.

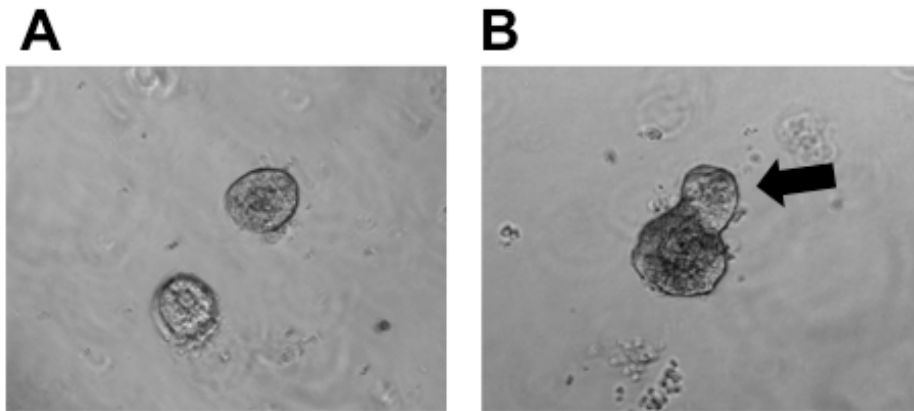


Figure 5.4 Organoids in culture form crypt buds. After 24-hours in culture, crypts ball up to form spheres (A). After 3-7 days in culture, organoids develop well-defined crypt-like buds (arrow) (B).

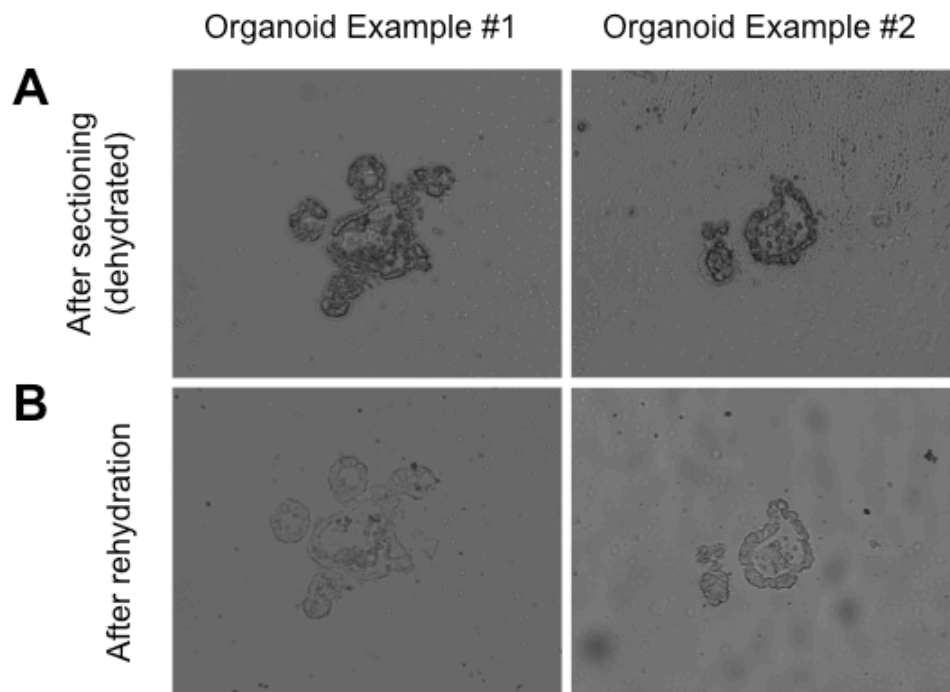


Figure 5.5 Sectioned organoids can be identified by light microscopy. Following sectioning, organoids can have the appearance of dust/debris (A). When rehydrated for immunofluorescence staining, characteristic epithelial morphology is observed (B).

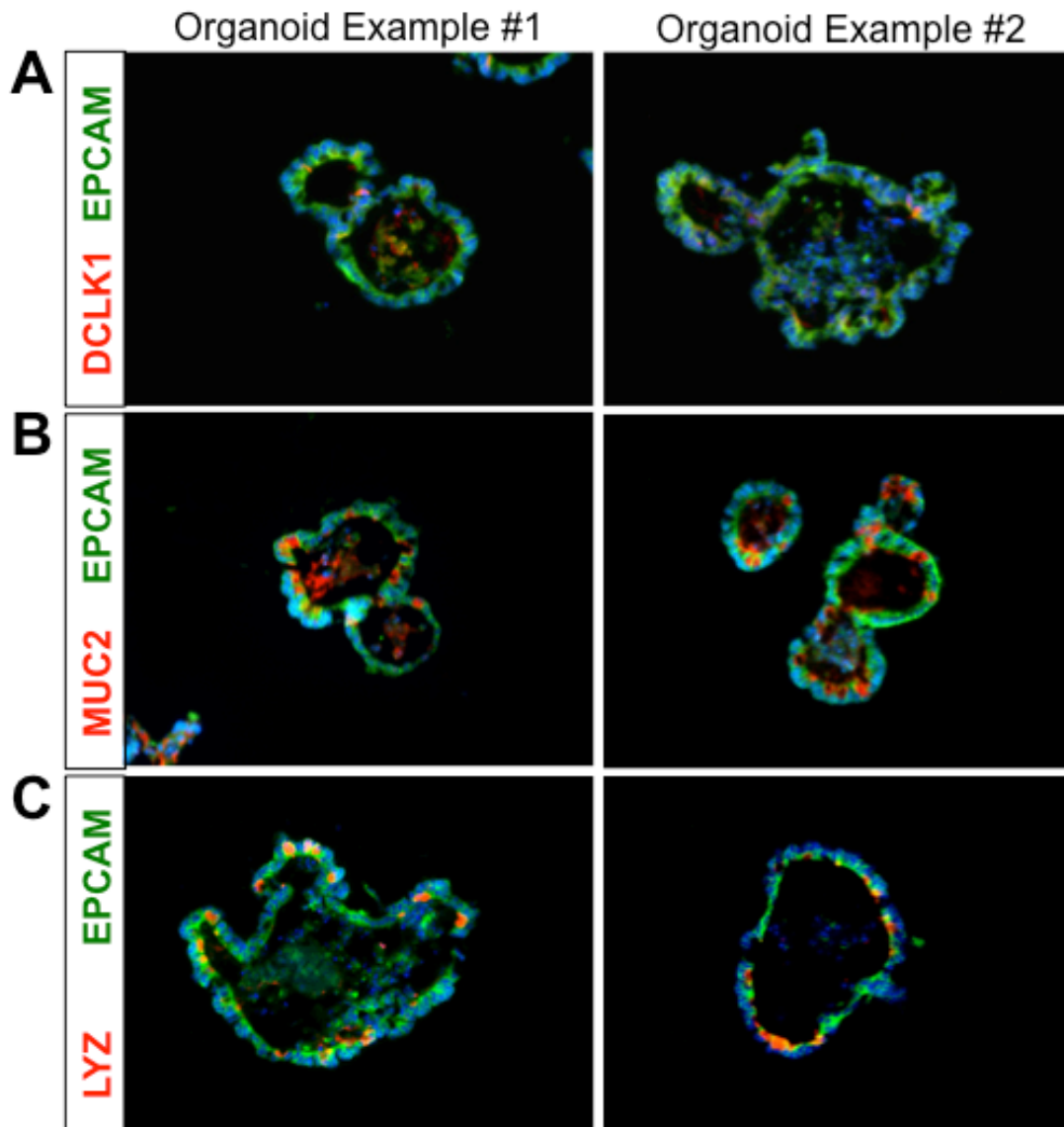


Figure 5.6 Wild-type intestinal organoids contain tuft, goblet, and Paneth cell populations. Canonical markers for tuft cells (DCLK1, A), goblet cells (MUC2, B), and Paneth cells (LYZ, C) can be used to assess secretory cell numbers in intestinal organoids by immunofluorescence.

Gene Name	Cell Type	TaqMan Gene Expression Assay ID
<i>18S</i>	Housekeeping Gene	Hs99999901_s1
<i>ChgA</i>	Enteroendocrine Cells	Mm00514341_m1
<i>Dclk1</i>	Tuft Cells	Mm00444950_m1
<i>Lyz2</i>	Paneth Cells	Mm00727183_s1
<i>Muc2</i>	Goblet Cells	Mm00458299_m1
<i>Sl</i>	Absorptive Enterocytes	Mm01210305_m1

Table 5.1 Suggested Taqman probes for qRT-PCR analysis

REFERENCES

1. Wheater, P. R. & Young, B. *Wheater's functional histology : a text and colour atlas*. (Churchill Livingstone/Elsevier, 2006).
2. Meran, L., Baulies, A. & Li, V. S. W. Intestinal Stem Cell Niche: The Extracellular Matrix and Cellular Components. *Stem Cells Int* 2017, 7970385 (2017).
3. Snippert, H. J. *et al.* Intestinal crypt homeostasis results from neutral competition between symmetrically dividing Lgr5 stem cells. *Cell* 143, 134–144 (2010).
4. Marshman, E., Booth, C. & Potten, C. S. The intestinal epithelial stem cell. *Bioessays* 24, 91–98 (2002).
5. Watson, A. J. M. & Hughes, K. R. TNF- α -induced intestinal epithelial cell shedding: implications for intestinal barrier function. *Annals NY Acad Sci* 1258, 1–8 (2012).
6. Grossmann, J. *et al.* Induction of apoptosis before shedding of human intestinal epithelial cells. *The American Journal of Gastroenterology* 97, 1421–1428 (2002).
7. Barker, N. Adult intestinal stem cells: critical drivers of epithelial homeostasis and regeneration. *Nat Rev Mol Cell Biol* 15, 19–33 (2014).
8. Wright, N. A. & Irwin, M. The kinetics of villus cell populations in the mouse small intestine. I. Normal villi: the steady state requirement. *Cell Tissue Kinet* 15, 595–609 (1982).
9. Treuting, P. M. & Dintzis, S. M. *Comparative anatomy and histology [electronic resource] : a mouse and human atlas*. (Elsevier, 2012).
10. Mowat, A. M. & Agace, W. W. Regional specialization within the intestinal immune system. *Nature Reviews Immunology* 14, 667–685 (2014).
11. Shroyer, N. F. *et al.* Intestine-specific ablation of mouse atonal homolog 1 (Math1) reveals a role in cellular homeostasis. *Gastroenterology* 132, 2478–2488 (2007).
12. Yang, Q., Bermingham, N. A., Finegold, M. J. & Zoghbi, H. Y. Requirement of Math1 for secretory cell lineage commitment in the mouse intestine. *Science* 294, 2155–2158 (2001).
13. van der Flier, L. G. & Clevers, H. Stem cells, self-renewal, and differentiation in the intestinal epithelium. *Annu. Rev. Physiol.* 71, 241–260 (2009).

14. van Es, J. H. *et al.* Notch/gamma-secretase inhibition turns proliferative cells in intestinal crypts and adenomas into goblet cells. *Nature* 435, 959–963 (2005).
15. Milano, J. *et al.* Modulation of notch processing by gamma-secretase inhibitors causes intestinal goblet cell metaplasia and induction of genes known to specify gut secretory lineage differentiation. *Toxicol. Sci.* 82, 341–358 (2004).
16. Fre, S. *et al.* Notch signals control the fate of immature progenitor cells in the intestine. *Nature* 435, 964–968 (2005).
17. VanDussen, K. L. & Samuelson, L. C. Mouse atonal homolog 1 directs intestinal progenitors to secretory cell rather than absorptive cell fate. *Developmental Biology* 346, 215–223 (2010).
18. Kim, Y. S. & Ho, S. B. Intestinal goblet cells and mucins in health and disease: recent insights and progress. *Curr Gastroenterol Rep* 12, 319–330 (2010).
19. Cheng, H. & Leblond, C. P. Origin, differentiation and renewal of the four main epithelial cell types in the mouse small intestine. V. Unitarian Theory of the origin of the four epithelial cell types. *Am. J. Anat.* 141, 537–561 (1974).
20. Rindi, G., Leiter, A. B., Kopin, A. S., Bordi, C. & Solcia, E. The ‘normal’ endocrine cell of the gut: changing concepts and new evidences. *Annals NY Acad Sci* 1014, 1–12 (2004).
21. Gerbe, F., Brulin, B., Makrini, L., Legraverend, C. & Jay, P. DCAMKL-1 expression identifies Tuft cells rather than stem cells in the adult mouse intestinal epithelium. *Gastroenterology* 137, 2179–80– author reply 2180–1 (2009).
22. Gerbe, F. & Jay, P. Intestinal tuft cells: epithelial sentinels linking luminal cues to the immune system. *Mucosal Immunol* 9, 1353–1359 (2016).
23. Clevers, H. C. & Bevins, C. L. Paneth cells: maestros of the small intestinal crypts. *Annu. Rev. Physiol.* 75, 289–311 (2013).
24. Ireland, H., Houghton, C., Howard, L. & Winton, D. J. Cellular inheritance of a Cre-activated reporter gene to determine Paneth cell longevity in the murine small intestine. *Dev. Dyn.* 233, 1332–1336 (2005).
25. Bevins, C. L. & Salzman, N. H. Paneth cells, antimicrobial peptides and maintenance of intestinal homeostasis. *Nat. Rev. Microbiol.* 9, 356–368 (2011).
26. Sato, T. *et al.* Paneth cells constitute the niche for Lgr5 stem cells in intestinal crypts. *Nature* 469, 415–418 (2011).

27. Potten, C. S., Owen, G. & Booth, D. Intestinal stem cells protect their genome by selective segregation of template DNA strands. *J. Cell. Sci.* 115, 2381–2388 (2002).
28. Roche, K. C. *et al.* SOX9 maintains reserve stem cells and preserves radioresistance in mouse small intestine. *Gastroenterology* 149, 1553–1563.e10 (2015).
29. Snippert, H. J. & Clevers, H. Tracking adult stem cells. *EMBO Rep.* 12, 113–122 (2011).
30. Richmond, C. A., Shah, M. S., Carlone, D. L. & Breault, D. T. Factors regulating quiescent stem cells: insights from the intestine and other self-renewing tissues. *The Journal of Physiology* 594, 4805–4813 (2016).
31. Barker, N. *et al.* Identification of stem cells in small intestine and colon by marker gene *Lgr5*. *Nature* 449, 1003–1007 (2007).
32. Sato, T. *et al.* Single *Lgr5* stem cells build crypt–villus structures in vitro without a mesenchymal niche. *Nature* 459, 262–265 (2009).
33. Mustata, R. C. *et al.* *Lgr4* is required for Paneth cell differentiation and maintenance of intestinal stem cells ex vivo. *EMBO Rep.* 12, 558–564 (2011).
34. de Lau, W. *et al.* *Lgr5* homologues associate with Wnt receptors and mediate R-spondin signalling. *Nature* 476, 293–297 (2011).
35. Nusse, R. & Clevers, H. Wnt/ β -Catenin Signaling, Disease, and Emerging Therapeutic Modalities. *Cell* 169, 985–999 (2017).
36. Gregorieff, A. *et al.* Expression pattern of Wnt signaling components in the adult intestine. *Gastroenterology* 129, 626–638 (2005).
37. Farin, H. F. *et al.* Visualization of a short-range Wnt gradient in the intestinal stem-cell niche. *Nature* 530, 340–343 (2016).
38. Krausova, M. & Korinek, V. Wnt signaling in adult intestinal stem cells and cancer. *Cell. Signal.* 26, 570–579 (2014).
39. Korinek, V. *et al.* Depletion of epithelial stem-cell compartments in the small intestine of mice lacking Tcf-4. *Nat Genet* 19, 379–383 (1998).
40. Fevr, T., Robine, S., Louvard, D. & Huelsken, J. Wnt/ β -catenin is essential for intestinal homeostasis and maintenance of intestinal stem cells. *Mol. Cell. Biol.* 27, 7551–7559 (2007).

41. Formeister, E. J. *et al.* Distinct SOX9 levels differentially mark stem/progenitor populations and enteroendocrine cells of the small intestine epithelium. *Am. J. Physiol. Gastrointest. Liver Physiol.* 296, G1108–18 (2009).
42. van der Flier, L. G. *et al.* Transcription factor achaete scute-like 2 controls intestinal stem cell fate. *Cell* 136, 903–912 (2009).
43. Schuijers, J., van der Flier, L. G., van Es, J. & Clevers, H. Robust cre-mediated recombination in small intestinal stem cells utilizing the olfm4 locus. *Stem Cell Reports* 3, 234–241 (2014).
44. van der Flier, L. G., Haegebarth, A., Stange, D. E., van de Wetering, M. & Clevers, H. OLFM4 is a robust marker for stem cells in human intestine and marks a subset of colorectal cancer cells. *Gastroenterology* 137, 15–17 (2009).
45. Blache, P. *et al.* SOX9 is an intestine crypt transcription factor, is regulated by the Wnt pathway, and represses the CDX2 and MUC2 genes. *The Journal of cell ...* (2004).
46. Bastide, P. *et al.* Sox9 regulates cell proliferation and is required for Paneth cell differentiation in the intestinal epithelium. *J. Cell Biol.* 178, 635–648 (2007).
47. Ramalingam, S., Daughtridge, G. W., Johnston, M. J., Gracz, A. D. & Magness, S. T. Distinct levels of Sox9 expression mark colon epithelial stem cells that form colonoids in culture. *Am. J. Physiol. Gastrointest. Liver Physiol.* 302, G10–G20 (2012).
48. Gracz, A. D. *et al.* A high-throughput platform for stem cell niche co-cultures and downstream gene expression analysis. *Nat. Cell Biol.* 17, 340–349 (2015).
49. Kosinski, C. *et al.* Gene expression patterns of human colon tops and basal crypts and BMP antagonists as intestinal stem cell niche factors. *Proc. Natl. Acad. Sci. U.S.A.* 104, 15418–15423 (2007).
50. Miyazono, K., Maeda, S. & Imamura, T. BMP receptor signaling: transcriptional targets, regulation of signals, and signaling cross-talk. *Cytokine Growth Factor Rev.* 16, 251–263 (2005).
51. Haramis, A.-P. G. *et al.* De novo crypt formation and juvenile polyposis on BMP inhibition in mouse intestine. *Science* 303, 1684–1686 (2004).
52. Batts, L. E., Polk, D. B., Dubois, R. N. & Kulesa, H. Bmp signaling is required for intestinal growth and morphogenesis. *Dev. Dyn.* 235, 1563–1570 (2006).
53. Qi, Z. *et al.* BMP restricts stemness of intestinal Lgr5(+) stem cells by directly suppressing their signature genes. *Nat Commun* 8, 13824 (2017).

54. Sato, T. & Clevers, H. Growing self-organizing mini-guts from a single intestinal stem cell: mechanism and applications. *Science* 340, 1190–1194 (2013).
55. Spence, J. R. *et al.* Directed differentiation of human pluripotent stem cells into intestinal tissue in vitro. *Nature* 470, 105–109 (2011).
56. Stelzner, M. *et al.* A nomenclature for intestinal in vitro cultures. *Am. J. Physiol. Gastrointest. Liver Physiol.* 302, G1359–63 (2012).
57. Miguel, J. C. *et al.* Epidermal growth factor suppresses intestinal epithelial cell shedding through a MAPK-dependent pathway. *J. Cell. Sci.* 130, 90–96 (2017).
58. Dignass, A. U. & Sturm, A. Peptide growth factors in the intestine. *Eur J Gastroenterol Hepatol* 13, 763–770 (2001).
59. Kim, K.-A. *et al.* Mitogenic influence of human R-spondin1 on the intestinal epithelium. *Science* 309, 1256–1259 (2005).
60. Miyoshi, H. & Stappenbeck, T. S. In vitro expansion and genetic modification of gastrointestinal stem cells in spheroid culture. *Nat Protoc* 8, 2471–2482 (2013).
61. Meijer, L., Flajolet, M. & Greengard, P. Pharmacological inhibitors of glycogen synthase kinase 3. *Trends in Pharmacological Sciences* 25, 471–480 (2004).
62. Yin, X. *et al.* Niche-independent high-purity cultures of Lgr5(+) intestinal stem cells and their progeny. *Nat. Methods* 11, 106–112 (2013).
63. Greenblatt, D. Y. *et al.* Valproic acid activates notch-1 signaling and regulates the neuroendocrine phenotype in carcinoid cancer cells. *Oncologist* 12, 942–951 (2007).
64. Stockhausen, M.-T., Sjölund, J., Manetopoulos, C. & Axelson, H. Effects of the histone deacetylase inhibitor valproic acid on Notch signalling in human neuroblastoma cells. *British Journal of Cancer* 2005 92:4 92, 6602309–759 (2005).
65. Sträter, J. *et al.* Rapid onset of apoptosis in vitro follows disruption of beta 1-integrin/matrix interactions in human colonic crypt cells. *Gastroenterology* 110, 1776–1784 (1996).
66. Jabaji, Z. *et al.* Use of Collagen Gel As an Alternative Extracellular Matrix for the In Vitro and In Vivo Growth of Murine Small Intestinal Epithelium. *Tissue Eng Part C Methods* 130510061312005 (2013). doi:10.1089/ten.tec.2012.0710
67. Gjorevski, N. *et al.* Designer matrices for intestinal stem cell and organoid culture. *Nature* 539, 560–564 (2016).

68. Leushacke, M. & Barker, N. Ex vivo culture of the intestinal epithelium: strategies and applications. *Gut* 63, 1345–1354 (2014).
69. Kim, T.-H., Escudero, S. & Shivdasani, R. A. Intact function of Lgr5 receptor-expressing intestinal stem cells in the absence of Paneth cells. *Proc. Natl. Acad. Sci. U.S.A.* 109, 3932–3937 (2012).
70. Farin, H. F., van Es, J. H. & Clevers, H. Redundant sources of Wnt regulate intestinal stem cells and promote formation of Paneth cells. *Gastroenterology* 143, 1518–1529.e7 (2012).
71. Roulis, M. & Flavell, R. A. Fibroblasts and myofibroblasts of the intestinal lamina propria in physiology and disease. *Differentiation* 92, 116–131 (2016).
72. Powell, D. W., Pinchuk, I. V., Saada, J. I., Chen, X. & Mifflin, R. C. Mesenchymal Cells of the Intestinal Lamina Propria. *Annu. Rev. Physiol.* 73, 213–237 (2011).
73. Lei, N. Y. *et al.* Intestinal subepithelial myofibroblasts support the growth of intestinal epithelial stem cells. *PLoS ONE* 9, e84651 (2014).
74. Teller, I. C. & Beaulieu, J. F. Interactions between laminin and epithelial cells in intestinal health and disease. *Expert Rev Mol Med* 3, 1–18 (2001).
75. Brizzi, M. F., Tarone, G. & Defilippi, P. Extracellular matrix, integrins, and growth factors as tailors of the stem cell niche. *Current Opinion in Cell Biology* 24, 645–651 (2012).
76. Perreault, N. *et al.* Epithelial vs Mesenchymal Contribution to the Extracellular Matrix in the Human Intestine. *Biochemical and Biophysical Research Communications* 248, 121–126 (1998).
77. Xu, R., Boudreau, A. & Bissell, M. J. Tissue architecture and function: dynamic reciprocity via extra- and intra-cellular matrices. *Cancer Metastasis Rev* 28, 167–176 (2009).
78. Aitken, K. J. & Bägli, D. J. The bladder extracellular matrix. Part I: architecture, development and disease. *Nat Rev Urol* 6, 596–611 (2009).
79. Nelson, C. M. & Bissell, M. J. Of Extracellular Matrix, Scaffolds, and Signaling: Tissue Architecture Regulates Development, Homeostasis, and Cancer. <http://dx.doi.org/10.1146/annurev.cellbio.22.010305.104315> (2006). doi:10.1146/annurev.cellbio.22.010305.104315
80. Yamamoto, S. *et al.* Heparan sulfate on intestinal epithelial cells plays a critical role in intestinal crypt homeostasis via Wnt/ β -catenin signaling. *Am. J. Physiol. Gastrointest. Liver Physiol.* 305, G241–G249 (2013).

81. Hynes, R. O. The Extracellular Matrix: Not Just Pretty Fibrils. *Science* 326, 1216–1219 (2009).
82. Muragaki, Y. *et al.* Mouse Col18a1 is expressed in a tissue-specific manner as three alternative variants and is localized in basement membrane zones. *Proc. Natl. Acad. Sci. U.S.A.* 92, 8763–8767 (1995).
83. de Mattos, B. R. R. *et al.* Inflammatory Bowel Disease: An Overview of Immune Mechanisms and Biological Treatments. *Mediators of Inflammation* 2015, 493012 (2015).
84. Tomasello, E. & Bedoui, S. Intestinal innate immune cells in gut homeostasis and immunosurveillance. *Immunol. Cell Biol.* 91, 201–203 (2013).
85. Reboldi, A. & Cyster, J. G. Peyer's patches: organizing B-cell responses at the intestinal frontier. *Immunological Reviews* 271, 230–245 (2016).
86. Spencer, J. & Sollid, L. M. The human intestinal B-cell response. *Mucosal Immunol* 9, 1113–1124 (2016).
87. van Wijk, F. & Cheroutre, H. Mucosal T cells in gut homeostasis and inflammation. *Expert Review of Clinical Immunology* 6, 559–566 (2010).
88. Cornes, J. S. Number, size, and distribution of Peyer's patches in the human small intestine: Part I The development of Peyer's patches. *Gut* 6, 225–229 (1965).
89. Tsuji, M. *et al.* Requirement for lymphoid tissue-inducer cells in isolated follicle formation and T cell-independent immunoglobulin A generation in the gut. *Immunity* 29, 261–271 (2008).
90. Pabst, O. *et al.* Cryptopatches and isolated lymphoid follicles: dynamic lymphoid tissues dispensable for the generation of intraepithelial lymphocytes. *European Journal of Immunology* 35, 98–107 (2005).
91. Trepel, F. Number and distribution of lymphocytes in man. A critical analysis. *Klin. Wochenschr.* 52, 511–515 (1974).
92. Moghaddami, M., Cummins, A. & Mayrhofer, G. Lymphocyte-filled villi: comparison with other lymphoid aggregations in the mucosa of the human small intestine. *Gastroenterology* 115, 1414–1425 (1998).
93. Bostick, J. W. & Zhou, L. Innate lymphoid cells in intestinal immunity and inflammation. *Experientia* 73, 237–252 (2016).

94. Spits, H. *et al.* Innate lymphoid cells—a proposal for uniform nomenclature. *Nature Reviews Immunology* 13, 145–149 (2013).
95. Klose, C. S. N. & Artis, D. Innate lymphoid cells as regulators of immunity, inflammation and tissue homeostasis. *Nat. Immunol.* 17, 765–774 (2016).
96. Artis, D. & Spits, H. The biology of innate lymphoid cells. *Nature* 517, 293–301 (2015).
97. Johansson, M. E. V. *et al.* The inner of the two Muc2 mucin-dependent mucus layers in colon is devoid of bacteria. *Proc. Natl. Acad. Sci. U.S.A.* 105, 15064–15069 (2008).
98. Vaishnava, S., Behrendt, C. L., Ismail, A. S., Eckmann, L. & Hooper, L. V. Paneth cells directly sense gut commensals and maintain homeostasis at the intestinal host-microbial interface. *Proc. Natl. Acad. Sci. U.S.A.* 105, 20858–20863 (2008).
99. Stadnyk, A. W. Intestinal epithelial cells as a source of inflammatory cytokines and chemokines. *Can. J. Gastroenterol.* 16, 241–246 (2002).
100. Niess, J. H. *et al.* CX3CR1-mediated dendritic cell access to the intestinal lumen and bacterial clearance. *Science* 307, 254–258 (2005).
101. Bekiaris, V., Persson, E. K. & Agace, W. W. Intestinal dendritic cells in the regulation of mucosal immunity. *Immunological Reviews* 260, 86–101 (2014).
102. Garrett, W. S., Gordon, J. I. & Glimcher, L. H. Homeostasis and inflammation in the intestine. *Cell* 140, 859–870 (2010).
103. Cerovic, V., Bain, C. C., Mowat, A. M. & Milling, S. W. F. Intestinal macrophages and dendritic cells: what's the difference? *Trends Immunol.* 35, 270–277 (2014).
104. Stagg, A. J., Hart, A. L., Knight, S. C. & Kamm, M. A. The dendritic cell: its role in intestinal inflammation and relationship with gut bacteria. *Gut* 52, 1522–1529 (2003).
105. Kaplan, G. G. The global burden of IBD: from 2015 to 2025. *Nat Rev Gastroenterol Hepatol* 12, 720–727 (2015).
106. Ananthakrishnan, A. N. Epidemiology and risk factors for IBD. *Nat Rev Gastroenterol Hepatol* 12, 205–217 (2015).
107. Baumgart, D. C. & Sandborn, W. J. Crohn's disease. *The Lancet* 380, 1590–1605 (2012).

108. Danese, S. & Fiocchi, C. Ulcerative Colitis. <http://dx.doi.org/10.1056/NEJMra1102942> 365, 1713–1725 (2011).
109. Liverani, E., Scaioli, E., Digby, R. J., Bellanova, M. & Belluzzi, A. How to predict clinical relapse in inflammatory bowel disease patients. *World J. Gastroenterol.* 22, 1017–1033 (2016).
110. Lichtenstein, G. R., Hanauer, S. B., Sandborn, W. J. Practice Parameters Committee of American College of Gastroenterology. Management of Crohn's disease in adults. *The American Journal of Gastroenterology* 104, 465–83– quiz 464– 484 (2009).
111. Sturm, A. & Dignass, A. U. Epithelial restitution and wound healing in inflammatory bowel disease. *World J. Gastroenterol.* 14, 348–353 (2008).
112. Neurath, M. F. Cytokines in inflammatory bowel disease. *Nature Reviews Immunology* 14, 329–342 (2014).
113. Okamoto, R. Epithelial regeneration in inflammatory bowel diseases. *Inflammation and Regeneration* 31, 275–281 (2011).
114. Bryant, R. V., Winer, S., Travis, S. P. L. & Riddell, R. H. Systematic review: histological remission in inflammatory bowel disease. Is 'complete' remission the new treatment paradigm? An IOIBD initiative. *Journal of Crohn's and Colitis* 8, 1582–1597 (2014).
115. Rieder, F., Brenmoehl, J., Leeb, S., Schölmerich, J. & Rogler, G. Wound healing and fibrosis in intestinal disease. *Gut* 56, 130–139 (2007).
116. Abbas, A. K., Cotran, R. S., Fausto, N., Kumar, V. & Robbins, S. L. *Pathologic basis of disease.* (Elsevier Saunders, 2005).
117. Hussey, G. S., Keane, T. J. & Badylak, S. F. The extracellular matrix of the gastrointestinal tract: a regenerative medicine platform. *Nat Rev Gastroenterol Hepatol* 14, 540–552 (2017).
118. Neurath, M. F. New targets for mucosal healing and therapy in inflammatory bowel diseases. *Mucosal Immunol* 7, 6–19 (2014).
119. Metcalfe, C., Kljavin, N. M., Ybarra, R. & de Sauvage, F. J. Lgr5+ Stem Cells Are Indispensable for Radiation-Induced Intestinal Regeneration. *Cell Stem Cell* 14, 149–159 (2014).
120. Lindemans, C. A. *et al.* Interleukin-22 promotes intestinal-stem-cell-mediated epithelial regeneration. *Nature* 528, 560–564 (2015).

121. Hanash, A. M. *et al.* Interleukin-22 protects intestinal stem cells from immune-mediated tissue damage and regulates sensitivity to graft versus host disease. *Immunity* 37, 339–350 (2012).
122. Kaiko, G. E. *et al.* The Colonic Crypt Protects Stem Cells from Microbiota-Derived Metabolites. *Cell* 165, 1708–1720 (2016).
123. Fakhoury, M., Negrulj, R., Mooranian, A. & Al-Salami, H. Inflammatory bowel disease: clinical aspects and treatments. *Journal of Inflammation Research* 7, 113–120 (2014).
124. van der Sloot, K. W. J., Amini, M., Peters, V., Dijkstra, G. & Alizadeh, B. Z. Inflammatory Bowel Diseases: Review of Known Environmental Protective and Risk Factors Involved. *Inflamm. Bowel Dis.* 23, 1499–1509 (2017).
125. Wolk, K. *et al.* IL-22 Induces Lipopolysaccharide-Binding Protein in Hepatocytes: A Potential Systemic Role of IL-22 in Crohn's Disease. *J. Immunol.* 178, 5973–5981 (2007).
126. Li, J. *et al.* Interleukin 23 regulates proliferation of lung cancer cells in a concentration-dependent way in association with the interleukin-23 receptor. *Carcinogenesis* 34, 658–666 (2013).
127. Singh, U. P. *et al.* Chemokine and cytokine levels in inflammatory bowel disease patients. *Cytokine* 77, 44–49 (2016).
128. Lejeune, D. *et al.* Interleukin-22 (IL-22) Activates the JAK/STAT, ERK, JNK, and p38 MAP Kinase Pathways in a Rat Hepatoma Cell Line. *J. Biol. Chem.* 277, 33676–33682 (2002).
129. Mizuno, S. *et al.* Cross-talk between ROR γ t⁺ innate lymphoid cells and intestinal macrophages induces mucosal IL-22 production in Crohn's disease. *Inflamm. Bowel Dis.* 20, 1426–1434 (2014).
130. Sandrin, D. *et al.* Diffusion of macromolecules in a polymer hydrogel: from microscopic to macroscopic scales. *Physical Chemistry Chemical Physics* 18, 12860–12876 (2016).
131. Young, M. E., Carroad, P. A. & Bell, R. L. Estimation of diffusion coefficients of proteins. *Biotechnol. Bioeng.* 22, 947–955 (1980).
132. Francis, K. & Palsson, B. O. Effective intercellular communication distances are determined by the relative time constants for cyto/chemokine secretion and diffusion. *PNAS* 94, 12258–12262 (1997).

133. Cortez, V. S., Robinette, M. L. & Colonna, M. Innate lymphoid cells: new insights into function and development. *Current Opinion in Immunology* 32, 71–77 (2015).
134. Geremia, A. *et al.* IL-23–responsive innate lymphoid cells are increased in inflammatory bowel disease. *Journal of Experimental Medicine* jem.20101712 (2011). doi:10.1084/jem.20101712
135. VanDussen, K. L. *et al.* Notch signaling modulates proliferation and differentiation of intestinal crypt base columnar stem cells. *Development* 139, 488–497 (2012).
136. Carulli, A. J. *et al.* Notch receptor regulation of intestinal stem cell homeostasis and crypt regeneration. *Developmental Biology* 402, 98–108 (2015).
137. Mah, A. T., Yan, K. S. & Kuo, C. J. Wnt pathway regulation of intestinal stem cells. *The Journal of Physiology* 594, 4837–4847 (2016).
138. Noah, T. K. & Shroyer, N. F. Notch in the Intestine: Regulation of Homeostasis and Pathogenesis. <http://dx.doi.org/10.1146/annurev-physiol-030212-183741> (2013). doi:10.1146/annurev-physiol-030212-183741
139. Iscove, N. N. & Nawa, K. Hematopoietic stem cells expand during serial transplantation in vivo without apparent exhaustion. *Current Biology* 7, 805–808 (1997).
140. Park, O. *et al.* In vivo consequences of liver-specific interleukin-22 expression in mice: Implications for human liver disease progression. *Hepatology* 54, 252–261 (2011).
141. Longman, R. S. *et al.* CX3CR1+ mononuclear phagocytes support colitis-associated innate lymphoid cell production of IL-22. *Journal of Experimental Medicine* jem.20140678 (2014). doi:10.1084/jem.20140678
142. Chen, Q. *et al.* Inactivation of STAT3 Signaling Impairs Hair Cell Differentiation in the Developing Mouse Cochlea. *Stem Cell Reports* 9, 231–246 (2017).
143. Hao, J.-Q. Targeting Interleukin-22 in Psoriasis. *Inflammation* 37, 94–99 (2014).
144. Jia, H.-Y. *et al.* Asymmetric stem-cell division ensures sustained keratinocyte hyperproliferation in psoriatic skin lesions. *Int. J. Mol. Med.* 37, 359–368 (2016).
145. Brand, S. *et al.* IL-22 is increased in active Crohn's disease and promotes proinflammatory gene expression and intestinal epithelial cell migration. *Am. J. Physiol. Gastrointest. Liver Physiol.* 290, G827–38 (2006).

146. Martin, J. C. J. *et al.* Interleukin-22 binding protein (IL-22BP) is constitutively expressed by a subset of conventional dendritic cells and is strongly induced by retinoic acid. *Mucosal Immunol* 7, 101–113 (2014).
147. Mizoguchi, A. *et al.* Clinical importance of IL-22 cascade in IBD. *J. Gastroenterol.* 53, 465–474 (2018).
148. Gong, S. *et al.* A gene expression atlas of the central nervous system based on bacterial artificial chromosomes. *Nature* 425, 917–925 (2003).
149. Van Landeghem, L. *et al.* Activation of two distinct Sox9-EGFP-expressing intestinal stem cell populations during crypt regeneration after irradiation. *Am. J. Physiol. Gastrointest. Liver Physiol.* 302, G1111–32 (2012).
150. Schneider, C. A., Rasband, W. S. & Eliceiri, K. W. NIH Image to ImageJ: 25 years of image analysis. *Nat. Methods* 9, 671–675 (2012).
151. Jansson, A., Harlen, M., Karlsson, S., Nilsson, P. & Cooley, M. 3D computation modelling of the influence of cytokine secretion on Th-cell development suggests that negative selection (inhibition of Th1 cells) is more effective than positive selection by IL-4 for Th2 cell dominance. *Immunol. Cell Biol.* 85, 189–196 (2007).
152. Carpenter, A. E. *et al.* CellProfiler: image analysis software for identifying and quantifying cell phenotypes. *Genome Biology* 2006 7:10 7, R100 (2006).
153. Otsu, N. A Threshold Selection Method from Gray-Level Histograms. *IEEE Trans. Syst., Man, Cybern.* 9, 62–66
154. Berry, M. V. Image Analysis and Mathematics Morphology. *Phys. Bull.* 34, 252 (1983).
155. Gracz, A. D., Ramalingam, S. & Magness, S. T. Sox9 expression marks a subset of CD24-expressing small intestine epithelial stem cells that form organoids in vitro. *Am. J. Physiol. Gastrointest. Liver Physiol.* 298, G590–600 (2010).
156. Crapo, P. M., Gilbert, T. W. & Badylak, S. F. An overview of tissue and whole organ decellularization processes. *Biomaterials* 32, 3233–3243 (2011).
157. Misiakos, E. P., Macheras, A., Kapetanakis, T. & Liakakos, T. Short bowel syndrome: current medical and surgical trends. *J. Clin. Gastroenterol.* 41, 5–18 (2007).

158. American Gastroenterological Association. American Gastroenterological Association medical position statement: short bowel syndrome and intestinal transplantation. *Gastroenterology* 124, 1105–1110 (2003).
159. Krishnamurthy, G. & Gupta, R. in *GI Surgery Annual 23*, 33–57 (Springer, Singapore, 2017).
160. Fishbein, T. M. Intestinal Transplantation. *N Engl J Med* 361, 998–1008 (2009).
161. Mazariegos, G. V. Intestinal transplantation: current outcomes and opportunities. *Curr Opin Organ Transplant* 14, 515–521 (2009).
162. Bitar, K. N. & Zakhem, E. Bioengineering the gut: future prospects of regenerative medicine. *Nat Rev Gastroenterol Hepatol* 13, 543–556 (2016).
163. Badylak, S. F. Xenogeneic extracellular matrix as a scaffold for tissue reconstruction. *Transplant Immunology* 12, 367–377 (2004).
164. Shirakigawa, N. & Ijima, H. in *Advances in Biomaterials for Biomedical Applications* (eds. Tripathi, A. & Melo, J. S.) 185–226 (Springer Singapore, 2017).
165. Kararli, T. T. Comparison of the gastrointestinal anatomy, physiology, and biochemistry of humans and commonly used laboratory animals. *Biopharm. Drug Dispos.* 16, 351–380 (1995).
166. Keane, T. J., Swinehart, I. T. & Badylak, S. F. Methods of tissue decellularization used for preparation of biologic scaffolds and in vivo relevance. *Methods* 84, 25–34 (2015).
167. Wang, Y. *et al.* Lineage restriction of human hepatic stem cells to mature fates is made efficient by tissue-specific biomatrix scaffolds. *Hepatology* 53, 293–305 (2011).
168. Seetapun, D. & Ross, J. J. Eliminating the organ transplant waiting list: The future with perfusion decellularized organs. *Surgery* 161, 1474–1478 (2017).
169. Graham, M. *et al.* Collagen content and types in the intestinal strictures of Crohn's disease. *Gastroenterology* 94, 257–265 (1988).
170. Lindberg, K. & Badylak, S. F. Porcine small intestinal submucosa (SIS): a bioscaffold supporting in vitro primary human epidermal cell differentiation and synthesis of basement membrane proteins. *Burns* 27, 254–266 (2001).
171. Kühn, K. Basement membrane (type IV) collagen. *Matrix Biol.* 14, 439–445 (1995).

172. Simon-Assmann, P., Keding, M., Arcangelis, A., Rousseau, V. & Simo, P. Extracellular matrix components in intestinal development. *Experientia* 51, 883–900 (1995).
173. Sandberg, M. M., Hirvonen, H. E., Elima, K. J. M. & Vuorio, E. I. Co-expression of collagens II and XI and alternative splicing of exon 2 of collagen II in several developing human tissues. *Biochemical Journal* 294, 595–602 (1993).
174. Wetzels, R. H. *et al.* Distribution patterns of type VII collagen in normal and malignant human tissues. *Am. J. Pathol.* 139, 451–459 (1991).
175. Miller, E. J. & Rhodes, R. K. Preparation and characterization of the different types of collagen. *Meth. Enzymol.* 82 Pt A, 33–64 (1982).
176. Gonzalez, L. M., Williamson, I., Piedrahita, J. A., Blikslager, A. T. & Magness, S. T. Cell Lineage Identification and Stem Cell Culture in a Porcine Model for the Study of Intestinal Epithelial Regeneration. *PLoS ONE* 8, e66465 (2013).
177. Salic, A. & Mitchison, T. J. A chemical method for fast and sensitive detection of DNA synthesis in vivo. *Proc. Natl. Acad. Sci. U.S.A.* 105, 2415–2420 (2008).
178. Gum, J. R. *et al.* Goblet cell-specific expression mediated by the MUC2 mucin gene promoter in the intestine of transgenic mice. *Am. J. Physiol.* 276, G666–76 (1999).
179. Ku, S. K., Lee, H. S. & Lee, J. H. An immunohistochemical study of the gastrointestinal endocrine cells in the C57BL/6 mice. *Anat Histol Embryol* 32, 21–28 (2003).
180. Sala, F. G. *et al.* A multicellular approach forms a significant amount of tissue-engineered small intestine in the mouse. *Tissue Eng Part A* 17, 1841–1850 (2011).
181. Gracz, A. D. *et al.* CD24 and CD44 Mark Human Intestinal Epithelial Cell Populations with Characteristics of Active and Facultative Stem Cells. *Stem Cells* 31, 2024–2030 (2013).
182. McCracken, K. W., Howell, J. C., Wells, J. M. & Spence, J. R. Generating human intestinal tissue from pluripotent stem cells in vitro. *Nat Protoc* 6, 1920–1928 (2011).
183. Badylak, S. F. The extracellular matrix as a biologic scaffold material☆. *Biomaterials* 28, 3587–3593 (2007).

184. Lu, P., Weaver, V. M. & Werb, Z. The extracellular matrix: a dynamic niche in cancer progression. *J. Cell Biol.* 196, 395–406 (2012).
185. Wolf, M. T. *et al.* A hydrogel derived from decellularized dermal extracellular matrix. *Biomaterials* 33, 7028–7038 (2012).
186. USDA, N. A. S. S. Livestock Slaughter 2016 Summary 04/19/2017. 1–69 (2017).
187. Badylak, S. F. & Gilbert, T. W. Immune response to biologic scaffold materials. *Semin. Immunol.* 20, 109–116 (2008).
188. Andrée, B., Bär, A., Haverich, A. & Hilfiker, A. Small Intestinal Submucosa Segments as Matrix for Tissue Engineering: Review. *Tissue Eng Part B Rev* (2013). doi:10.1089/ten.TEB.2012.0583
189. Ansaloni, L. *et al.* Hernia repair with porcine small-intestinal submucosa. *Hernia* 11, 321–326 (2007).
190. Armitage, S., Seman, E. I. & Keirse, M. J. N. C. Use of surgisis for treatment of anterior and posterior vaginal prolapse. *Obstet Gynecol Int* 2012, 376251 (2012).
191. Mostow, E. N., Haraway, G. D., Dalsing, M., Hodde, J. P. & King, D. Effectiveness of an extracellular matrix graft (OASIS Wound Matrix) in the treatment of chronic leg ulcers: A randomized clinical trial. *Journal of Vascular Surgery* 41, 837–843 (2005).
192. Bejjani, G. K., Zabramski, J. Durasis Study Group. Safety and efficacy of the porcine small intestinal submucosa dural substitute: results of a prospective multicenter study and literature review. *J. Neurosurg.* 106, 1028–1033 (2007).
193. Bibbo, C. The porcine small intestinal submucosa (SIS) patch in foot and ankle reconstruction. *J Foot Ankle Surg* 49, 123–127 (2010).
194. Danese, S., Bonovas, S. & Peyrin-Biroulet, L. Positioning Ustekinumab in Crohn's Disease: From Clinical Evidence to Clinical Practice. *Journal of Crohn's and Colitis* 11, 1258–1266 (2017).
195. Tillack, C. *et al.* Anti-TNF antibody-induced psoriasiform skin lesions in patients with inflammatory bowel disease are characterised by interferon- γ -expressing Th1 cells and IL-17A/IL-22-expressing Th17 cells and respond to anti-IL-12/IL-23 antibody treatment. *Gut* 63, 567–577 (2014).
196. Garreta, E. *et al.* Tissue engineering by decellularization and 3D bioprinting. *Materials Today* 20, 166–178 (2017).

197. Bissell, M. J., Hall, H. G. & Parry, G. How does the extracellular matrix direct gene expression? *Journal of Theoretical Biology* 99, 31–68 (1982).
198. Moltke, von, J., Ji, M., Liang, H.-E. & Locksley, R. M. Tuft-cell-derived IL-25 regulates an intestinal ILC2-epithelial response circuit. *Nature* 529, 221–225 (2016).
199. Howitt, M. R. *et al.* Tuft cells, taste-chemosensory cells, orchestrate parasite type 2 immunity in the gut. *Science* 351, 1329–1333 (2016).
200. Gerbe, F. *et al.* Intestinal epithelial tuft cells initiate type 2 mucosal immunity to helminth parasites. *Nature* 529, 226–230 (2016).
201. Gerbe, F., Legraverend, C. & Jay, P. The intestinal epithelium tuft cells: specification and function. *Experientia* 69, 2907–2917 (2012).
202. Höfer, D. & Drenckhahn, D. Identification of brush cells in the alimentary and respiratory system by antibodies to villin and fimbrin. *Histochemistry* 98, 237–242 (1992).
203. Bezençon, C. *et al.* Murine intestinal cells expressing Trpm5 are mostly brush cells and express markers of neuronal and inflammatory cells. *J. Comp. Neurol.* 509, 514–525 (2008).
204. Bamias, G. & Cominelli, F. Role of type 2 immunity in intestinal inflammation. *Curr. Opin. Gastroenterol.* 31, 471–476 (2015).
205. Annunziato, F., Romagnani, C. & Romagnani, S. The 3 major types of innate and adaptive cell-mediated effector immunity. *J. Allergy Clin. Immunol.* 135, 626–635 (2015).
206. Bjercknes, M. *et al.* Origin of the brush cell lineage in the mouse intestinal epithelium. *Developmental Biology* 362, 194–218 (2012).